# GEOMORPHIC INFLUENCES ON SOIL DEVELOPMENT AND SOIL ORGANIC MATTER DYNAMICS IN CENTRAL JACKSON COUNTY, WISCONSIN

By

Kristine Emma Gruley

A dissertation submitted in partial fulfillment of

the requirements for the degree of

Doctor of Philosophy

(Geography)

At the

UNIVERSITY OF WISCONSIN-MADISON

2015

Date of final oral examination: 12/12/14

The dissertation is approved by the following members of the Final Oral Committee:

Dr. Joseph A. Mason, Professor, Geography
Dr. John W. (Jack) Williams, Professor, Geography
Dr. Erika Marín-Spiotta, Assistant Professor, Geography
Dr. Eric C. Carson, Assistant Professor, Environmental Sciences
Dr. Peter M. Jacobs, Professor, Geography and Geology, UW-Whitewater

**ACKNOWLEDGEMENTS**

It seems appropriate to start by acknowledging my undergraduate mentor and committee member, Dr. Peter Jacobs. His charismatic teaching style and enthusiasm for soils were instrumental in my decision to pursue graduate studies in physical geography. I appreciate his generosity, both in time spent chatting about my project, academia, and life in general, as well as in access to lab equipment, training, and teaching opportunities at UW-Whitewater. I am certain that I would not be here without his guidance and encouragement throughout my education.

I am greatly indebted to my advisor, Dr. Joe Mason, who supported me with grants and advocated for me throughout my time here at UW-Madison. I am so thankful for his advice and amazingly quick turnaround for feedback on my chapters and job application materials. Joe also supplied much of the equipment and supplies necessary to complete this project and never hesitated to talk through ideas when I was stuck.

I would like to acknowledge the rest of my committee, Dr. Jack Williams, Dr. Eric Carson, and Dr. Erika Marín-Spiotta. Erika, in particular, has been a continual source of encouragement during my time at UW-Madison. Her support in both my academic and non-academic pursuits has been vital to my success. I would also like to specially thank Dr. Jim Knox for being on my committee, use of his lab equipment, and letting me camp out in his lab during much of my PhD. I was excited to share an interesting finding with him shortly before he passed— clod of a suspected buried soil in silt that he thought looked much like Roxana Silt.

Several people need to be acknowledged who helped me complete lab work. Thank you to Sara Allen at UW-Platteville, who spent countless hours drying, crushing, and sieving my samples, running particle size analysis, and picking out modern organic fragments from a subset of my samples. Thank you to Elmo Rawling and the TREEs lab at UW-Platteville for the use of equipment and funding for my research while I was a faculty fellow there. Thanks to Gretchen Kamps, who was a great support at UW-

Platteville and acquired a coveted soil tape for me to take great profile pictures! Thank you also to Mengyu Liang at UW-Madison, who worked on most of my pH samples.

I also need to thank various people from the department who helped get me through my PhD. Sharon Kahn was a major support to me in countless ways—helping me navigate through my degree and future career options, and for sharing her experiences in academia and life. I will forever appreciate her open door policy and willingness to chat about anything. Additionally, many friends and colleagues I have encountered during my time here need to be recognized. I would like to especially thank Colin Belby, Paul Reyerson, Henry Loope, and Jacquelyn Gill for introducing me to the department, their time spent training me in the lab, and the countless discussions that expanded my way of thinking about Quaternary topics among others. I also need to especially thank Emily Atkinson and Sam Munoz as colleagues, but also for their friendship and support during the last couple years of my PhD. They, along with Jen Holmstadt, Sierra Munoz, Jessica Blois, Kelly Haslam, Amanda Eggen, and the Gruley clan, encouraged me during difficult times over the last couple years of my PhD, but also provided much needed fun and relief.

Finally, I need to thank my husband, Joel Gruley. Without his love and support, I may never have finished. He was my trusty field assistant during much of my fieldwork and had the pleasure of having to dig through three fragipans and then sitting for hours while I cleaned and described soil profiles. He also did more than his fair share of housework and never wavered in his belief that I would finish. He continues to broaden my geographical perceptions and be my source of calm.

This research was supported by the National Science Foundation under grant number BCS-0751750 made to Joe Mason, and by the Leopold Geomorphology fellowship from the Geography department at UW-Madison.

## TABLE OF CONTENTS

## *List of Figures*

## *List of Tables*

## *Abstract*

Sandy and silty mantles in central Jackson County were investigated to characterize, identify, and document past or present geomorphic and pedogenic processes as well as soil organic matter dynamics operational in this landscape. LiDAR, particle size, and silt geochemical data suggest the sand mantle is typically 30 – 100 cm, no more than 5 m thick, and covers much of the low-relief terrain landscape as a result of widespread eolian activity. The sand mantle acted largely as a surface of transport where saltating sands caused fine-grained material to be re-entrained to be deposited farther downwind. Eolian silt associated with deglaciation is only preserved as silty mantles in the most protected positions along the east and southeast aspects of large bedrock ridges. Silty eolian/colluvial mantles are rich in both coarse and fine silt; whereas, silt found in the sandy mantle in windward locations is dominantly fine silt. Thus, much of the fine silt was likely deposited near the end of widespread eolian activity.

Without these silty additions, a continuum of podzolization processes would likely dominate the sandy soils based on drainage from Entisols in higher positions to aquic Spodosols in toeslopes. Silty soils have greater inputs of reworked loess are highly acidic and generally unproductive, however, the pedogenic pathway is pushed from podzolization to lessivage. Bisequal soils with an upper E-Bt and lower Ex-Btx are common in these settings. Comparisons of lower sequa characteristics between catena positions suggest lateral flow and translocation through both silty and sandy catenas is an important process in this landscape.

Soil organic matter (SOM) was compared to fresh organic matter (OM), clay mineralogy and particle size data. SOM in the upper 30 cm show increasing $\delta^{15}N$ and $\delta^{13}C$ values and decreasing C:N values with depth, which suggests increased decomposition with depth. In sandy profiles with impeded drainage, podzolization resulted in less decomposed OM protected by organic-mineral complexes with depth. These results point to the importance of understanding the geomorphology and sedimentology of soil parent materials in SOM research as well as the importance of using sampling protocols that are based on horizons rather than incremental depths.

## CHAPTER 1 : INTRODUCTION

Deposits of windblown dust (loess) occur in many parts of the world, and are often associated with glacial and periglacial environments (Smith 1942; Frye et al. 1962; Smalley 1966; Ruhe and Olson 1980; Pye 1984; Bettis et al. 2003). Until recently, the Midwestern conceptual model of loess dispersion, linking loess deposits to broad river valleys that carried meltwater and sediment from the Laurentide Ice Sheet (LIS), has been a dominant explanation for loess deposits in the Midwest (Smith 1942; Snowden and Priddy 1968; Ruhe and Olson 1979; Follmer 1996; Mason 2001; Bettis et al. 2003). Thick loess deposits are often demonstrated or presumed to be derived from adjacent broad river valleys and valley trains (Smalley 1966; Ruhe and Olson 1980; Ruhe 1983; Grimley 2000; Bettis et al. 2003). In this model, rivers that drain glacial ice are typically sediment-rich, and during times of low flow, fine sands and silts are deflated from valley trains and broad river valleys and are subsequently deposited downwind (Smith 1942; Ruhe 1954; Frye et al. 1962; Fehrenbacher, White, Ulrich et al. 1965; Ruhe and Olson 1979; Johnson and Follmer 1989).

However, some loess deposits in North America are separated from their source areas by a transportation surface, on which saltating sands result in repeated silt re-entrainment until migrating sand is trapped by a topographic barrier allowing silt to accumulate downwind (Mason et al. 1999; Mason et al. 2003; Sweeney et al. 2007; Schaetzl and Loope 2008). Source areas are less readily identifiable for loess deposits that do not lie adjacent to large river valleys or valley trains. In addition to loess deposits spatially separated from their sources, relatively thin and/or discontinuous accumulations of loess are increasingly being investigated as they may provide insight into local and regional paleoenvironmental conditions at the time of eolian activity (Jacobs et al. 2011; Stanley and Schaetzl 2011; Schaetzl and Attig 2013)

Furthermore, understanding the geomorphology in areas where a relatively thin eolian mantle overlies other parent materials is a particularly important component to interpreting pedogenesis in these soils. The state factor model (Jenny 1941) of soil development remains an important framework within

which soil morphology can be understood by changes in one of the five factors in soil formation—climate, organisms (flora and fauna), relief, parent material, or time. In many locations strict application of the state factor model is difficult or impossible due to the presence of lithologic discontinuities, vegetation and hydrology changes with slope, and hillslope processes that not only change parent material characteristics, but also the time factor. In these situations, the catena concept is a better framework in which to understand pedogenesis on topography with moderate relief (Sommer and Schlichting 1997). The catena concept combines the basic tenets of the state factor model with the process-systems model (Simonson 1959) that better explains intra-profile changes in horizonation, in conjunction with the idea that soils on slopes are genetically linked (Hall et al. 1983).

In addition, much of our understanding about soil organic carbon (SOC) dynamics is based on implied static soils/landscapes as well as the dynamics of relatively shallow (surface) accumulations of soil organic matter (SOM). This bias ignores relatively large accumulations of SOC at depths >30 cm that are common in some landscapes (Stone et al. 1993; Grand and Lavkulich 2011). Carbon stored at depth may be important for at least two reasons: 1) relatively fresh C can be stabilized when dissolved organic matter (DOM) is translocated and precipitated at depth where microbial processes are impeded (Schwendenmann and Veldkamp 2005), and 2) the potential for long-term sequestration is high since mean residence times (MRT) at depth are commonly on the order of millennia (Holzhey et al. 1975; Trumbore 2000). In addition, C with a long MRT tends to be common in waterlogged soils with nutrient-poor parent materials, resulting in large accumulations of subsurface SOC (Buurman and Jongmans 2005), in which case, SOC in these landscapes may provide insight into past climate or vegetation dynamics.

Predicting future SOC dynamics associated with climate change requires complex understanding of how C stabilization mechanisms, ecosystems, and landscapes respond to change (Trumbore and Czimczik 2008). For this reason, it is important to not only analyze how carbon is stored spatially across the landscape and vertically within the soil profile, but also how modern and past geomorphic processes affect C storage in these landscapes.

With this background in mind, the focus of this research is the low relief, sandy landscape of central Jackson County, Wisconsin, within the northwest part of the Central Sand Plain. This study area presents an excellent opportunity to test the hypothesis that eolian processes played a key role in forming the sandy surficial mantle of the region. First, this sand-mantled landscape is generally low-relief, but contains prominent, isolated bedrock ridges which may have served to trap enough saltating sand to protect small areas of dust accumulation on their lee sides. If the results support the hypothesized role of eolian processes in this landscape, this will also provide additional support for the Jacobs et al. (2011) hypothesis that the Central Sands region acted as a surface of transport allowing distantly sourced loess to reach south-central Wisconsin. After the parent materials are identified and characterized, I will investigate how relatively small amounts of eolian fine grained sediments may affect soil development and SOM dynamics in an otherwise sandy landscape.

### *Research Objectives*

This study has three main research objectives:

(1) To identify, characterize, and document the geomorphic processes associated with the sandy and silty mantles in central Jackson County.
    a. What can the surface mantles suggest about the past and/or present geomorphic processes affecting this landscape?
    b. Is external loess detectable in this landscape?

(2) To document, characterize, and discuss pedogenic processes operational in this landscape with respect to parent material identified.
    a. How do relatively minor silt accumulations affect pedogenesis in a dominantly sandy landscape?
    b. What soil forming factors influence pedogenesis in sandy vs. silty mantles?

(3) To document, characterize, and discuss the dynamics of SOM in this dominantly sandy landscape.

a. How does the amount and character of SOM change with depth?

b. How does SOM differ between sandy and silty mantles?

## *Regional setting*

### Geology and Geomorphology

The study area is situated within central Jackson County, east of the Black River (Figure 1.1). West of the Black River, loess and loess-derived colluvium blanket the deeply dissected, bedrock controlled topography (Figure 1.2A). However, loess is largely absent east of the Black River. There, much of the landscape has low relief and relatively low drainage density, and is blanketed by up to a few meters of sandy sediment overlying Cambrian sandstone. Several prominent bedrock ridges with steep, dissected slopes rise above this low-relief terrain, and were important for the sampling strategies described below.

This area lacks evidence of glaciation and therefore is within the Driftless Area, approximately 10 km west of the Glacial Lake Wisconsin basin. During glaciations, this region undoubtedly experienced

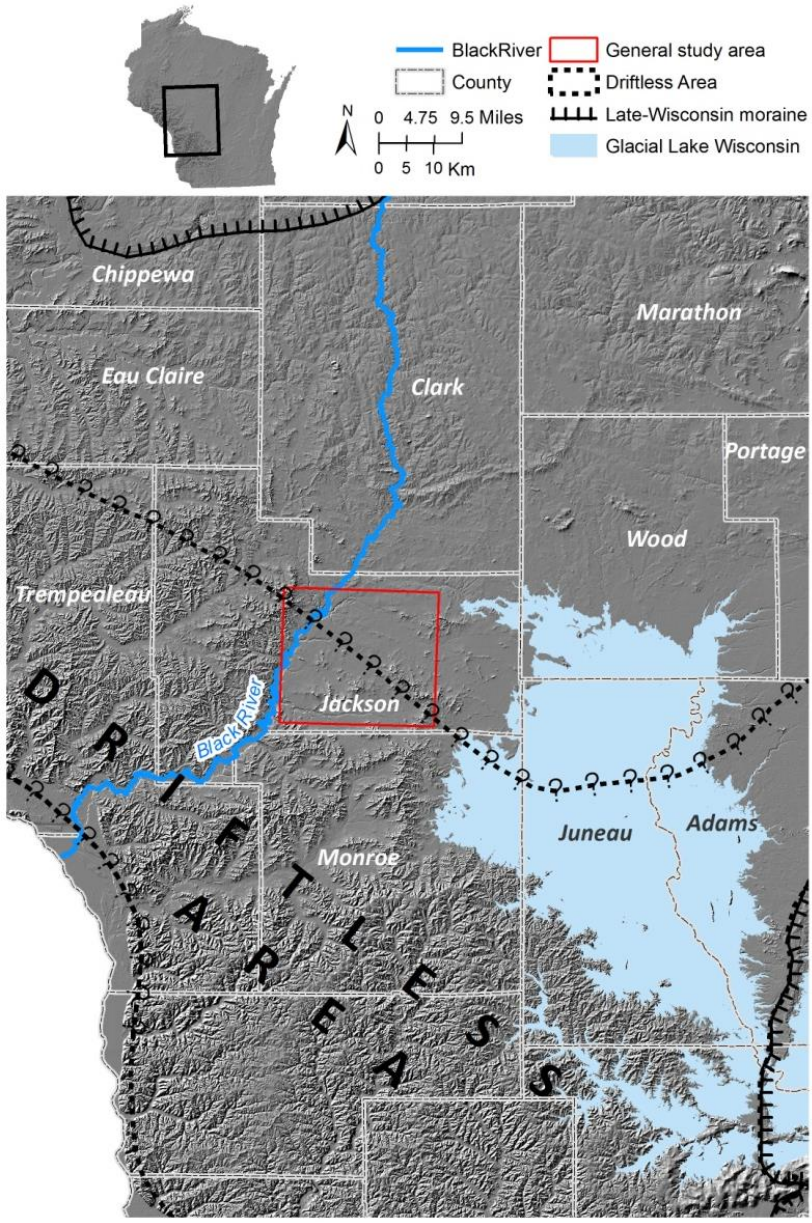


**Figure 1.1:** Hillshaded DEM of central Wisconsin showing Jackson and surrounding counties, the extent of Glacial Lake Wisconsin, and the extent of the Driftless Area. The Black River is highlighted in blue. The general study area is outlined in red.

periglacial conditions, evident by many relict permafrost features found within and adjacent to the Driftless Area (Black 1965; Johnson 1990; Clayton et al. 2001). Thus, Clayton and Madison (1983) postulated that the low-relief landscape east of the Black River largely resulted from periglacial hillslope erosion. Additionally, a thin sandy mantle that commonly covers pebble- and cobble-sized ventifacts occupies most of this landscape (Mickelson et al. 1983; Langton and Simonson 1998). The sand mantle continues towards the southeast where it crosses the regional drainage divide between the Black River basin and the Glacial Lake Wisconsin basin and subsequently merges with the sand plains of Glacial Lake Wisconsin (Clayton and Madison 1983) (Figure 1.2). This stone-free sand mantle that continues to the southeast into the Glacial Lake Wisconsin basin, is postulated to have acted as a transport surface, carrying re-entrained dust farther downwind towards the Oneota Escarpment (Jacobs et al. 2011). Although much attention has been given to the Glacial Lake Wisconsin landscape (Clayton and Attig 1987, 1989; Rawling et al. 2008; Jacobs et al. 2011) and the high-relief, loess covered terrain of the Driftless Area (Knox et al. 1982; Mickelson et al. 1982; Leigh and Knox 1994; Jacobs et al. 1997; Mason and Knox 1997), little if any research has focused on the sandy landscape between the two areas.

Underlying most of the low-relief topography is the Mount Simon Formation (Figure 1.2D), a Cambrian sandstone unit that is characterized by poorly sorted beds which are dominantly composed of coarse (~700 μm) and medium (~250 μm) quartz grains (Asthana 1969; Ostrom 1970; Distefano 1973) (Table 1.1). Median grain size for the Mt. Simon Formation is 277 μm (medium sand); although, siltstones and shale partings and laminae are a minor constituent throughout (Asthana 1969; Ostrom 1970). Towards the top of the Mt. Simon, medium and coarse lithologies alternate with finer-grained beds typical of the Eau Claire Formation, which if present, is likely less than 3 m thick within central Jackson County (Ostrom 1970).

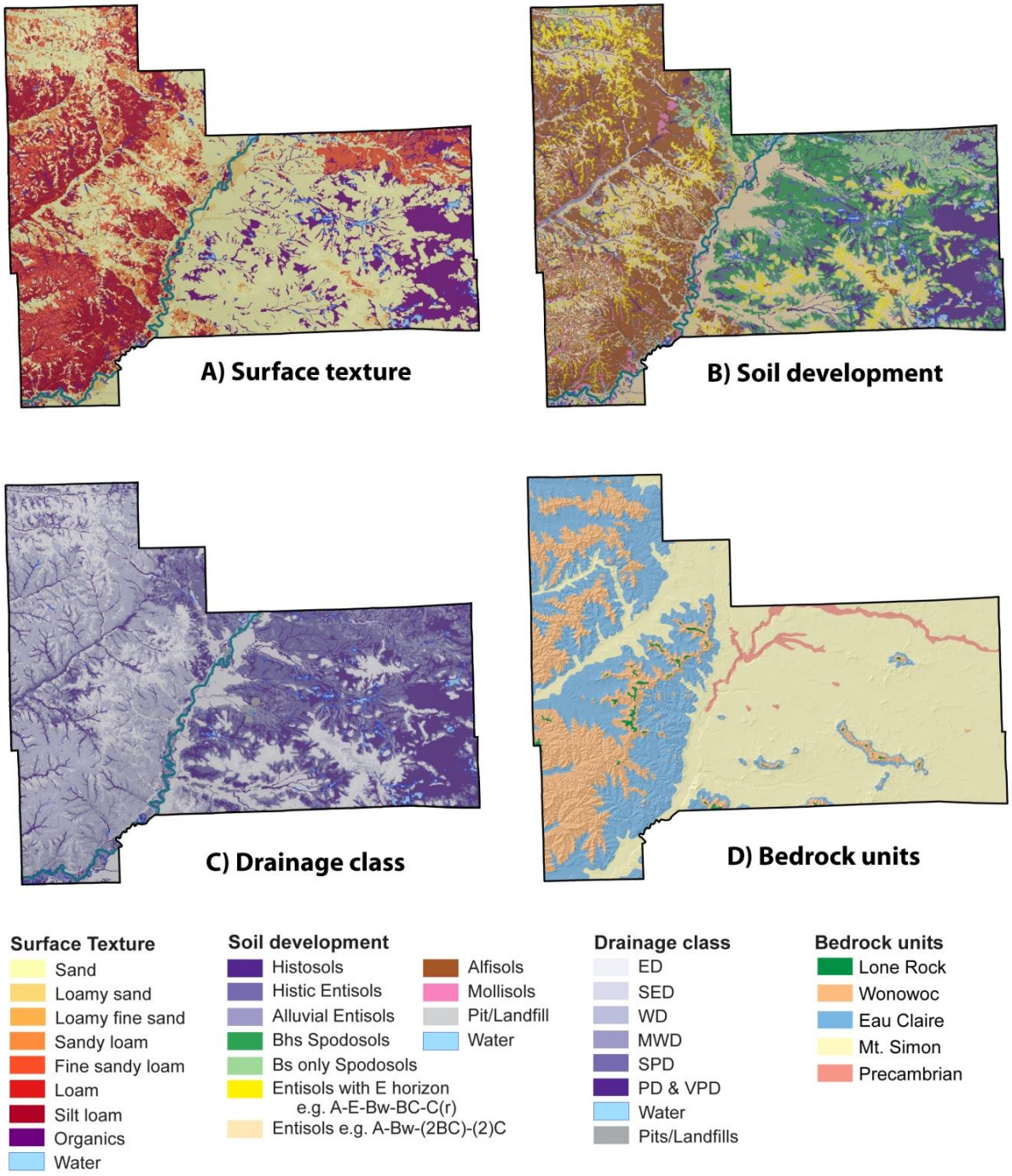


**Figure 1.2:** Maps of Jackson County soil characteristics and bedrock units. **A:** Surface textures. **B:** Soil development. **C:** Drainage class. **D:** Bedrock units. Much of the low relief terrain east of the Black River consists of wet, sandy, Aquic Spodosols and Histosols underlain by Mt. Simon Sandstone. Better drainage occurs in this area where relief is higher, especially where prominent bedrock ridges composed of Wonowoc Sandstones and Alfisols only occur in small isolated patches near these bedrock ridges. However, west of the river, the terrain is generally higher and more dissected and soils are dominantly better drained Alfisols. Sandy Entisols only occur on the ridge tops and as eolian sand ramps upslope from larger valleys. (After Langton and Simonson, 1998; Brown, 1995; using SSURGO data and shaded relief of 30 m NED data).

**Table 1.1:** Cambrian sandstone units commonly cropping out in central Wisconsin.

| Group | Formation | | Common grain size range (µm) | Mean grain size (µm) | Feldspar content | Other minerals | Clay mineralogy |
|---|---|---|---|---|---|---|---|
| Tunnel City Group | Lone Rock | Reno Member | 88-250[a] | 172[a] | < 50 % K-feldspar, no plag[c] | Dolomite, mica [b] | 20-50% G [a] |
| | | Birkmose Member | Silt-fine sand [b] | 125 [b] | < 50 % K-feldspar, no plag[c] | Dolomite/calcite cement [b] | 15-45% G [a] |
| Elk Mound Group | Wonewoc | Ironton Member | 114-400[d] | 322[e] | 1.1%; Silt-rich beds as high as 5%[d] | Zircon, tourmaline >> garnet >Leucoxene, Ilmenite; Hematite and limonite coat quartz grains in the upper beds[d] | I (Al-rich)>>I(.7)/M >>K; More G towards top[d] |
| | | Galesville Member | 114-400[d] | 207[f] | 1.1%; Silt-rich beds as high as 5%[d] | 95.2% Q; Zircon>tourmaline>> garnet,Leucoxene, Ilmenite [d] | |
| | Eau Claire | | <63-125[f] | 88[g] 46[f] | >40%; mostly orthoclase, K-spar ave 33%; plagioclase present (1.8%) [f, h] | Zircon, tourmaline, garnet (all concentrated in finer grains) [f] | I (Al-rich)>>I(.7)/M >>C >K, G [h] |
| | Mt. Simon | | 250-700[f] | 277[g] | <15% up to 40% concentrated in Csi and VFS; 1/3 detrital microcline[f]; (< 2% detrital microcline/plag[g]); orthoclase overgrowths | Zircon, tourmaline, garnet (all concentrated in finer grains) [f] | I (Al-rich)>>I(.7)/M >>C>K [h] |

a: (Eoff 2008)
b:(Berg 1954)
c: (Ostrom 1970; Stablein and Dapples 1977)
d: (Emrich 1966)
e: (Andrew 1965), coarse skewed particle size analysis.
f: (Distefano 1973), sample bias for finer grained beds.
g: (Asthana 1969)
h: (Morrison 1968)

The Wonewoc Formation caps the isolated ridges rising above the low-relief areas. The Galesville Member of the Wonewoc Formation unconformably overlies the Eau Claire Formation where present (or the Mt. Simon Formation where the Eau Claire is absent), and is dominantly composed of moderate- to well-sorted, massively and cross-bedded fine and medium sands (Ostrom 1970; Odom 1975). According to Distefano (1973), Galesville sandstones contained a range of 114 μm (very fine sand) to 400 μm (medium sand) with the median grain size of 207 μm (fine sand). The upper member of the Wonewoc Formation, the Ironton, is characterized by poorly sorted, even-bedded, fine to coarse-grained sandstone with common glauconite and silt-rich beds (Ostrom 1970; Odom 1975). At Saddle Mound, in northern Jackson County, the median grain size of the Ironton is 322 μm according to Andrew (1965). Small, isolated remnants of the Lone Rock Formation, a fine-grained, glauconite-rich sandstone (Emrich 1966), can be found in the highest locations within the study area overlying the Wonewoc Formation. The Lone Rock Formation has typical particle sizes ranging from silt (<63 μm) to 250 μm (medium sand), with means between 125 and 172 μm (Eoff 2008).

Feldspar is present in most samples of these Cambrian strata, but it is highly concentrated in the finest fractions, especially coarse silt and very fine sands (Distefano 1973; Odom 1975) (Table 1.1). The overwhelming majority of feldspar is K-feldspar, with microcline comprising the detrital components and orthoclase comprising much of the overgrowths (Asthana 1969; Distefano 1973; Odom 1975). Plagioclase is rarely identified in sand grain point counts from Cambrian Sandstones, but in some cases can make up < 2% of sand grains (Asthana 1969; Distefano 1973; Odom 1975).

**Soils**

An eolian sand mantle up to 2 m thick blankets a large part of the study area east of the Black River, with organic soils occupying many of the lowest areas (Langton and Simonson 1998) (Figure 1.3 inset). Finer textured soils (loams and silt loams) derived from varying amounts of loess inputs occur on uplands west of the Black River and on the lee (east) sides of the few, prominent bedrock ridges, e.g. Wildcat Ridge, in central Jackson County (see Chapter 2). Bedrock controlled uplands are typically

mapped as Boone sands, which have a 20 and 40 cm thick sandy mantle overlying bedrock. Some of the knife-edge ridges have less than 5 cm of sand overlying consolidated bedrock, whereas slightly broader summits and shoulders on the lee side (east) of prominent bedrock ridges have more fines in the solum

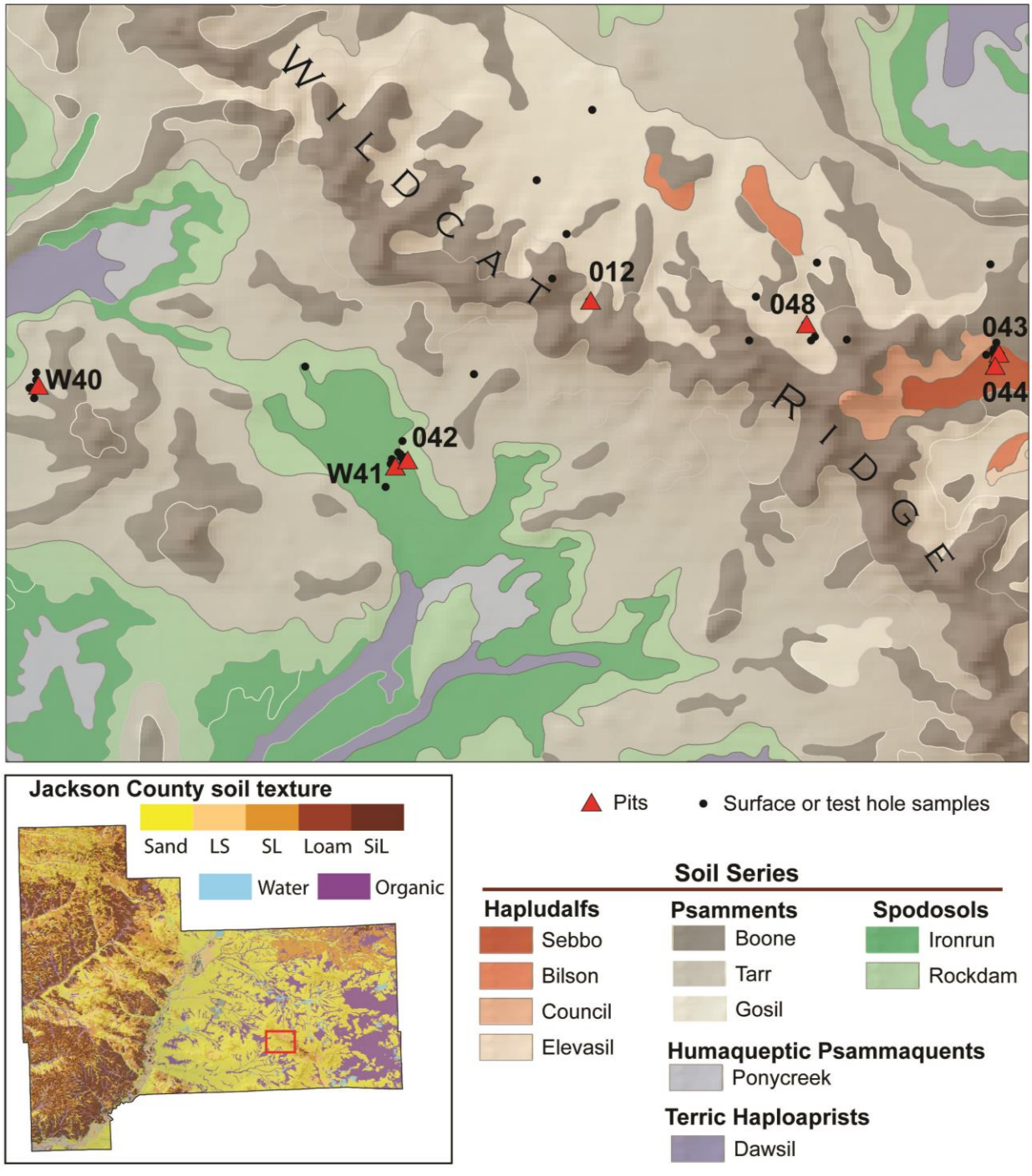


**Figure 1.3:** Map of soil development for central Jackson County, WI (after Langton and Simonson 1998 using SSURGO and shaded relief of 30 m NED data).

and some soils have argillic horizons and are mapped as Elevasil sandy loams. Tarr sands are mapped over vast areas of central Jackson County, where <2 m of eolian sand mantle bedrock residuum and/or colluvium. Tarr sands often ramp onto windward aspects of prominent bedrock ridges; whereas on immediately adjacent lee aspects, Gosil loamy sands are mapped. In these places, Gosil loamy sands extend <1.5 km east of Wildcat Ridge before eolian fines decrease and Tarr sands are mapped.

In a few of the most isolated and protected lee footslopes, finer-textured Alfisols are mapped. Merit and Bilson soils are mapped where the silt loam or sandy loam mantle overlies siliceous sandy colluvium or bedrock residuum. Where relatively thick loamy mantles occur, Sebbo loams and Council silt loams are mapped. As the eolian sand mantle transitions from somewhat excessively drained higher landscape positions to lower landscape positions where drainage is increasingly impeded, soils change from Entisols to Spodosols, and finally to Histosols. Here, Tarr sands transition to Rockdam sands and then to Ironrun sands, increasing in spodic development with decreasing drainage. Ponycreek mucks and Dawsil mucky peats are mapped in the lowest position on the landscape.

In summary, this landscape is dominated by Entisols in drier landscape position (lower backslope and higher) formed into a sandy eolian mantle with Spodosols and Alfisols formed into sandy and silty mantles, respectively, in lower landscape positions. Both silty and sandy mantles overlie Cambrian sandstone residuum, and thus, presumably contain a lithologic discontinuity with coarser material below. These similar parent materials that primarily differ in silt content within the solum present a good opportunity to investigate the influence of relatively minor accumulations of eolian dust on soil development.

## Environment & vegetation

### *Glacial and Late-Glacial Environments*

At present, the only long, continuous paleoecological record going back to the late glacial period from within the Driftless Area is from Devil's Lake (Maher 1982; Baker et al. 1992), however, this data can be supplemented using studies from areas immediately west and north of the Driftless Area in

Minnesota and northern Wisconsin to provide a regional context for paleoenvironments and vegetation from the Late Pleistocene to the present. Thus, paleovegetation and geomorphic evidence suggest much of the DA and surrounding region experienced a periglacial climate during the LGM. Relict permafrost features, including ice-wedge casts, patterned ground, and talus streams, have been recognized across the state of Wisconsin (Black 1965; Johnson 1986; Clayton et al. 2001). These features, especially ice-wedge polygons, are indicative of permafrost, as actively forming wedges spatially coincide with the area of continuous permafrost (Péwé 1966, 1983, 1984; French 1996). Closely associated with permafrost and periglacial environments are 1) tundra communities, which overly areas of continuous permafrost, and 2) boreal forest communities, which often overly areas of discontinuous permafrost (Price 1972; Carter et al. 1987). In central Minnesota, pollen data suggest taxa consistent with tundra communities occurred between 24.4 and 17.5 ka[1] (Birks 1976). Thus, while the Laurentide Ice Sheet (LIS) was at its maximum extent between approximately 26 and at least 21 ka (Carson et al. 2012), the landscape of the DA was likely underlain by continuous permafrost (Black 1965; Clayton et al. 2001) and dominated by herb taxa associated with tundra communities (Birks 1976; Overpeck et al. 1992).

As the climate warmed following the LGM, the geomorphic landscape and vegetation adjusted to the new climatic conditions. As the permafrost melted, the thickness of the seasonally thawed (active) layer likely increased (Price 1972). Permafrost at depth, however, restricts water percolation which can lead to slope destabilization via increased runoff, solifluction, and mass wasting (Carter et al. 1987; French 1996). In the Driftless Area, accelerated solifluction and mass wasting associated with a permafrost-dominated landscape is known to have occurred between 22.5 and 13.6 ka (Mason 1995; Mason and Knox 1997).

During this time of increasing landscape instability, vegetation assemblages also changed due to the independent migration of individual taxa (Overpeck et al. 1992; Williams et al. 2004). By approximately 18 ka, the tundra-like environment had shifted towards an open spruce parkland, which

[1] All age estimates are reported in calibrated calendar years before present (1950). Ages that were originally reported in RC years BP have been converted to calendar years using Calib 6.0 (Reimer et al. 2009).

was similar to modern boreal forest but were likely more open because pollen assemblages contained slightly higher amounts of sedge and Artemisia (Overpeck et al. 1992; Williams et al. 2004). By approximately 16 ka, temperate coniferous and deciduous taxa migrated into the DA forming a mixed parkland biome, which has no modern analog (Williams et al. 2001; Webb et al. 2004; Wright et al. 2004). After 16 ka, continued migration of individual taxa (both at and within range margins) accelerated and vegetation abundances increased with increasing atmospheric $CO_2$ levels into the early Holocene (Williams et al. 2004). Presumably, the increase in vegetation cover stabilized periglacial landscapes within/near the DA, which likely limited supply of sediment for loess deposits by approximately 12 ka (Stanley 2008a).

## Holocene Environments

### *Early Holocene*

Temperature and moisture reconstructions from central Minnesota suggest climate during the early Holocene was generally cool and humid with gradually increasing episodes of aridity until 8 ka (Camill et al. 2003; Nelson and Hu 2008). Similarly, multi-proxy records from two lakes in Illinois suggest aridity gradually increased from 10 to 8.5 ka (Nelson et al. 2006). During the onset of the Holocene, *Pinus* (especially *Pinus banksiana and/or resinosa*) rapidly increased in abundance replacing *Picea* in central Minnesota and north central Wisconsin (Heide 1984; Wright et al. 2004). In central Minnesota, *Picea* remained a component of vegetation assemblages until approximately 10 ka when an *Ulmus-Ostrya* community greatly increased in abundance across the landscape (Camill et al. 2003). By ~9 ka, modern vegetation assemblages were established in the upper Midwest; however, the relative importance of these taxa on the landscape varied throughout the Holocene due to changing temperatures and humidity (Overpeck et al. 1992; Camill et al. 2003).

### *Mid-Holocene*

In general, climate in the Midwest abruptly shifted towards warmer and drier conditions at approximately 8 ka and persisted until approximately 4 ka (Baker et al. 2002; Camill et al. 2003);

however, the intensity of the aridity was neither spatially nor temporally homogeneous throughout the Midwest during this period (Nelson and Hu 2008; Williams et al. 2010). Vegetation continued to change during the mid-Holocene in response to the changing climate, albeit at slower rates after 7 ka (Williams et al. 2004). By 8 ka, prairie and deciduous forest taxa dominated most vegetation assemblages west and south of the DA (Webb et al. 1983; Camill et al. 2003; Nelson et al. 2006). Prairie taxa (including C4 grasses) expanded at the expense of deciduous taxa by ~6 ka (Baker et al. 2002; Camill et al. 2003; Nelson et al. 2006). Prairie expansion especially occurred in open woodlands, at woodland margins, and on floodplain openings (Baker et al. 2002). Decreasing moisture availability probably would have inhibited reproduction and survival of juvenile tree taxa, and at the same time reduced fuel loads of grasslands via decreased net primary production (Nelson et al. 2004; Umbanhowar et al. 2006). In this region, therefore, fire seems to be largely a product of changes in vegetation due to climate change rather than a driver (Webb et al. 1983; Nelson et al. 2004; Umbanhowar 2004; Nelson et al. 2006; Umbanhowar et al. 2006; Nelson and Hu 2008). However, at local scales, edaphic, topographic, and fire regime characteristics had a stong influence on the local vegetation patterns (Webb et al. 1983; Grimm 1984).

Topography and edaphic characteristics as well as changes in seasonality of precipitation probably enhanced the effects of climate change on both geomorphology and vegetation. Moisture stress would have affected the driest sites first, e.g. *Ulmus* was found to have declined at ~6 ka from upland settings and by 5.5 ka from lowland settings (Baker et al. 2002). Evidence that the decreased moisture availability likely occurred during the summer can be found in speleothem and macrofossil records from northeast Iowa, which also corroborate the increase of C4 plants at this time (Baker et al. 2002). Furthermore, fluvial sedimentation and stream morphology suggests large floods between 6 and 4.5 ka were a direct consequence of drier summers, which not only increased the dominance of prairie taxa, but also likely led to an overall decrease in vegetation cover and consequently increased runoff (Knox 1985; Baker et al. 2002).

***Late-Holocene through present***

Multiple lines of evidence suggest humidity slowly increased between 4 and 2 ka in the region surrounding the Driftless Area (Camill et al. 2003; Umbanhowar et al. 2006). While the increase in moisture availability likely promoted reproduction and juvenile growth of deciduous forest taxa, it also supported increased net primary production of prairie taxa, which led to increased fire intensity/frequency (Camill et al. 2003; Nelson et al. 2006; Umbanhowar et al. 2006). As a result, reforestation responded much more slowly during this time compared to the retreat of forests at the onset of mid-Holocene aridity (Umbanhowar et al. 2006). Forest expansion was typically in the form of oak woodlands and savannas, which occupied much of the Midwest by ~3 ka (Baker et al. 2002; Camill et al. 2003; Umbanhowar et al. 2006). Topographic firebreaks and expansion of oak woodlands likely created increased protection for fire intolerant deciduous taxa i.e., maples (*Acer),* basswood *(Tilia),* and elms *(Ulmus*), allowing them to slightly expand in some areas (Camill et al. 2003). While these mesic taxa did not replace the oak woodlands until 300 years B.P. in central Minnesota (Umbanhowar et al. 2006), the highly dissected, loess-mantled topography of the DA likely protected large areas dominated by mesic and conifer taxa throughout much of the late-Holocene (Davis 1977). However, jack pine (*Pinus banksiana)* or red pine (*P. resinosa)* probably occurred instead of oak woodlands on sandier sites within the northern DA (Wright et al. 2004).

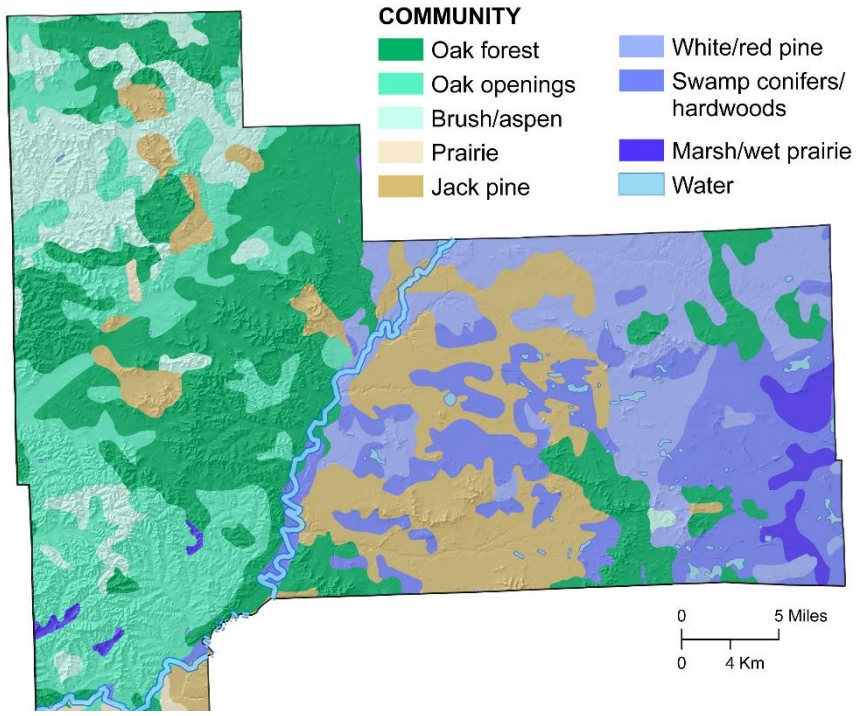


**Figure 1.4:** Map of pre-settlement vegetation. Soils formed in loess typically area associated with oak forest or savannah, whereas jack pine stands typically were found on drier, sandy soils (After Finley 1976).

According to the pre-settlement vegetation map of Wisconsin (Finley, 1976), much

of the area west of the Black River was occupied by open or closed oak forest on the silty uplands, with some isolated spots where prairie or brush vegetation occur (Figure 1.2, Figure 1.4) (Finley 1976). East of the Black River, oak forests are mapped only where isolated high-relief remnants of the Wonowoc formation rise above the sandy low-relief terrain. Jack pine occur both east and west of the Black River in sandy soils, however, it is much more common along with red pines and white pines (*P.strobus*) in the low-relief terrain east of the river. Swamp conifers/hardwoods and marsh/wet prairie are mapped in the lowest positions on the landscape (Figure 1.2, Figure 1.4) (Finley 1976).

Modern vegetation within central Jackson County is primarily mixed hardwood forest. Red pine plantations are common in this sandy landscape, and row crops are planted in the few locations where silty soils occur. In low areas where drainage is impeded, relatively large white pines (*Pinus strobus*) are common along with swamp white oaks (*Quercus bicolor*), black oaks (*Quercus velutina*) red maple (*A. rubrum*), and aspen (*Populus tremuloides*). Bracken fern (*Pteridium*) commonly occupy the forest floor, and in some locations, white pine saplings create dense undergrowth (Figure 1.5A). In siltier soils, the canopy vegetation is composed of relatively young black oaks (*Quercus velutina*), sugar maple *(A. saccharum),* and white birch *(Betula)*; sedges are the dominant vegetation type on the forest floor (Figure 1.5B).


**Figure 1.5:** Vegetation typical of foot and toeslope positions in A: sandy soils and B: silty-loamy soils. Photographs by K. Gruley July 2010.

# CHAPTER 2 : GEOMORPHOLOGY AND SOIL PARENT MATERIALS IN CENTRAL JACKSON COUNTY, WI


## *Abstract*

LiDAR data from Monroe and Juneau Counties show landforms that suggest widespread eolian activity resulted in an eolian mantle covering the low relief terrain associated with the central sand plains of Wisconsin. Particle size distributions of profiles suggest the eolian sand sheet is mostly between 30 and 100 cm thick and covers much of the landscape in central Jackson County and the surrounding low-relief terrain of the Central Sand Plain; however, in places with larger parabolic dunes, the eolian sand may be up to 5 m thick. Eolian silt associated with the period of deglaciation is only preserved in the most protected landscape positions along the east and southeast aspects of large bedrock ridges. This silty eolian/colluvial mantle found in protected leeward locations is rich in both coarse and fine silt; whereas, silt found in the sandy mantle in windward locations is dominantly fine silt that was likely deposited near the end of or after the time of widespread eolian activity. The abundance of dune forms and the absence of silt deposits across the majority of the sandy terrain suggest this landscape acted largely as a surface of transport where fine materials deposited from suspension were entrained by saltating sands across the surface. Most of the silt and finer material was carried farther downwind, perhaps into the Glacial Lake Wisconsin basin, only to be redistributed even farther downwind, presumably onto the Oneota Cuesta. If this is the case, loess on the Green Bay lobe is a mixture of fine sediments from multiple sources including the Cambrian landscape of west-central Wisconsin, outwash and valley train deposits associated with the Upper Mississippi River Valley, and very fine materials from distant western sources.


## *Introduction*

Many of the thick loess deposits in North America have been studied in detail, providing clues into the chronology of unstable periods in which loess deflation and deposition occurred, as well as stable periods of soil development (Willman and Frye 1970; Follmer 1996; Bettis et al. 2003). These thick deposits, especially within the Central Lowlands of the US, are often demonstrated or presumed to be derived from

adjacent broad river valleys and valley trains (Smalley 1966; Ruhe and Olson 1980; Ruhe 1983; Grimley 2000; Bettis et al. 2003). In this model, rivers that drain glacial ice are typically sediment-rich, and during times of low flow, fine grained sediment is deflated from valley trains and broad river valleys due to strong winds, minimal vegetation, and saltating sands and is subsequently deposited downwind (Smith 1942; Ruhe 1954; Frye et al. 1962; Fehrenbacher, White, Ulrich et al. 1965; Ruhe and Olson 1979; Johnson and Follmer 1989) (Figure 2.1A). However, some loess deposits in North America are separated from their source areas by a transportation surface, on which saltating sands result in repeated silt re-entrainment until migrating sand is trapped by a topographic barrier allowing silt to accumulate downwind (Mason et al. 1999; Mason et al. 2003; Sweeney et al. 2007; Schaetzl and Loope 2008; Luehmann et al. 2013) (Figure 2.1B). Source areas are less readily identifiable for loess deposits that do not lie adjacent to large river valleys or valley trains. In addition to loess deposits spatially separated from their sources, relatively thin and/or discontinuous accumulations of loess are increasingly being investigated as they may provide insight into local and regional paleoenvironmental conditions at the time of eolian activity (Jacobs et al. 2011; Stanley and Schaetzl 2011; Schaetzl and Attig 2013).

Eolian depositional processes result in downwind trends of thickness and/or particle size distribution (PSD) in loess deposits that can used to determine wind direction, and therefore, source areas (Smith 1942; Fehrenbacher, White, Beavers et al. 1965; Putman et al. 1988; Johnson and Follmer 1989; Mason 2001; Stanley and Schaetzl 2011; Luehmann et al. 2013). Additionally, other loess properties e.g.., chemical composition, mineralogy, and magnetic susceptibility, have been used to determine the source area and/or the provenance of the sediment (Ruhe and Olson 1980; Grimley et al. 1998; Mason and Jacobs 1998; Aleinikoff et al. 1999; Grimley 2000; Muhs and Bettis 2000; Schaetzl and Loope 2008; Stanley and Schaetzl 2011).

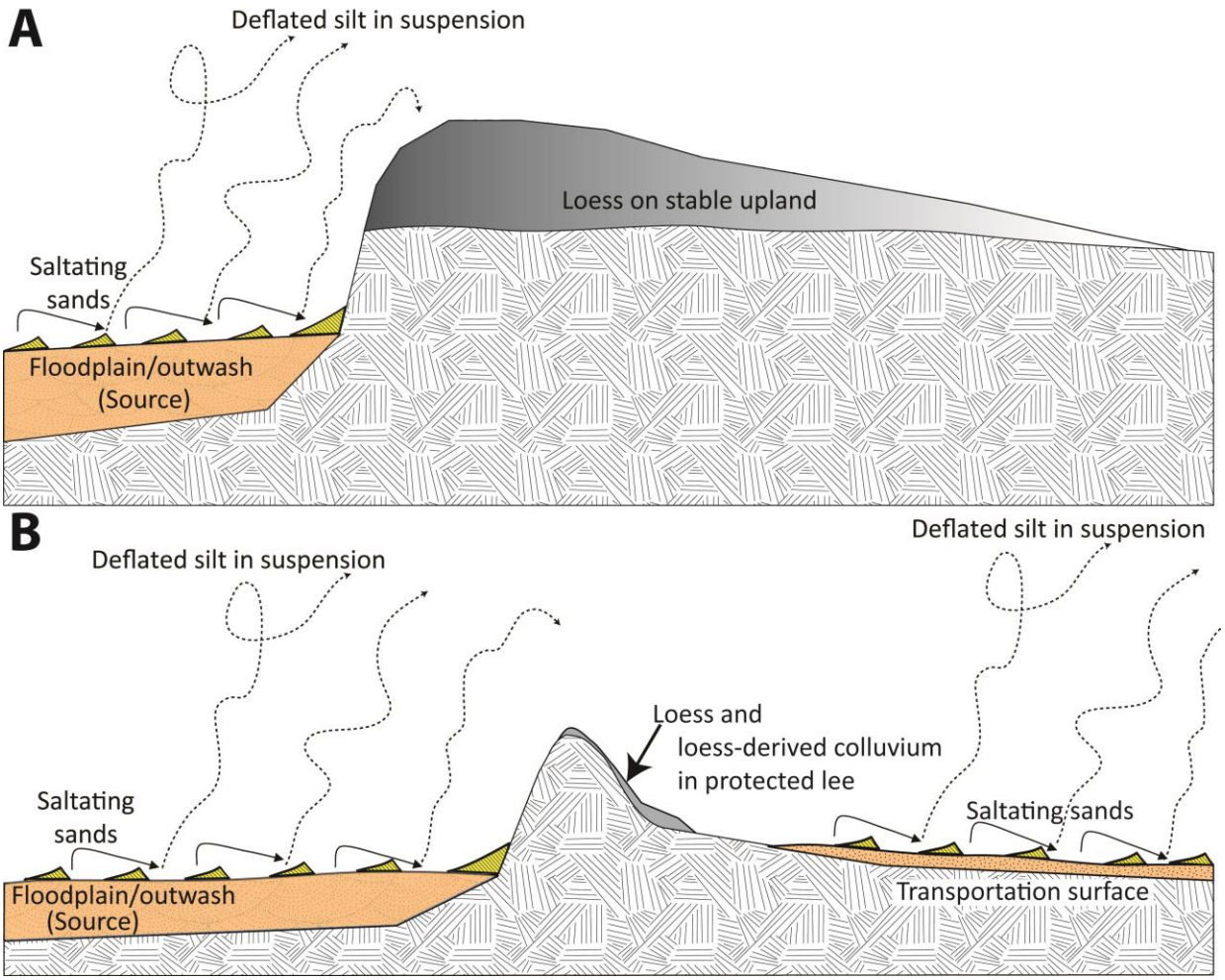


**Figure 2.1:** Diagrams of loess distribution/deposit models that illustrate the interaction of eolian processes with topography. **A:** The Midwestern model of loess distribution where large river valleys carrying sediment-rich meltwater from the Laurentide Ice Sheet are interpreted or demonstrated to be source areas for wedge-shaped loess deposits downwind. During times of low flow, strong winds deflate the outwash/alluvium. Eolian processes separate the sediment due to size fractions with fine and medium sand saltating along the surface, potentially forming dunes and finer grained sediment carried in suspension to be deposited downwind. **B.** Transportation surface model where a relatively low-relief surface allows saltating sand to migrate across the surface. Fine silt and clay carried in suspension is re-entrained by strong winds and saltating sands until a topographic barrier hinders sand migration allowing fine sediment carried in suspension to remain deposited in protected lee locations, and perhaps on summits, if broad/stable enough. Orange = Areas subject to blowing sand; yellow = active sand dunes; gray tones = loess. (After Tsoar and Pye 1987; Mason et al. 1999; Leuhmann et al. 2013).

In Wisconsin, the thickest total accumulations of loess are adjacent to the Mississippi River (Figure 2.2), where they are typically 10-12 m thick (Hole 1950 (reprinted 1968); Leigh and Knox 1994) and the loess tends to systematically thin to <1m toward the east over a distance of 40 km (Leigh and Knox 1994). Yet, relatively thick loess also occurs in south central Wisconsin that is separated from the thick loess deposits adjacent to the Mississippi River Valley by large areas with little to no discrete loess accumulation (Hole 1950 (reprinted 1968); Jacobs et al. 2011). Jacobs et al. (2011) proposed at least part of the relatively thick loess in south central Wisconsin was sourced from the Mississippi Valley region and was re-entrained southeastward across the Central Sands region, which likely acted as a surface of transport based on thickness and PSD trends as well as clay and silt mineralogy comparisons with potential source areas. Schaetzl (2012) questioned these conclusions based on kriged maps of particle size data and the lack of obvious dune fields over the majority of the Central Sands region, and instead favored a more local loess source, namely the Glacial Lake Oshkosh basin. However, the dismissal of an eolian sand mantle covering much of the Central Sand Plain is unwarranted based only on the lack of obvious dune fields. Low-relief coversands and sand sheets (also referred to as sandy loess) are widely recognized eolian features associated with periglacial conditions during the Late Pleistocene across Europe (Catt 1977; Ruegg et al. 1983; Koster 1988; Schwan 1988, 1991; Kasse 1997; Bateman and Huissteden 1999; Kasse 2002); but have received little attention in North America (Lea and Waythomas 1990; Markewich et al. 2009).

In this chapter I use particle size, silt mineralogy, and silt geochemistry data, in combination with mapping and statistical analysis to test the hypothesis that eolian processes are primarily responsible for the characteristics of the surficial sediment mantle in central Jackson County and to identify any evidence for alternative hypotheses attributing that mantle to periglacial hillslope processes or bioturbation and slopewash. The relative contribution of eolian processes to formation of the surficial mantle in the study area has important implications for a hypothesis on loess sources and transport paths in Wisconsin that was proposed by Jacobs et al. (2011).

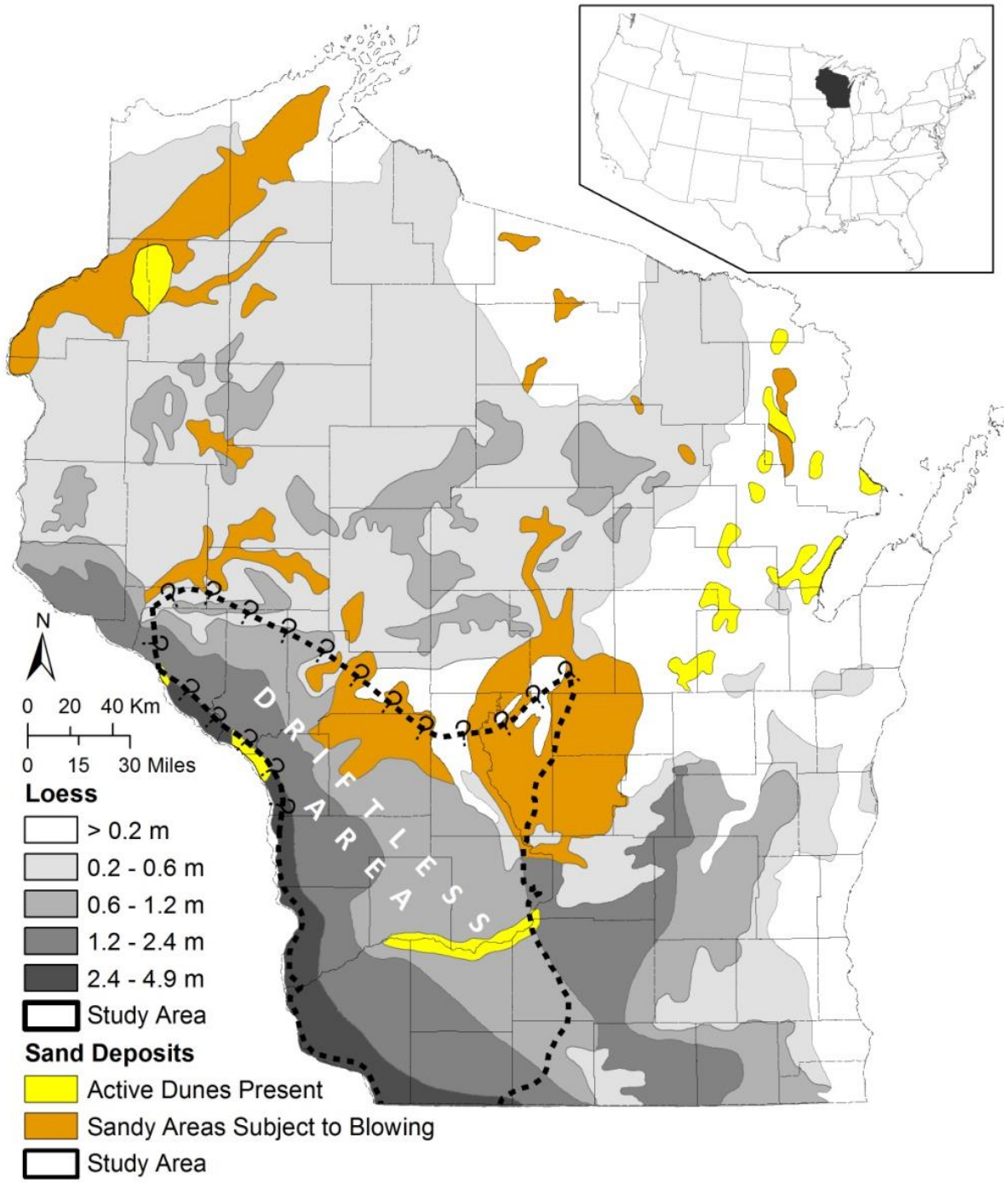


**Figure 2.2:** Map of loess and sand deposits in Wisconsin. Loess is shown in gray tones where darker = thicker. White areas represent surfaces where loess accumulation is less than 20 cm or absent. Yellow areas signify areas of active dunes; whereas orange areas signify sandy areas that are subject to eolian activity. After Hole 1950.

Central Jackson County, within the northwest part of the Central Sand Plain presents an excellent opportunity to test the hypothesis that eolian processes played a key role in forming the sandy surficial mantle of the region. First, this sand-mantled landscape is generally low-relief, but contains prominent, isolated bedrock ridges which may have served to trap enough saltating sand to protect small areas of dust accumulation on their lee sides. Second, LiDAR-based digital elevation models are now available for the surrounding counties (Monroe and Juneau), providing high resolution topographic data for similar landscapes. If the results support the hypothesized role of eolian processes in this landscape, this will also provide additional support for the Jacobs et al. (2011) hypothesis that the Central Sands region acted as a surface of transport allowing distantly sourced loess to reach south-central Wisconsin.

## *Background*

Until recently, the Midwestern conceptual model of loess dispersion, linking loess deposits to broad river valleys that carried meltwater and sediment from the Laurentide Ice Sheet (LIS), has been a dominant explanation for loess deposits in the Midwest (Smith 1942; Snowden and Priddy 1968; Ruhe and Olson 1979; Follmer 1996; Mason 2001; Bettis et al. 2003). In this model, glacial ice grinds rock fragments into dominantly silt-sized grains, which are transported, sorted, and deposited as outwash in broad river valleys draining the ice sheet (Smalley 1966, 1975; Ruhe 1983). In times of low flow, sediment from the broad river channels and floodplains can be deflated by prevailing strong winds (Frye et al. 1962; Johnson and Follmer 1989). Deflated sands saltate—bounce—across the floodplain and possibly terrace landscapes and in the process, deflate silt and clay sized particles, which can become re-entrained and carried further downwind. In this model, eolian sand cannot escape the valley walls, allowing silt to remain deposited on higher elevation surfaces downwind. Thus, loess deposits explained by the Midwestern model are thickest immediately adjacent to broad river valleys and thin downwind.

More recently, Mason et al. (1999) expanded a surface roughness theory of eolian transport described by Tsoar and Pye (1987) to take into account changes in landscape relief. In this study, Mason et al. (1999) provided a supplemental approach for loess deposits that are separated from the source area

by a low-relief surface of transport (little, if any net loess accumulation). In this model, sands saltate along this low-relief surface, deflating silt and clay sized particles that become re-entrained and carried further downwind. This process continues until the sand grains fall into a steep sided valley or get trapped against a steep topographic break, e.g., an escarpment, preceding an area of increased relief. Protected from saltating sand grains, the sediment in suspension is deposited, and remains deposited, in downwind areas. In this process, an abrupt boundary between the area of thin and thick loess deposits often coincides with a steep-sided stream valley too small to be a glaciofluvial source (Mason et al. 1999) or on the escarpment/upland itself (Schaetzl and Loope 2008).

## *Materials and Methods*

### Field methods

In order to characterize soil particle size distribution across the study area, to test for spatial patterns consistent with eolian processes, surface soil samples were collected from the Black River eastward with an emphasis on collecting samples from near Wildcat Ridge. General target locations for sample collection was based on a stratified design based on variations in surface texture and soil development (Langton and Simonson 1998), as well as distance from the Black River, and various geomorphic positions and aspects (i.e. leeward and windward) with respect to Wildcat Ridge. A judgmental schema, which may have introduced bias, was used once in the field to place sample locations, for example locations with obvious disturbance (i.e. tree throw and pine plantation furrows) were avoided when possible. In total, 86 surface samples were collected at a depth of 5-10 cm across the general study area using a standard bucket auger. Additional samples were collected in 10 cm depth increments at some sites. Information recorded at each site included: depth of gravels, changes in sediment consolidation, presence and estimation of the character of lamellae and lamina, redox features, and depth to water table, and general comments about the geomorphology and vegetation. The coordinates of each soil sample were also recorded using a Garmin GPS 76 unit.

Seven profiles were excavated for detailed analysis of particle size distribution, clay mineralogy, and pH. General locations for soil profile excavations were targeted prior to fieldwork based on digital soil survey (SSURGO) and elevation data using a stratified sampling method. Targeted locations aimed to represent 1) a relatively isolated windward (west aspect) lower backslope of an unprotected ridge or mound (site W40), 2) a footslope and toe slope from a semi-protected location on the windward side (west aspect) of Wildcat Ridge (W42 and W41), 3) a footslope or lower backslope position located within the Wildcat Ridge complex (R12), 4) a protected footslope on the lee side (east aspect) of Wildcat Ridge (L48), and 5) a less-protected footslope and toeslope on the lee side of Wildcat Ridge (L43 and L44) (Figure 2.3).

Because Wildcat Ridge and other ridges in the area are narrow and have a little (< 30 cm) loose sediment overlying consolidated bedrock, summit and shoulder positions were avoided. Once in the field, five to ten test holes were inspected using a bucket auger within a ~50 $m^2$ area of each target location, making sure to avoid evidence of disturbance. The placement of these test holes may have introduced bias, as a judgmental sampling schema was used to avoid evidence of disturbance and maintain approximately the same context of landscape position and micropotography in an attempt to minimize differences in soil formation factors. This approach was unavoidable, however, given the limited number of points that could be sampled in the time available. Each test hole was numbered and latitude/longitude coordinates were recorded along with qualitative soil characteristic data such as approximate depth to horizons encountered, texture, and coarse fragments. Based on test hole qualitative data, the location deemed to represent a typical soil profile for the target area was selected for soil pit excavations. Soil profiles were excavated, described, and sampled according to NRCS guidelines (Schoeneberger et al. 2002). In addition, one set of samples was also collected in 10 cm increments for particle size comparison to auger data.

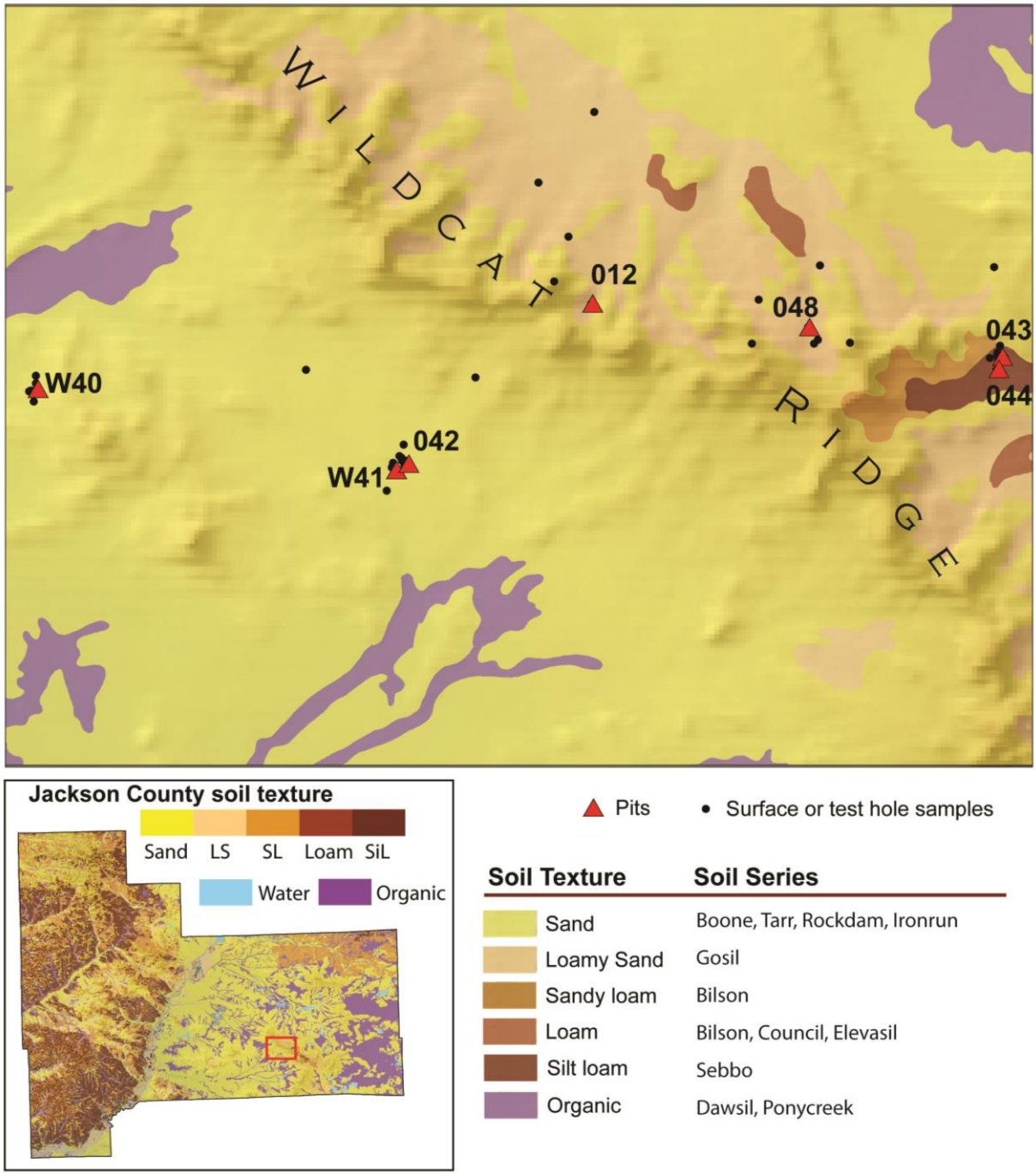


**Figure 2.3:** Map of soil profile locations and SSURGO soils data according to soil texture. Yellow hues represent soils mapped as sands at the surface; hues become increasingly browner hues with an increase of fine texture. Organic soils are shown in purple.

**Particle Size Analysis**

Samples used in pipette analysis were pretreated with 10 mL of 30% $H_2O_2$ and heated to ~60 °C for five hours to remove organic matter. Samples rich in OM were treated with an additional 5-10 mL of 30% $H_2O_2$ and heated to ~60 °C for another five hours. All samples were then heated to 100°C for 20 minutes to destroy unreacted $H_2O_2$. Following OM removal, samples were treated with 10 mL of $(NaPO_3)_{13}{\cdot}Na_2O$ in about 200 mL DI water, and shaken for 10 hours. Sand was separated by wet sieving using a 63 μm mesh before transferring the samples to 1000 mL cylinders for determination of clay content using the method described by (Gee and Bauder 1986).Following pipette analysis, samples were re-agitated in the cylinders and allowed to settle for 24 hr. Approximately 750 ml of clay suspension was then collected for X-ray diffraction (XRD) analysis, from above the depth to which all silt should have settled, based on Stoke's Law. This process was repeated after adding water to bring the volume back up to 1000 mL, until the resulting suspension was clear or light gray in color after 24 hr settling, indicating minimal remaining clay (Grimley 1996). The remaining sediment (2-63 μm) was collected for mineralogical and geochemical analyses.

Fragments of OM not completely destroyed by chemical oxidation ($H_2O_2$ or NaClO) treatment have little effect on pipette data because they weigh so much less than the sand fraction. However in laser diffraction, OM fragments, particularly in surface horizon samples, can be "seen" as larger sediment particle sizes, which can make the data less reproducible and/or skew the particle size distribution even after sonication (Figure 2.4). In Figure 2.4, a chemically treated sample has coarser sand and silt modes because of coarse OM fragments remaining. Notice that the chemically treated samples are different from each other based on whether the coarse OM fragments happened to be captured by the measurement. In both chemically treated samples, the silt fractions are much lower compared to the treatment described below.

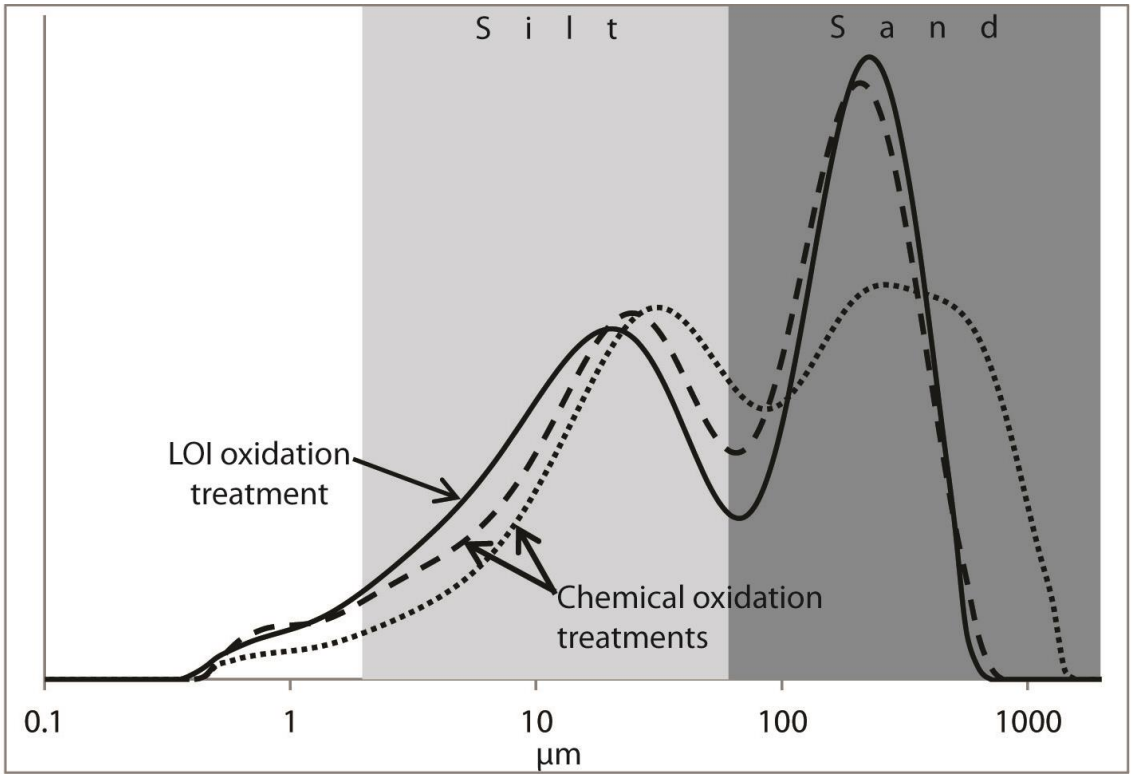


**Figure 2.4:** Laser particle size distributions of samples L44 EB after repeated sonication treatments at 6 minute intervals vs. chemical oxidation treatments of $H_2O_2$ or CaClO. LOI oxidation produces more fine silt with a finer silt mode and slightly more very fine clay compared to chemical oxidation treatments.

In order to remove coarse organic matter for laser particle size analysis, all samples were ignited at 360°C for 2 hours (Belby 2009). Particle size distributions of samples were analyzed using a Malvern Laser Diffractor (Malvern Instruments Ltd., Malvern, UK) after being dispersed with 10 ml NaPO4 and sonicated for 6 minutes. To ensure disaggregation and full dispersion, samples were repeatedly sonicated and measured at 6 minute increments until a reproducible pattern was observed (Figure 2.5). Because the sample size needed for PSD laser analysis is so small, duplicate samples were measured using the same protocol. To minimize sample bias, the final measurements for the original and duplicate samples were averaged. Thus, the final measurements used in analysis represent the average of two PSD measurements.

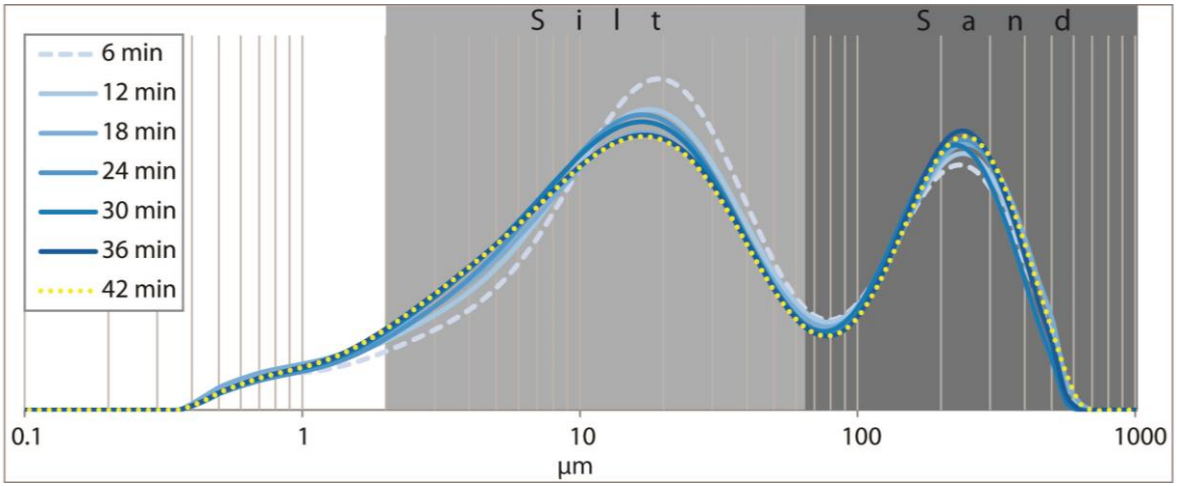


**Figure 2.5:** Laser particle size distributions of sample L44 EB after repeated sonication treatments at 6 minute intervals. Notice the first measurement shows a silt mode ~20 µm, but after repeated sonications, the silt mode shifts to ~17 µm. Very fine silt (2-10 µm) and clay amounts increase with repeated sonication treatments at the expense of coarse silt and sand microaggregates.

## Silt Mineralogy

Silt mineralogy was analyzed using UW-Whitewater's RigakuMiniFlex X ray diffractometer employing Cu Kα radiation. Silt fractions (2-63 µm) were ground using a McCrone Micronising Mill for 2.5 min with water prior to XRD analysis to reduce particle sizes to <20 µm, to produce a more homogeneous sample. Randomly oriented powder samples were analyzed within the 25–31.5 2θ range with a scan speed of 1° per minute and a 0.02 step. After adjusting the resulting diffractograms by aligning the quartz peak to 3.34 Å, peak intensities (counts per second) and background values for quartz (3.34 Å), K-feldspar (microcline 3.24 Å), and plagioclase (albite 3.19 Å) were quantified by JADE (Materials Data, Inc.). Net peak intensities were calculated for each mineral by subtracting the background value from the peak intensity value. Net peak intensities were converted to mineral percentages using peak intensity factors determined by Grimley (1996, 2000). Feldspar percentages were normalized to quartz percentages creating P/Q and K/Q ratios as an indicator of the relative plagioclase and K-feldspar content in each sample.

**Energy Dispersive X-Ray Florescence (eXRF)**

Major and trace element contents in micronized silt samples were measured using UW-Whitewater's hand-held Tracer IV-SD (Bruker Corporation) X-ray fluorescence (XRF) instrument, with a Soil and GeoQuantTr method configuration for geochemical data. Each measurement ran for 120s; three measurements were performed on each sample, shaking between measurements. The three measurement values and errors were averaged, resulting in a single value and measurement error estimate for each sample.

**Mapping methods**

Surface texture and soil development maps were created using NRCS SSURGO data and soil series descriptions specific to Jackson County, Wisconsin (Langton and Simonson 1998). At the surface, sand is the dominant soil texture covering a large part of the study area east of the Black River; organic material blankets many of the lowest areas (Langton and Simonson 1998) (Figure 1.2).

Texture maps using primary data from this study were made by joining laser particle size data to the spatial coordinates of corresponding soil samples in ArcMap 10.2 software (ESRI, Redlands, CA). Particle size contents were classified into three or four classes based on histogram clusters for each fraction using the same graduated color scheme; yellows representing the least contents and dark browns representing the highest contents.

**Principle Component Analysis (PCA)**

Principle component analysis (PCA) reduces a large number of variables to a smaller set of independent variables that represent much of the observed variation among samples. The results can be interpreted in terms of major axes of variation in the sample set. Percentage data that sum to 100% (e.g. particle size fractions) were logratio transformed as recommended by Kucera and Malmgren (1998) prior to PCA analysis, by taking the log of the sample divided by the geometric mean, expressed in an equation as:

$$S_{tr} = ln\left(\frac{S_1}{(S_1 * S_2 * \ldots S_n)^{\frac{1}{n}}}\right)$$

where $S_{tr}$ is the transformed grain size fraction value, $S_1$ is the percentage of the grain size fraction. PCA was performed using R 3.1.1 (The R Foundation for Statistical Computing) using the PRINCOMP module with COR=TRUE in order to scale each variable similarly.

## *Results*

### Regional evidence for eolian activity

Topography in Jackson County can be categorized into three basic types: 1) open, low-relief terrain, 2) moderate-relief terrain with bedrock knobs, and 3) bedrock ridge topography. Using the same 30m DEM, these three types of terrain can also be found to the south, in Monroe County, and to the east, in Juneau County, both of which have high resolution LiDAR data available (Figure 2.6-Figure 2.8).

In areas of open, low-relief terrain, numerous parabolic dunes are apparent using the LiDAR data (Figure 2.6), but are not apparent on the 30m DEM. The height of the parabolic dunes is often relatively low (1.4 to 2 m), but can exceed 5 m in some instances. Small dunes, which are typically low-relief (< 2 m) tend to have long axes between 0.1 and 0.6 km in length and are oriented northwest to southeast. Larger, elongated parabolic dunes can extend >1.8 km in length. In low areas often mapped as Dawson peat or Loxley mucky peat, dune forms cannot be identified. It is likely eolian sand was trapped as a sand sheet in these wet areas, preventing dune formation.

In this study, moderate-relief topography includes areas where the low-relief topography gives way to bedrock knobs (e.g., Figure 2.7); numerous dune forms are apparent in these areas in Monroe and Juneau counties. For example, small linear accumulations of eolian sand can be found on terrace edges, particularly on the southeastern side of the stream. As the terraces step up to higher topography these accumulations of eolian sand on terrace edges transition to small, poorly defined parabolic dunes (Figure 2.7 C,E). Small, poorly formed parabolic dunes typically have 0.5-1 m relief and are approximately 50

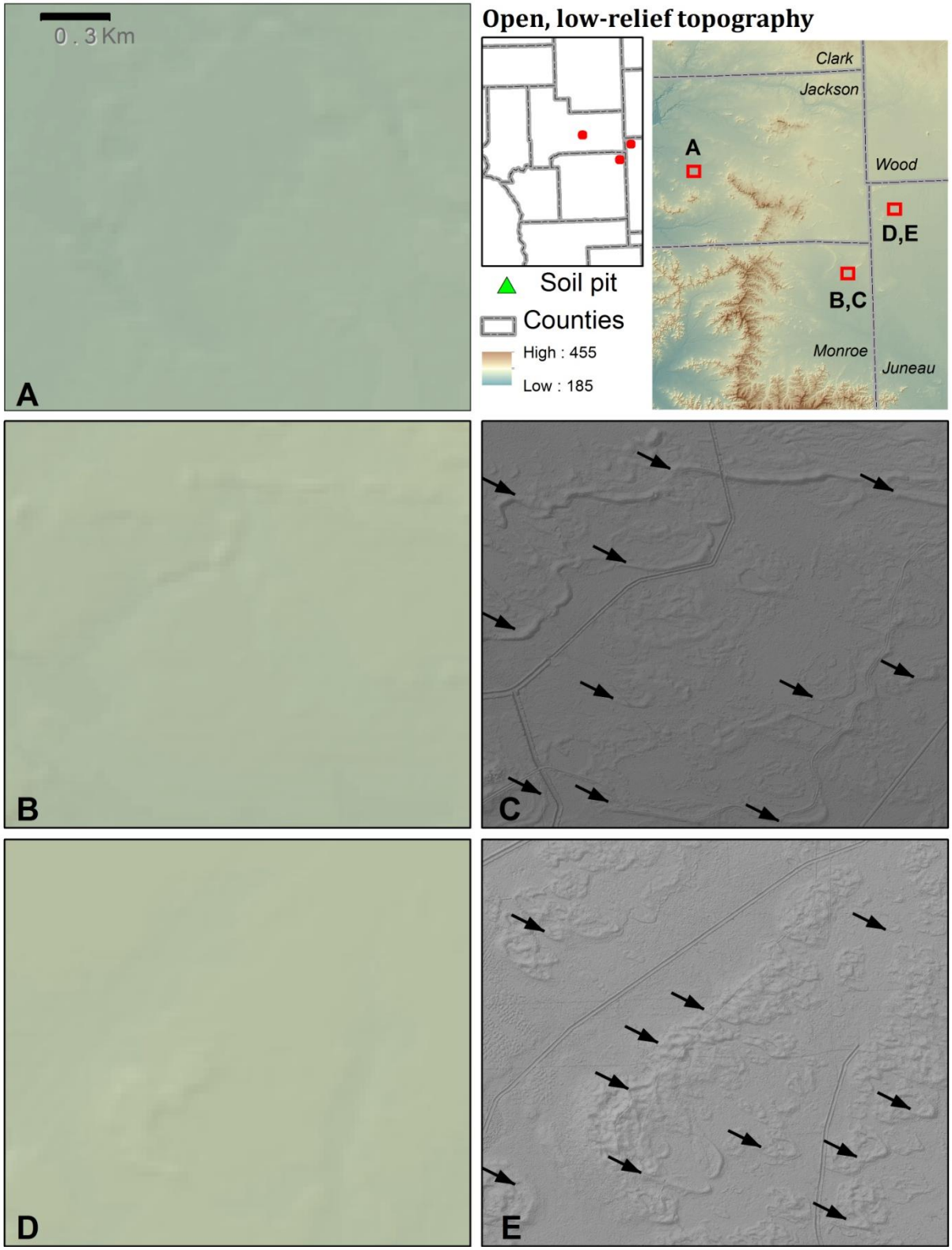


**Figure 2.6:** Maps comparing open, low-relief topography in Jackson County with similar topography in Monroe and Juneau Counties. Scale is 1:20,000 for all maps. Arrows point to arms of parabolic dunes and indicate paleowind direction. **A:** 30m DEM shaded relief of Jackson County. **B:** 30m DEM shaded relief of Monroe County. **C:** LiDAR shaded relief of the same area shown in B. **D:** 30m DEM shaded relief of Juneau County. **E:** LiDAR shaded relief of the same area shown in D.

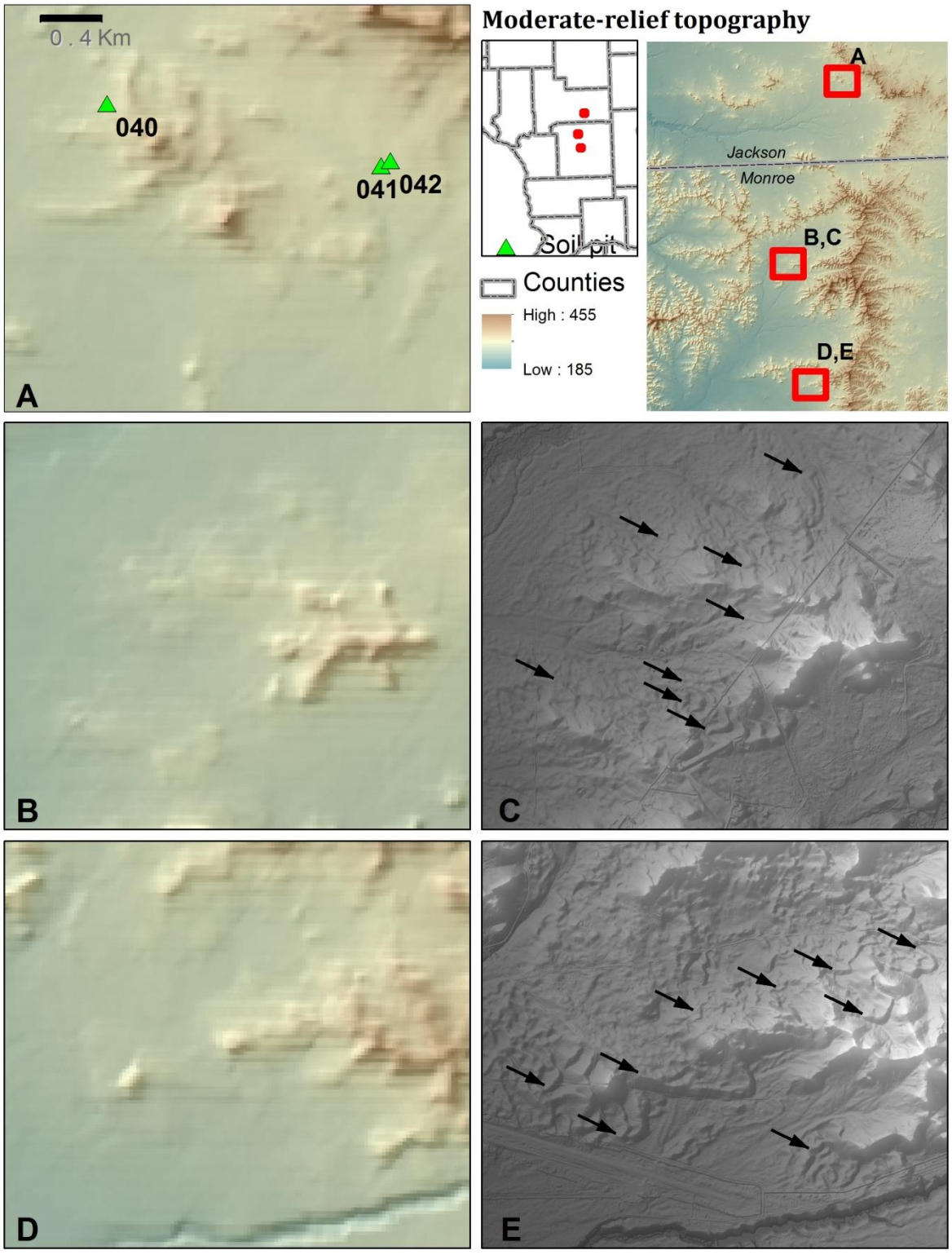


**Figure 2.7:** Maps comparing moderate bedrock-controlled topography in Jackson County with similar topography in Monroe and Juneau Counties. Scale is 1:20,000 for all maps. Arrows point to arms of parabolic dunes and indicate paleowind direction. **A:** 30m DEM shaded relief of Jackson County. **B:** 30m DEM shaded relief of Monroe County. **C:** LiDAR shaded relief of the same area shown in B. **D:** 30m DEM shaded relief of Juneau County. **E:** LiDAR shaded relief of the same area shown in D.

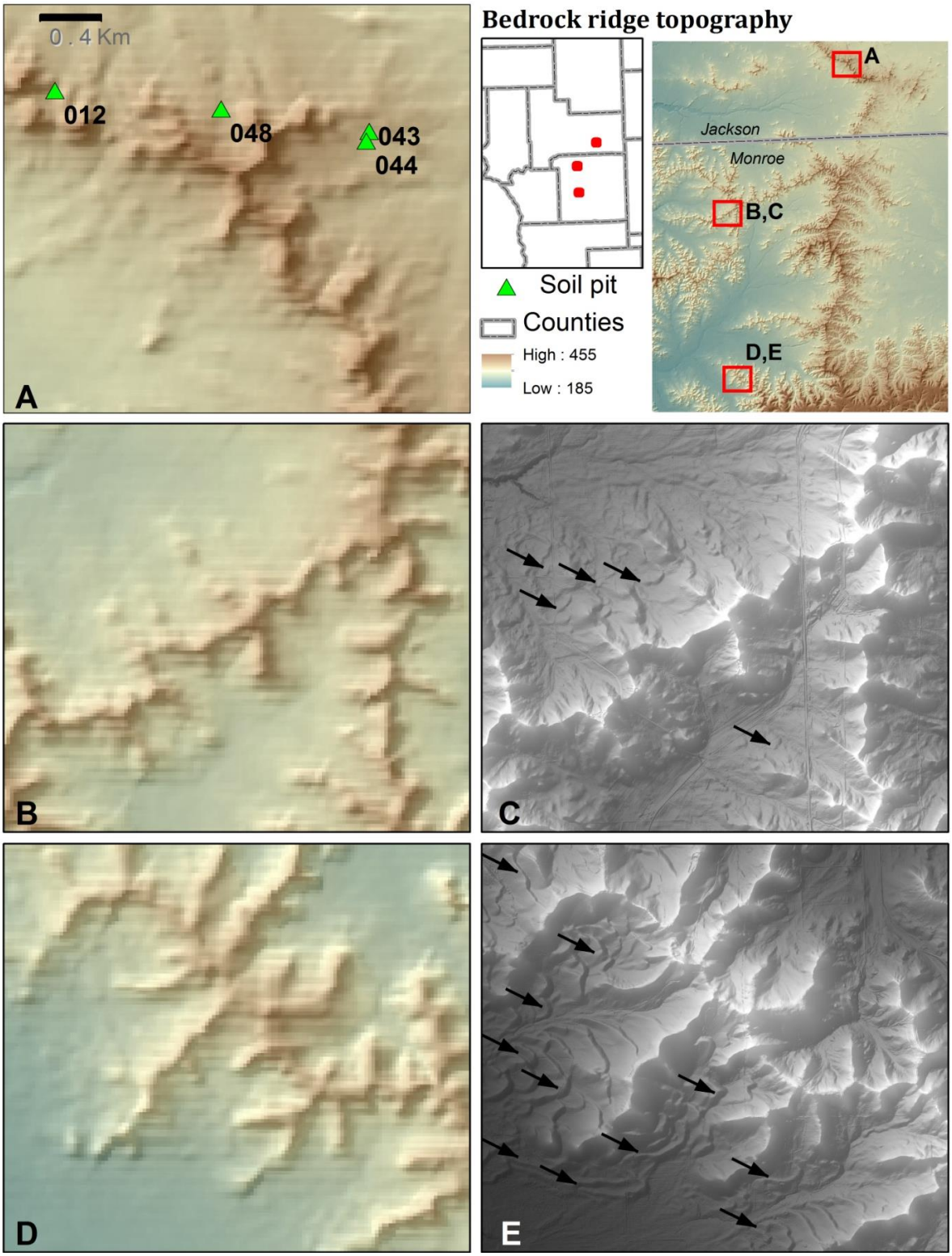


**Figure 2.8:** Maps comparing bedrock ridge topography in Jackson County with similar topography in Monroe and Juneau Counties. Scale is 1:20,000 for all maps. Arrows point to arms of parabolic dunes and indicate paleowind direction. **A:** 30m DEM shaded relief of Jackson County. **B:** 30m DEM shaded relief of Monroe County. **C:** LiDAR shaded relief of the same area shown in B. **D:** 30m DEM shaded relief of Juneau County. **E:** LiDAR shaded relief of the same area shown in D.

m in diameter and have a hummocky appearance. Farther from the stream on higher land, the small parabolic dunes transition to moderately- and well-defined parabolic dunes, which are typically < 3.5 m in relief and < 150 m wide. However, the southern arm of the large parabolic dune in the center of Figure 2.7E has a relief of ~12 m. Notice that only the largest dunes show up as slight relief on the 30 m DEM; even then, the coarse resolution obscures the dune form. The transition from transverse to parabolic dunes may suggest a transition from more abundant sand to more abundant vegetation in a semi-arid environment, but more likely reflects modifications to the dunes during the tail end of eolian activity.

Areas with bedrock ridge topography in Monroe and Juneau counties also have dune forms revealed by LiDAR data (Figure 2.8). In areas slightly protected from westerly-northwesterly winds, poorly formed parabolic dunes with 0.5 – 3 m of relief and diameters of 50-100 m transition to larger and better formed parabolic dunes climbing up the windward side of a bedrock ridge (Figure 2.8C). In less protected areas, parabolic dunes are well-formed and a prominent feature of the landscape (Figure 2.8E). In these cases, the parabolic dunes have 3.5 – 5 m of relief, and are between 150 and 350 m long, although some can reach up to 1 km long along open, low relief topography. Notice in Figure 2.7E, parabolic dunes breach the bedrock ridge and continue on the lower slope positions on the southeastern aspect. Only lee aspects that are most protected from northwesterly and westerly winds remain free of dune forms.

Based on LiDAR data from similar topographic settings in nearby Monroe and Juneau Counties, it is reasonable to expect that much of Jackson County has been similarly affected by eolian sand transport and dune formation. Therefore, much of central and eastern Jackson County likely acted as a surface of transport for migrating sands originating from the surrounding landscape, the Black River, and potentially from farther west. Dunes in Monroe, Juneau, and likely Jackson Counties are typically lower in relief than the parabolic dunes in the Glacial Lake Wisconsin basin that were the focus of Rawling et al. (2008), which suggests sand availability was more limited in the study area during the time of intense eolian activity (Lea and Waythomas 1990). Sand supply could have been limited in the study area by seasonal environmental conditions such as high groundwater tables, snow cover, permafrost depth, and/or

vegetation cover (Schwan 1988; Lea and Waythomas 1990), particularly in low-relief, open areas of Jackson, Juneau, and Monroe Counties.

### Particle size data for surface samples

The texture class of 80 surface samples collected in central Jackson County ranges from sand to silt loam, of which 39 have loamy sand texture and 27 have a sandy loam texture (Figure 2.9). Most of the samples with finer textures (silt loams and sandy loams) were collected on the eastern slopes of Wildcat Ridge (Figure 2.9). The few exceptions are samples 20, 23, 34, 41-2, 41-3, 41-5, and 41-7. Sample 20 was collected within a red pine plantation with prominent disturbance (30 cm furrows). The other five samples were collected from locations where the water table was found within 20 cm of the surface. Due to the mucky nature of the surface samples and dark color after LOI, it is likely that organic matter (i.e. charcoal fragments) contributes much of the apparent silt content in these samples. Not only are the silt modes coarser compared to less organic-rich samples (Figure 2.10), but organic-rich samples had to be sonicated twice as long, sometimes > 1hr, before the laser diffraction pattern stabilized.

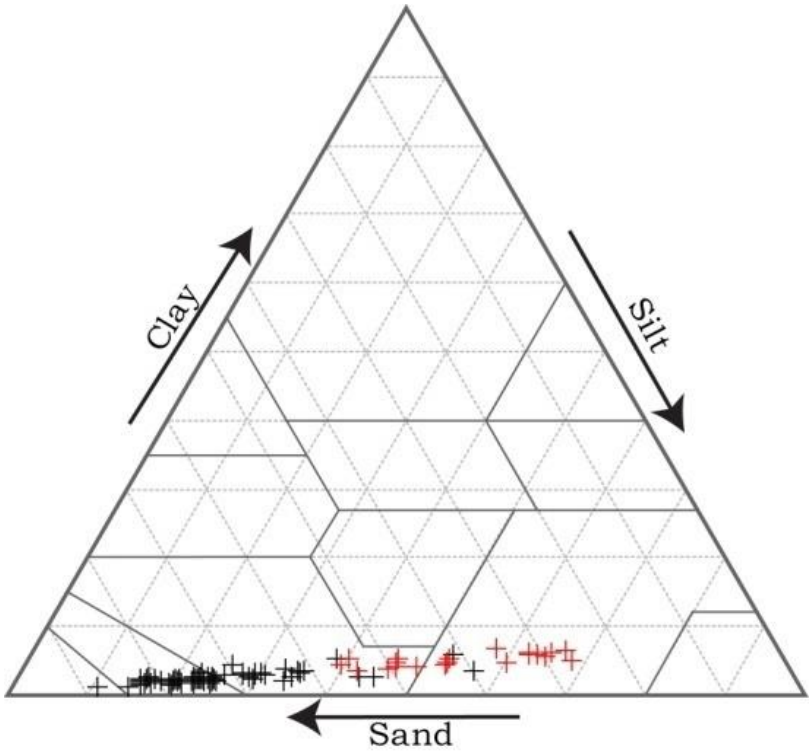


**Figure 2.9:** Texture of 80 surface samples collected in central Jackson County, WI. Samples shown in red were collected on the lee side of Wildcat Ridge.

Detailed laser analysis reveals a bimodal PSD for surface samples, which may also be used to further discriminate outliers. Except for outlier samples discussed above, the silt mode for surface samples ranges between 11 and 22

µm (Figure 2.11); the mean silt mode is 17.3 µm and the median is 17.8 µm (Table 2.1). The sand mode is more variable, ranging between 224 and 502 µm, with a mean of 344.9 µm and a median of 355.7µm (Table 2.1). Medium sand contents are likely derived locally from either the Mt. Simon Sandstone (mean sand mode: 315 µm; median grain size: 277 µm (Distefano 1973)) or the Wonowoc Sandstone (median grain size: 207 (Emrich 1966)) (Table 1).

PSD modes can help discriminate subtle lithologic discontinuities because the modes reflect the depositional process (Schaetzl and Luehmann 2013). Likewise, detailed PSDs can be used to identify outliers that should be excluded from further sedimentological analysis. For example, surface samples across the study area are dominantly bimodal; however, samples collected at sites 34 and 46 are clear outliers since they are trimodal, with an extra mode of approximately 75 µm (Figure 2.11). Samples collected from site 046 were located within an obvious colluvial apron extending from a very steep

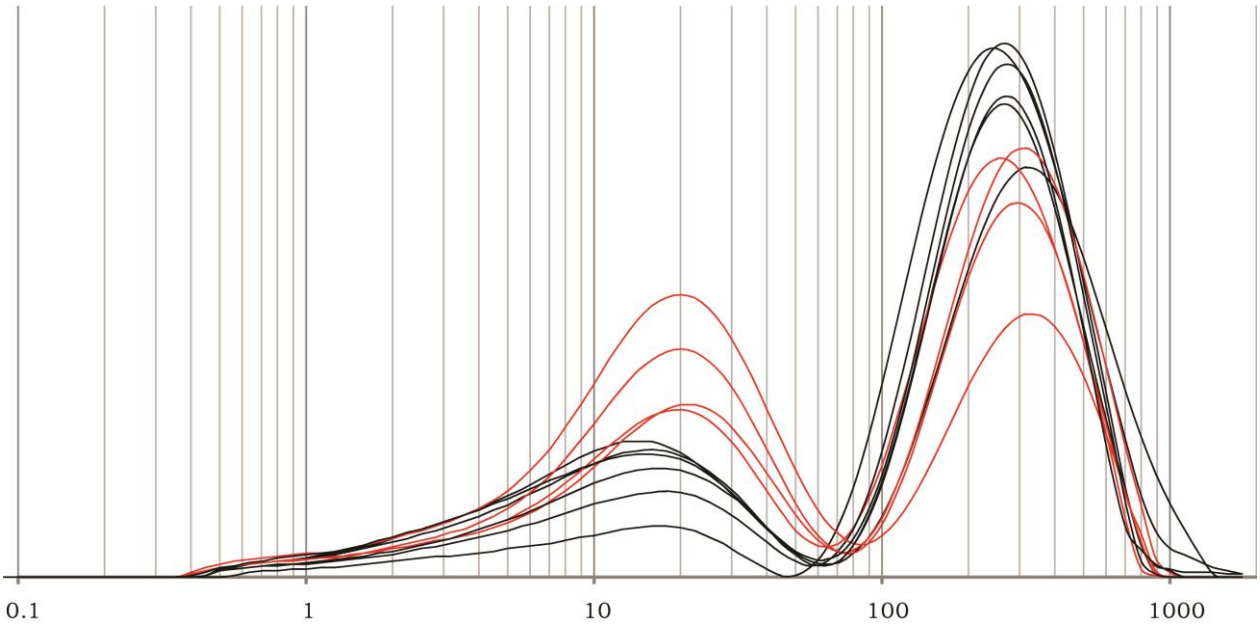


**Figure 2.10:** Laser particle size data for surface samples collected near site W41, which is mapped as Ironrun-Ponycreek complex in this heterogeneous soilscape. The samples with abnormally high coarse silt contents are shown in red are poorly drained Hummaqueptic Psamments (Ponycreek mucks); whereas samples shown in black are Typic Endoaquods (Ironrun sands) with less organic matter.

section of Wildcat Ridge, capped by Lone Rock sandstone. Lone Rock sandstones tend to be finer textured with a mean between 125 and 175 µm (Table 1). The fine sand mode for sample 34 cannot be explained. Based on the low sand mode, silt mode in the fine-medium silt range, relatively high clay

content, and abundant round feldspar and quartz granules in the upper 30 cm, the parent material may be an isolated outwash remnant or a silty, fine sand bed within the upper Mount Simon Sandstone.

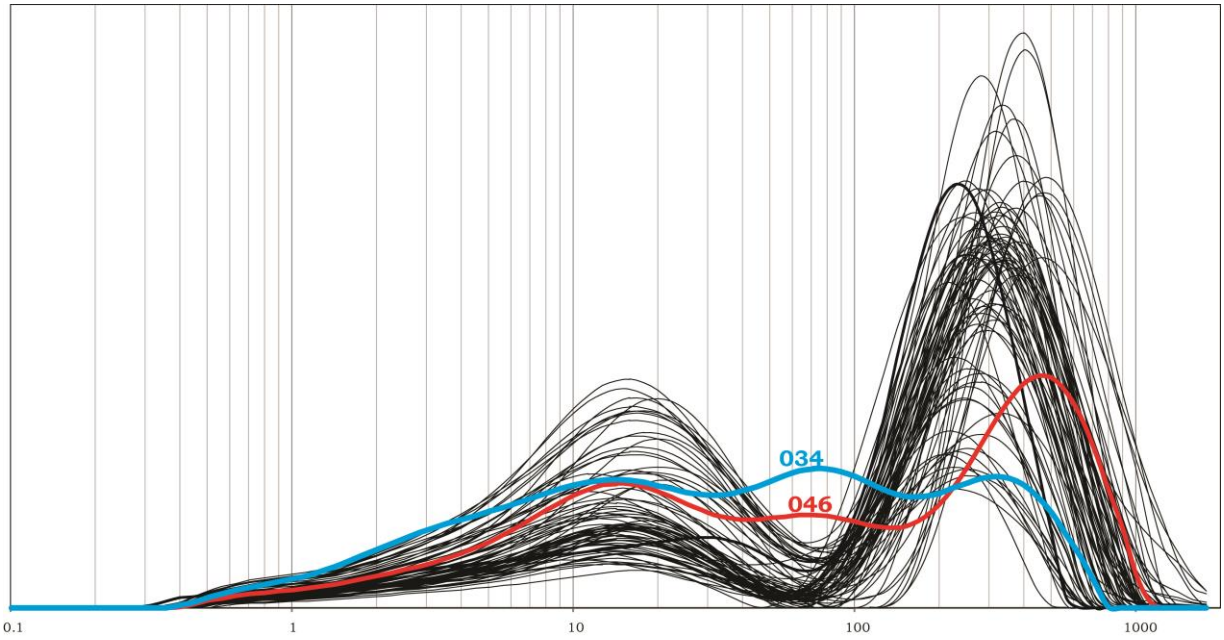


**Figure 2.11:** Detailed laser particle size distribution of all 80 surface samples collected across central Jackson County, WI. Site 034, shown in blue, and site 046, shown in red, have prominent trimodal distributions and are clear outliers compared to other surface samples.

**Table 2.1:** Silt and sand modes for surface samples collected across central Jackson County, WI.

| Sample | Depth (cm) | Silt mode (µm) | Sand mode (µm) | Sample | Depth (cm) | Silt mode (µm) | Sand mode (µm) | Sample | Depth (cm) | Silt mode (µm) | Sand mode (µm) | Sample | Depth (cm) | Silt mode (µm) | Sand mode (µm) |
|---|---|---|---|---|---|---|---|---|---|---|---|---|---|---|---|
| 001 | 0-9 | 15.9 | 399.1 | 027 | 5-10 | 15.9 | 399.1 | W40-7 | 5-10 | 17.8 | 355.7 | L43 | 5-10 | 20.0 | 282.5 |
| 001B | 4-13 | 14.2 | 563.7 | 028 | 5-10 | 14.2 | 447.7 | W40-8 | 5-10 | 20.0 | 355.7 | L43-1 | 5-10 | 20.0 | 224.4 |
| 002 | 5-1 | 15.9 | 447.7 | 029 | 5-10 | 15.9 | 399.1 | W41 | 5-10 | 17.8 | 282.5 | L43-3 | 5-10 | 17.8 | 282.5 |
| 006 | 5-8 | 15.9 | 251.8 | 030 | 5-10 | 14.2 | 502.4 | W41-1 | 5-10 | 15.9 | 355.7 | L43-4 | 5-10 | 20.0 | 317.0 |
| 008 | 5-10 | 17.8 | 355.7 | 031 | 5-10 | 12.6 | 502.4 | W41-2 | 5-10 | 22.4 | 282.5 | L43-5 | 5-10 | 17.8 | 317.0 |
| 010 | 5-10 | 14.2 | 317.0 | 032 | 5-10 | 11.2 | 447.7 | W41-3 | 5-10 | 20.0 | 282.5 | L43-6a | 5-10 | 12.6 | 317.0 |
| 011 | 5-10 | 14.2 | 399.1 | 033 | 5-10 | 15.9 | 447.7 | W41-4 | 5-10 | 20.0 | 317.0 | L43-6b | 5-10 | 20.0 | 251.8 |
| R12 | 0-5 | 22.4 | 251.8 | 034 | 5-10 | 15.9 | 355.7 | W41-5 | 5-10 | 22.4 | 355.7 | L43-7 | 5-10 | 20.0 | 282.5 |
| 013 | 5-10 | 15.9 | 355.7 | 035 | 5-10 | 14.2 | 355.7 | W41-6 | 5-10 | 22.4 | 355.7 | L44 | 5-10 | 17.8 | 282.5 |
| 014 | 5-10 | 15.9 | 355.7 | 036 | 5-10 | 15.9 | 502.4 | W41-7 | 5-10 | 22.4 | 317.0 | L44-1 | 5-10 | 20.0 | 282.5 |
| 015 | 5-10 | 17.8 | 317.0 | 037 | 5-10 | 15.9 | 355.7 | W41-8a | 5-10 | 17.8 | 317.0 | L44-2 | 5-10 | 17.8 | 251.8 |
| 017 | 5-10 | 17.8 | 282.5 | 038 | 5-10 | 15.9 | 399.1 | W41-9b | 5-10 | 17.8 | 317.0 | L44-3 | 5-10 | 20.0 | 282.5 |
| 018 | 5-10 | 17.8 | 282.5 | 039 | 5-10 | 17.8 | 355.7 | W42 | 5-10 | 12.6 | 447.7 | L44-4 | 5-10 | 17.8 | 251.8 |
| 019 | 5-10 | 15.9 | 317.0 | W40 | 5-10 | 15.9 | 317.0 | W42-1 | 5-10 | 15.9 | 355.7 | L44-5 | 5-10 | 17.8 | 251.8 |
| 020 | 5-10 | 15.9 | 317.0 | W40-1 | 5-10 | 15.9 | 355.7 | W42-2 | 5-10 | 15.9 | 355.7 | 045 | 5-10 | 17.8 | 317.0 |
| 021 | 5-10 | 17.8 | 282.5 | W40-2 | 5-10 | 17.8 | 399.1 | W42-3 | 5-10 | 14.2 | 399.1 | 046 | 5-10 | 15.9 | 502.4 |
| 022 | 5-10 | 15.9 | 317.0 | W40-3 | 5-10 | 17.8 | 282.5 | W42-4 | 5-10 | 15.9 | 355.7 | 047 | 5-10 | 15.9 | 317.0 |
| 023 | 5-10 | 17.8 | 355.7 | W40-4 | 5-10 | 20.0 | 317.0 | W42-5 | 5-10 | 15.9 | 317.0 | 049 | 5-10 | 17.8 | 355.7 |
| 025 | 5-10 | 15.9 | 399.1 | W40-5 | 5-10 | 17.8 | 317.0 | W42-7 | 5-10 | 14.2 | 355.7 | 050 | 5-10 | 31.7 | 251.8 |
| 026 | 5-10 | 17.8 | 399.1 | W40-6 | 5-10 | 17.8 | 355.7 | W42-9 | 5-10 | 12.6 | 355.7 | 051 | 5-10 | 17.8 | 355.7 |
| | | | | | | | | | | | | | ***Mean*** | ***17.3*** | ***344.9*** |
| | | | | | | | | | | | | | ***Median*** | ***17.8*** | ***355.7*** |
| | | | | | | | | | | | | | ***High*** | ***22.4*** | ***502.4*** |
| | | | | | | | | | | | | | ***Low*** | ***11.2*** | ***224.4*** |

**Spatial patterns of surface sample particle size**

Analysis of 75 surface samples reveals spatial patterns with respect to particle size distribution (Figure 2.12). Samples with the coarsest median grain sizes (350-425 µm) are dominantly located in areas of low-relief terrain, especially near the Black River (Figure 2.12A). Samples with finer medians, i.e., more contents of finer materials tend to be located near Wildcat Ridge (area of detailed inset maps in Figure 2.12). Samples collected west of Wildcat Ridge have median grain sizes that range between 150 and 250 µm, whereas samples with median grain sizes finer than 150 µm are only found immediately east of Wildcat Ridge. Although the sediment is mostly rounded quartz grains and is likely derived from local bedrock sources, it is unlikely that hillslope redistribution was the primary depositional process because relatively high concentrations of particles finer than 125µm do not occur equally on all aspects of Wildcat Ridge. Instead, relatively high contents of fractions finer than 125 µm were likely deposited on the eastern, lee side of Wildcat Ridge by eolian processes.

Silt to medium sand ratio data show similar patterns as median data (Figure 2.12B). The underlying Cambrian sandstone formations are probably the dominant source of these materials; however, the underlying sandstone lithologies cannot explain the surface texture patterns within central Jackson County. Finer surface textures (sandy loams to silt loams) do not consistently overlie the finer-grained Eau Claire or Lone Rock Formations, and therefore where they overlie the Mt. Simon Formation they are likely not a result of finer beds in that unit (Figure 1.2, Figure 2.12). Samples with the least amount of silt tend to be in areas of open, low-relief terrain. Slightly elevated silt contents can be found in samples immediately adjacent to the Black River, likely as a result of floodplain sedimentation or eolian reworking of floodplain deposits. The majority of samples with moderate to high silt to medium sand ratios tend to cluster near Wildcat Ridge. Most importantly, samples with the most silt are all located immediately east of Wildcat Ridge, which is strongly suggestive of eolian processes in which a topographic barrier that prevents the continuation of saltating sands across the landscape allows for silt to be deposited immediately downwind.

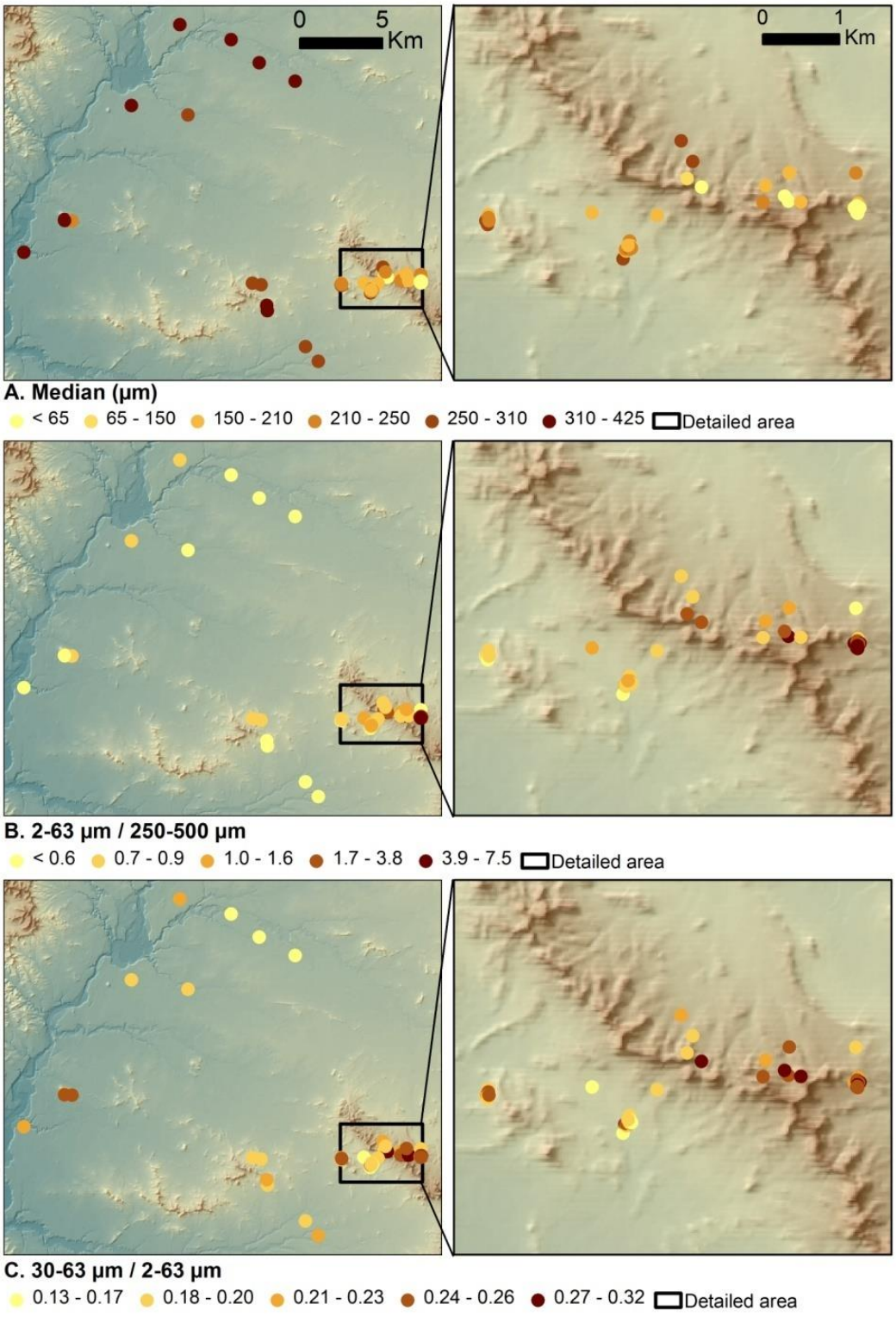


**Figure 2.12:** Map of particle size data from surface samples collected across central Jackson County, WI. Yellow represents lowest values and darker browns represent higher values. Note content amounts differ for each size fraction mapped. A: median grain size (µm); B: ratio of silt (2-63 µm) to medium sand (250-500 µm); C: ratio of coarse silt (30-63 µm) to total silt.

The ratio of coarse silt (30 – 63 μm) to total silt shows more complicated patterns. Figure 2.12C shows increasing coarse silt from north to south along the Black River. Although this trend could be associated with the characteristics of the bedrock, the more likely explanation is related to the regional topography west and northwest of the Black River. North and north-northwest of the study area, the landscape is sandy and relatively low relief. Stanley and Schaetzl (2011) documented that this landscape acted as a surface of transport for the central-Wisconsin loess sheet. In this scenario, silt deposited on this landscape was likely re-entrained by sand migrating across this low relief surface. Towards the south, particularly beginning in the north-central part of the study area, the topography immediately west and northwest of the Black River is highly dissected and mantled by loess. This loess-mantled landscape probably influenced silt patterns in central Jackson County providing more silt size material for re-entrainment and deposition downwind.

A closer look at the samples surrounding Wildcat Ridge reveals coarse silt is most abundant east of Wildcat Ridge, a pattern consistent with eolian processes. Coarse silt is lower west of Wildcat Ridge where sand was likely saltating across the surface. Coarse silt was normalized to total silt contents, so areas with low amounts of coarse silt have, therefore, relatively higher accumulations of fine silt. While the proportion of fine silt makes up most of the silt content in windward locations, fine silt is still abundant on in surface samples on in lee side locations as well. These additions of fine silt likely blanketed the area, both on the windward and lee areas, after the period of large scale eolian sand migration ended and vegetation stabilized.

**PSD of selected profiles**

The trend of greater silt contents for samples collected on the lee side of Wildcat Ridge continues from the surface with depth. In general, soil profiles on the windward side of Wildcat Ridge have much less silt and clay compared to profiles on the lee side (Figure 2.13). Maximum silt contents on windward aspects range between 16 and 24.5%; whereas on lee aspects, the maximum silt contents range between 34.7 and 56.2%. Silt contents are usually highest at the surface and decrease with depth with the

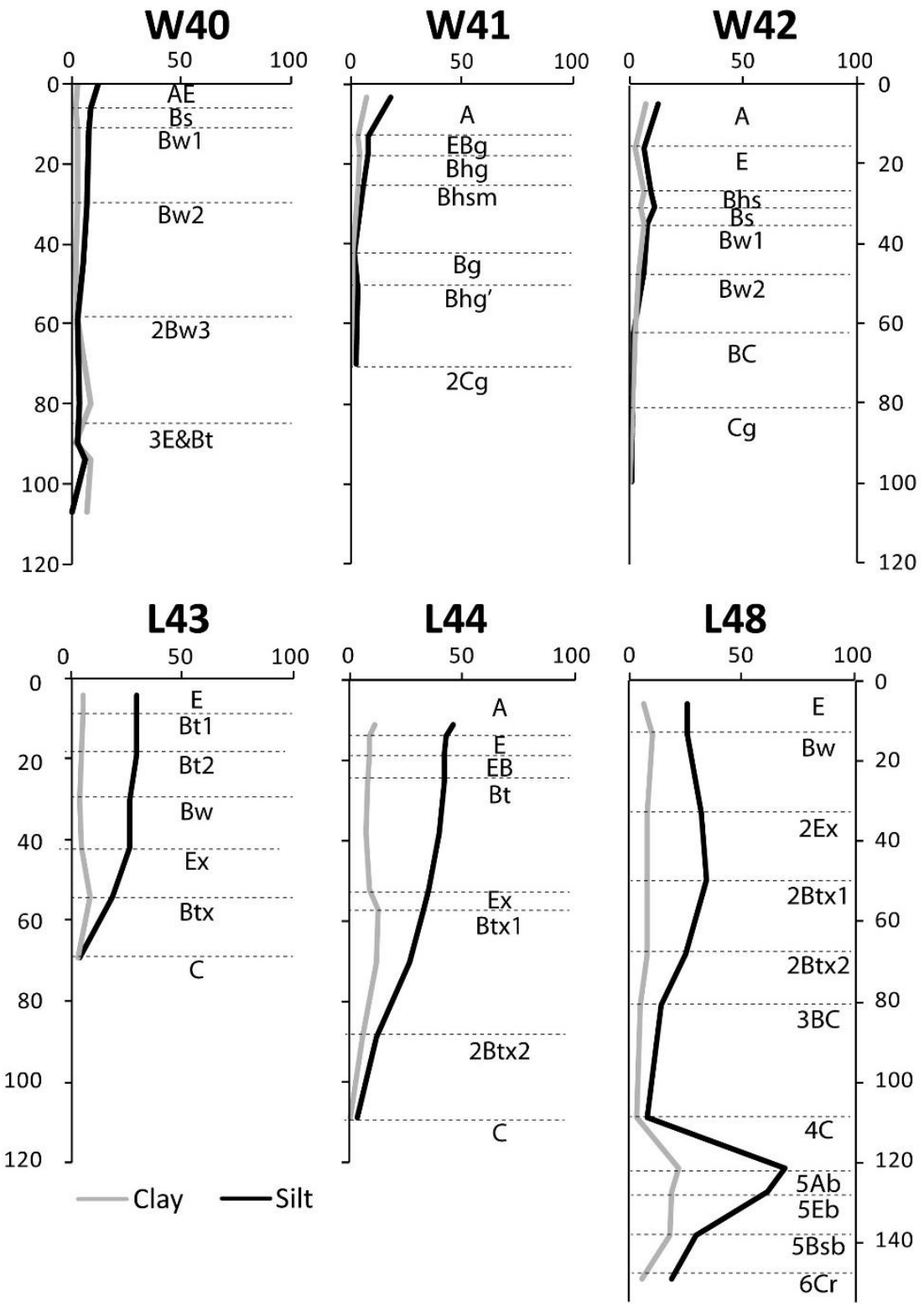


**Figure 2.13:** Particle size distribution with depth based on pipette data. Windward profiles: W40, W41, W42. Lee profiles: L43, L44, L48.

exception of site L48, where colluvial deposits overlie siltier deposits at a depth of 34 cm. (Abundant sandstone flagstones and cobbles can be found in a lobate apron that extends from the steep slope of Wildcat Ridge 2-3m past site L48). Silt in the upper profiles of windward sites decreases rapidly with depth from the surface, whereas lee sites tends to decrease more slowly with depth until the lithologic discontinuity with the underlying bedrock residuum, where a steep drop in silt content occurs. Again the notable exception is in site L48, which shows a steep increase in silt (and clay) contents at 125 cm and contains a buried soil (see chapter 3 for buried soil description). The difference in silt contents with depth in upper profiles support a scenario of long term eolian silt accumulation on the lee side of topographic barriers and a final pulse of wide-scale fine silt deposition occurring after the time of major eolian activity.

**Detailed windward profiles and relation to parent materials**

Laser diffraction data reveal much more detailed PSD changes with depth (Figure 2.14). For instance, the sand mode of both windward and lee profiles tends to remain consistent (~250 µm with fine and medium sand contents between 10 and 15%) in upper horizons and become more variable with depth. At depth, the sand mode tends to become finer (~200 µm) and/or coarser (~300 µm) and typically increases in fine and medium sand contents at the expense of all other particle size fractions (Figure 2.14). This transition from consistent sand modes to inconsistent sand modes tends to coincide with field-based interpretations of a lithologic discontinuity between an upper mantle and sandstone residuum substratum.

In windward locations, a sandy mantle ranges between ~25 cm and 150 cm thick based on field data. The sand mantle is thinnest on the sideslopes and shoulders of prominent bedrock ridges and in low-lying wet areas such as site W41, where sand modes fluctuate practically to the surface (Figure 2.14). However, most windward sites tend to be similar to profiles W40 and W42, with relatively low silt contents and consistent sand mode in the upper 59 and 81 cm, respectively. In these windward profiles, the silt modes tend to be finest at or near the surface (~15 µm) and gradually increase to ~22 µm with depth.

Locations on the lee side of Wildcat Ridge have much siltier mantles ranging in thickness between 50 and 100 cm overlying colluvium or bedrock residuum. Profiles L43 and L44 are typical examples of lee profiles, where the silty mantle is 70 or 90 cm thick. Unlike the windward profiles, silt modes in these profiles tends to start off with modes ~15 µm, increasing slightly (to ~22 µm) half way through the mantle then fining to ~15 µm again deeper in the silt mantle before abruptly shifting to < 25µm in the underlying sandstone residuum.

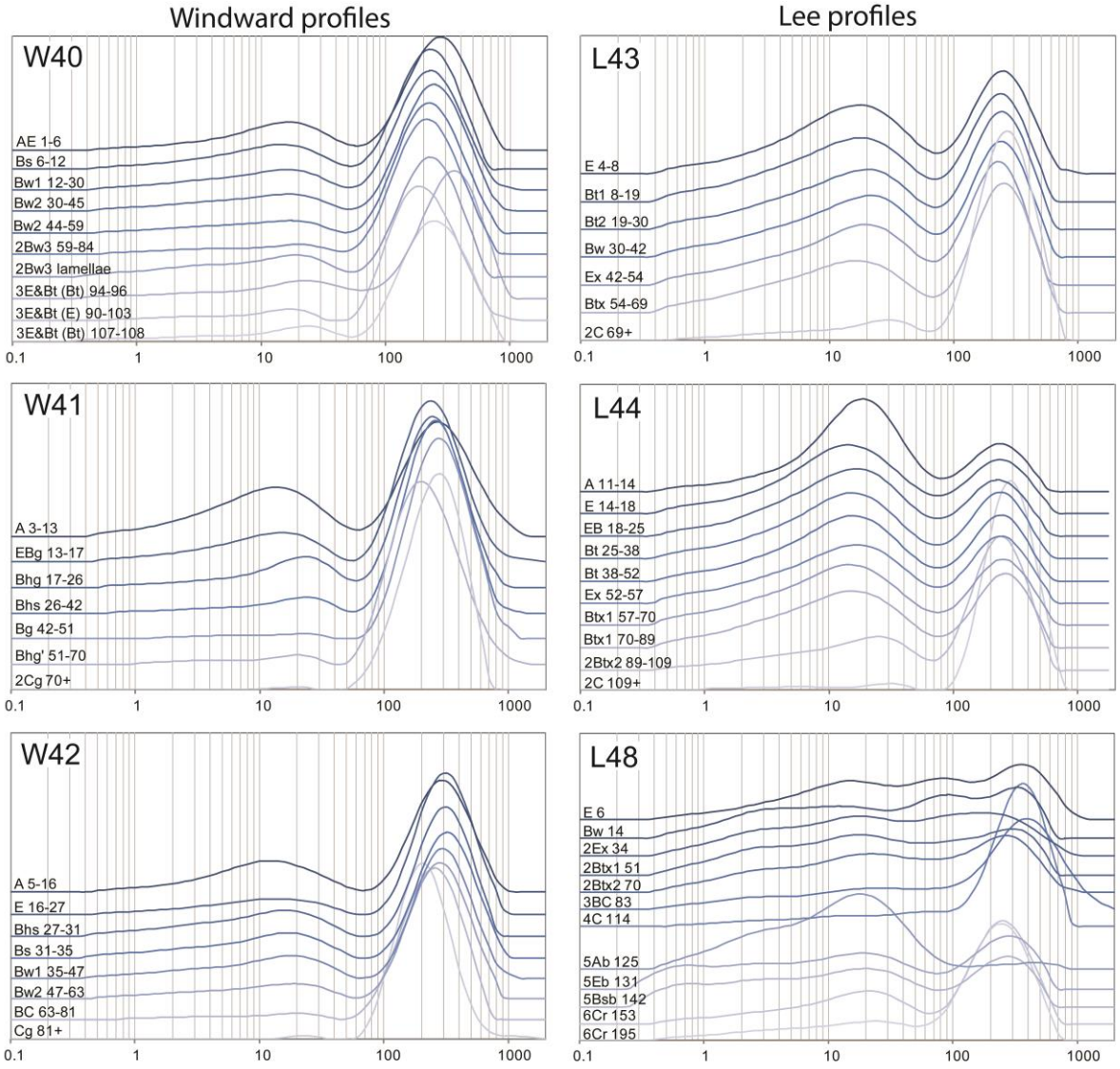


**Figure 2.14:** Laser particle size data with depth for windward and lee profiles.

Laser PSD data confirms a complex accumulation of parent materials at site L48. The top 34 cm of soil are formed in a colluvial apron described above. Based on the trimodal distribution with a very fine sand mode, this colluvial material likely derives from very fine grained Lone Rock sandstone beds that cap the adjacent Wildcat Ridge. Silt contents increase between 34 and 70 cm, which is very similar to the silty mantle found at nearby sites L43 and L44. Underlying the silty mantle is a 13 cm thick layer of very flaggy and gravelly sand, which in turn overlies stratified sand. The stratified sand overlies a buried soil at 125 cm, that can be readily be identified by a sharp increase in silt and clay. Finally, sandstone residuum is interpreted to underlie the silty buried soil at 153 cm.

**Silt mineralogy**

As expected, quartz represents an overwhelming majority of the minerals identified in all 58 samples analyzed in the seven profiles, averaging 71.1% with a maximum amount measured in the A horizon of profile W41 and the lowest amount occurring in a lamella within sandstone residuum in profile W40 (Figure 2.15; Appendix 3). Plagioclase and K-feldspar occur in all samples, and in general, tend to increase slightly in parent materials interpreted to be sandstone residuum. Most profiles show a slight decrease in feldspar at the surface, which is likely a result of weathering in these acidic soils. K-feldspar contents ranged between 30.8% (Bw of L48) and 6.1% (W41 A) with an average of 16.0%. Plagioclase ranged between 26.5% (a lamella within sandstone residuum in profile W40) and 6.5% (L48 E) with an average of 13.1%. Based on JADE peak identification, all of the plagioclase is albite and the K-feldspar is dominantly microcline with orthoclase and sanidine occurring commonly as well.

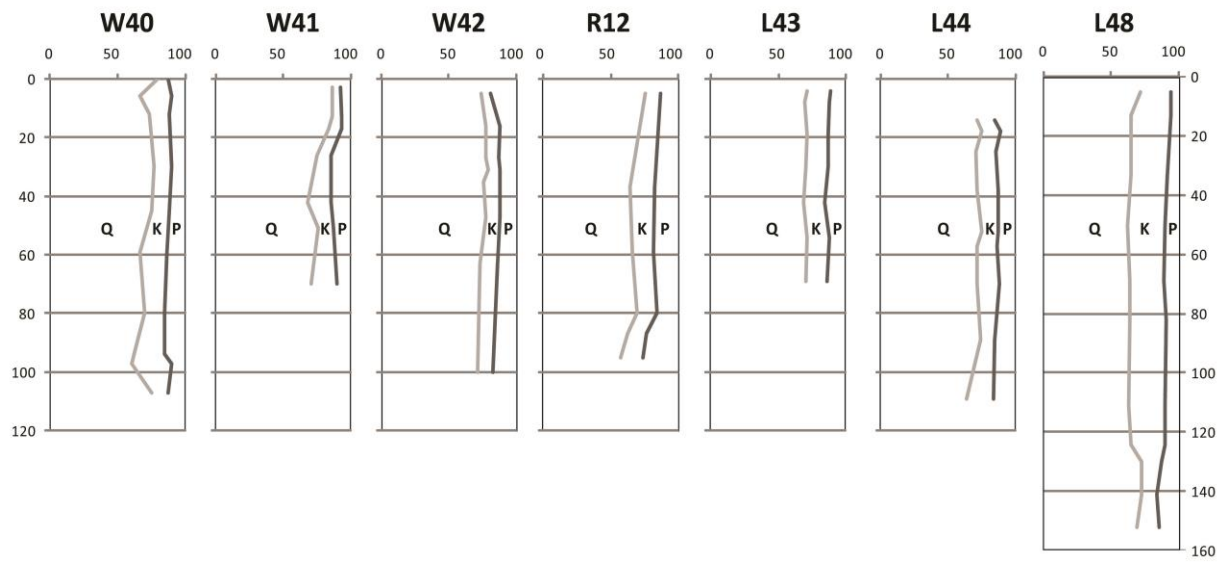


**Figure 2.15:** Cumulative silt mineralogy with depth for soil profiles in central Jackson County, WI. Q=quartz; K=K-feldspar; P=plagioclase feldspar.

In windward profiles, K-feldspar tends to be highest in bedrock residuum, whereas in the lee profiles K-feldspar contents tend to be highest mid-profile. The ratio of plagioclase peak height to that of quartz (P/Q) is generally <5% for both windward and lee profiles; although in a few bedrock residuum samples, the P/Q ratio exceeded 10%. In general, the ratio of K-feldspar peak height to quartz (K/Q) peak height (M=5.8%, SD= 2.5) is not significantly different from the P/Q peak height ratio (M=5.3%, SD=1.8), $t(57)=1.171$, $p > 0.05$. Windward P/Q ratios (M=4.8%, SD=1.3) were also not significantly different from lee ratios (M=5.7%, SD=2.0), $t(24)= -2.0$, $p > 0.05$; however, windward K/Q ratios (M=4.7%, SD=2.5) are significantly lower than those of lee samples (M=6.6%, SD=2.3), $t(24)= -2.3$, $p < 0.05$.

Peoria Loess elsewhere in Wisconsin tends to have similar K/Q values, which are not significantly different from those found in this study (Table 2.2). For example, K/Q ratios of Peoria Loess in southwestern and the Driftless Area of Wisconsin (Jacobs et al. 2011) and in central Wisconsin just north of the study area (Stanley 2008a) tend to be ~4%, and in this study K/Q is 5.7%. Upper Peoria Loess farther south in Illinois tends to have significantly lower K/Q ratios compared to silt in central

Jackson County, $p$ <0.01 (Table 2.2). Silt P/Q ratios of Peoria Loess in Illinois and Wisconsin are significantly higher ($p < 0.001$) than those found in this study (Table 2.2).

**Table 2.2:** Statistical results of XRD silt mineralogy in this study compared to that of Peoria Loess in Illinois and Wisconsin.

| | **This study (2-63 µm)** | | **Grimley 1996 (8-63 µm)** | | **Jacobs et al 2011 (8-63 µm)** | | | | **Stanley 2008 (20-45 µm)** | | | |
|---|---|---|---|---|---|---|---|---|---|---|---|---|
| | **K/Q** | **P/Q** | **K/Q** | **P/Q** | **K/Q (loess)** | **P/Q (loess)** | **K/Q (DA)** | **P/Q (DA)** | **K/Q (loess)** | **P/Q (loess)** | **K/Q (SST)** | **P/Q (SST)** |
| **N** | 58 | 58 | 43 | 43 | 24 | 24 | 10 | 10 | 20 | 20 | 10 | 10 |
| **Min.** | 1.8 | 2.2 | 2.8 | 4.4 | 2.4 | 3.2 | 2.6 | 6.7 | 1.6 | 3.5 | 5.5 | 0 |
| **Max.** | 12.2 | 13.1 | 5 | 7.8 | 6 | 10.9 | 5.9 | 10.8 | 5.4 | 10.8 | 37.1 | 0 |
| **Median** | 5.4 | 5 | 3.6 | 6.5 | 3.9 | 7.4 | 3.9 | 8.4 | 3.9 | 6.7 | 19.9 | 0 |
| **Mean** | 5.8 | 5.3 | 3.7 | 6.3 | 3.9 | 7.6 | 4.0 | 8.7 | 3.7 | 7.0 | 20.3 | 0 |
| **SD** | 2.5 | 1.8 | 0.5 | 0.9 | 0.9 | 1.8 | 1.1 | 1.3 | 0.9 | 1.7 | 10.0 | 0 |
| ***t =*** | | | ***-4.328*** | ***3.313*** | ***1.608*** | ***-6.748*** | ***2.182*** | ***-6.722*** | ***1.883*** | ***-4.738*** | ***-4.243*** | ***15.493*** |
| ***Sig.*** | | | *** | ** | | *** | | *** | | *** | *** | *** |

K/Q= peak height ratio of K-feldspar to quartz; P/Q = peak height ratio of plagioclase to quartz; DA = Driftless Area loess; SST = sandstone; N= number of samples; min.= minimum value; max.= maximum value, SD = standard deviation; Sig. = significance.
** $p < 0.01$
*** $p < 0.001$

Silt mineralogy (20-45 µm) of bedrock residuum samples collected in southern Clark County (20 km north of the study area) tended to have significantly different K/Q and P/Q ratios ($p < 0.001$) with much more K-feldspar and no detectable plagioclase amounts. The plagioclase discrepancy between samples interpreted to be bedrock residuum in this study compared to bedrock mineralogy of Stanley (2008a) could reflect a difference in the particle sizes analyzed. The over representation of K-feldspar in sandstone samples analyzed by Stanley (2008a) may be due to feldspar concentration in finer size fractions of Cambrian sandstones (Odom 1975), and a contaminant dilution by quartz in the 45-63 µm fraction. Likewise, since plagioclase is slightly more susceptible to abrasion, it should be more concentrated in a finer fraction, which might explain why plagioclase is found in total silt collected from central Jackson County bedrock residuum and not in bedrock samples collected by Stanley (2008). Alternatively, this discrepancy might be due to the lithologic character of the bedrock units or sample collection differences. In Jackson County, the samples were collected in the C horizon near the base of the solum in quartzarenitic sandstone residuum; whereas Stanley's (2008a) bedrock samples were

collected from shale partings in bedrock outcrops or relatively thick beds of shale residuum. It is also possible that in the sandy bedrock residuum samples of this study, very fine, relatively plagioclase-rich silt may have translocated into the upper residuum along with clay, opposed to the bedrock and shale residuum samples from Stanley (2008a), which are less likely to be influenced by translocation of very fine silt contents either because 1) samples lack an overlying soil profile or 2) fine-grained shale residuum would limit/prevent fine silt translocation. Furthermore, the silt mineralogy in the mantle of central Jackson County is different than loess from glacial sources found elsewhere in Wisconsin and the Driftless Area (Jacobs et al. 2011) or in Illinois (Grimley 1996, 2000). Although the 8-63 µm fraction of unaltered loess was analyzed by Grimley (1996) and Jacobs et al. (2011), rather than the 2-63 µm fractions used in this study, this is unlikely to account for the relative difference in plagioclase contents. Instead, the difference in plagioclase content may reflect a greater contribution from Cambrian bedrock to the silt in the eolian mantle of Jackson County, than to loess elsewhere in the region.

**eXRF data**

Titanium to Zirconium ratios (Ti:Zr) of the silt fraction (2-63 µm) tend to be highest at the surface and decrease with depth in all profiles (Figure 2.16). Although Zr contents are relatively stable in each profile, Ti contents decrease to nearly zero in sediment interpreted to be bedrock residuum, especially for windward profiles. Except for the poorly drained soil (W41), Ti:Zr ratios decrease gradually with depth; whereas, in silty lee profiles, Ti:Zr ratios remain relatively consistent with depth before declining rapidly in the BC and C horizons. Note that the dramatic Ti:Zr increase in profile L48 coincides with the buried soil in especially silty material. In site W41, the relatively rapid decrease at approximately 20 cm coincides with the water table.

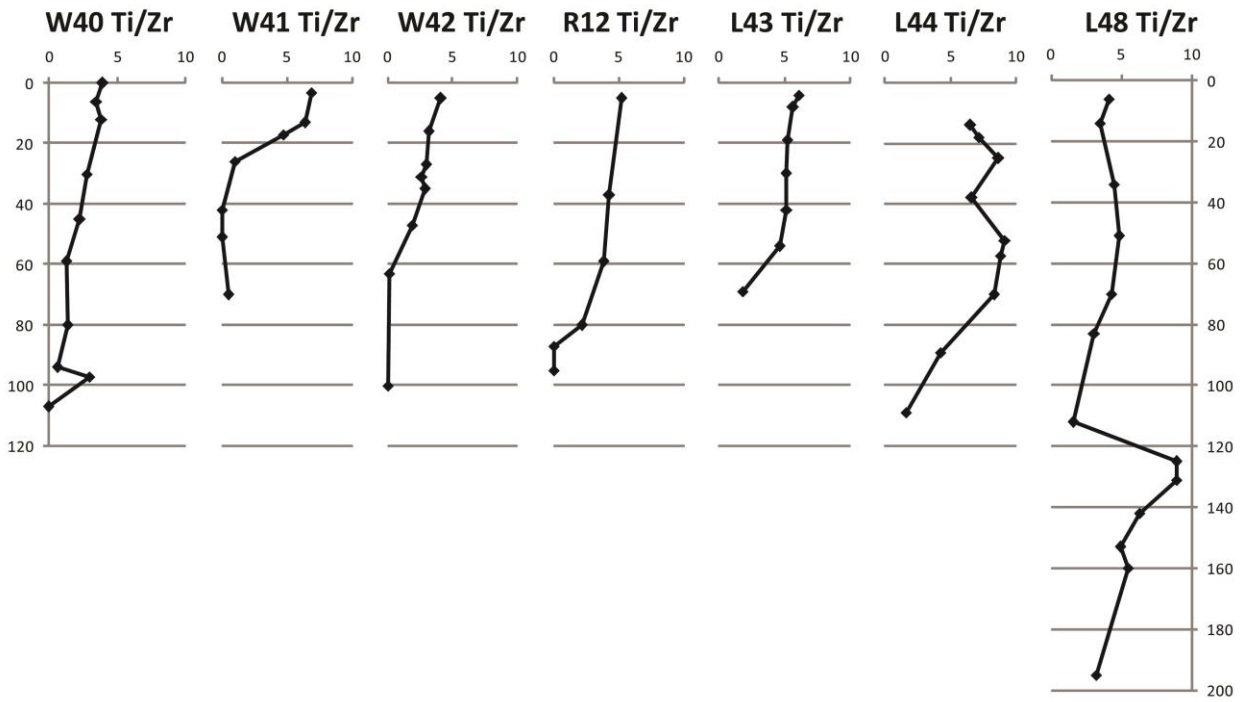


**Figure 2.16:** Depth trends of Ti:Zr in the silt fraction (2-63 µm) for soil profiles in central Jackson County, WI . Windward profiles: W40, W41, W2; Ridge profile: R12; Lee profiles: L43, 44, 48.

Although Ti is slightly more labile, Ti and Zr are both considered to be relatively immobile in temperate region soils (Jackson and Sherman 1953). Therefore, Ti:Zr ratios are expected to increase slightly, if they change at all, with depth in a homogenous parent material. The decreasing Ti:Zr ratio with depth in these profiles suggests the parent materials in these soils are heterogeneous and silt contents are likely derived from different sources (Reheis 1990; Stiles and Stensvold 2008). That is, silt in the upper profile is not likely derived completely from local bedrock residuum sources as nearly all bedrock residuum samples have little, if any, Ti in the silt fraction. A better explanation is that some proportion of silt was derived through eolian transport from more distant sources. Probable sources of this non-local silt may include the Mississippi and Chippewa rivers, which drained the Laurentide Ice Sheet during the last glaciation and/or fine atmospheric dust from loess sources farther west on the Great Plains. Given that the silt modes for most surficial mantle samples are <25 µm, it is possible that much of this silt fraction was derived from dust sources hundreds of kilometers away (Tsoar and Pye 1987), possibly from the

Mississippi or Chippewa River Valleys. Future work should look at the geochemical differences between silt fractions. Driftless Area loess in southwestern Wisconsin is thought to be derived largely from Mississippi River Valley trains (Knox et al. 1982; Muhs et al. 2003), although there was probably a large contribution from pre-Illinoian glacigenic sediments west of the Mississippi and from the Des Moines lobe of the ice sheet even farther west (Mason et al. 1994). Fine dust addition, possibly from more distant sources, becomes evident in the upper part of Late Pleistocene loess in the Midwest (Mason and Jacobs 1998). According to Stiles and Stensvold (2008), southwestern Wisconsin loess samples tend to have Ti:Zr ratio between 10.4 and 13.1. Since silty surface samples in Jackson County tend to have Ti:Zr ratios < 7, and all samples have ratios <10, it is possible that silt contents in Jackson County represent a mixture of silt derived from both local bedrock sources (with low Ti contents) and more distant regional loess sources (with higher Ti contents) such as sediment derived from the Laurentide Ice Sheet.

**Principal component analysis (PCA)**

Based on lab data discussed above, particle size fractions were simplified to three variables for PCA analysis: median, silt to medium sand ratio, and coarse silt to total silt ratio. Other variables include Ti/Zr ratios, XRD silt mineralogy percentages of quartz, plagioclase, and K-feldspar, and pH. Results of PCA performed on 58 samples from 7 locations within the study area show that the first three principal components explain 77% of the variance in the sample set (Table 2.3). Median grain size loads positively (0.52) on principal component (PC) 1; whereas silt to medium sand and titanium to zirconium ratios have negative loadings (-0.40 and -0.56, respectively). PC1, which explains 32% of the variance in the data, thus is interpreted to indicate parent material categories 1) coarse grained bedrock residuum with low titanium and 2) silt-rich samples with relatively high titanium contents. The second component, which accounts for an additional 29% of the variance, mainly reflects quartz contents (0.59) versus K-feldspar (-0.60) contents, with minor loadings of coarse silt: total silt ratios (-0.30) and pH (-0.31). PC2 likely reflects both parent material influence (more quartz in coarser textured mantles) and weathering trends (more K-feldspar and higher pH with depth). Almost all of the variables load to some extent on PC3,

which accounts for an additional 16% of the variance. Plagioclase contents (0.59) and coarse silt to silt ratios (-0.55) are the dominant variables loading on PC3. Low coarse silt-to-total silt ratios, by definition, are high in fine silt, and thus, plagioclase and fine silt contents are positively correlated on PC3 and may relate to weathering trends or inherited mineralogy of the fine silt additions.

**Table 2.3:** Principal component analysis loadings and summary for variables associated with parent material characteristics.

| **Loadings** | **Comp.1** | **Comp.2** | **Comp.3** | **Comp.4** | **Comp.5** | **Comp.6** | **Comp.7** | **Comp.8** |
|---|---|---|---|---|---|---|---|---|
| Median | **0.52** | 0.22 | -0.21 | | | 0.31 | **-0.67** | 0.22 |
| Si:MS | **-0.40** | -0.22 | 0.33 | -0.27 | | **0.77** | | |
| Csi:Si | | -0.30 | **-0.55** | **0.64** | -0.22 | 0.36 | | |
| quartz | | **0.59** | | | -0.37 | | 0.28 | **0.61** |
| K-feldspar | | **-0.60** | -0.25 | -0.29 | | -0.21 | | **0.66** |
| plagioclase | 0.31 | | **0.59** | **0.60** | 0.26 | | | 0.35 |
| pH | 0.35 | -0.31 | 0.30 | | **-0.82** | | | |
| Ti:Zr | **-0.56** | | 0.20 | | | -0.33 | **-0.68** | |
| **Importance of components:** | **Comp.1** | **Comp.2** | **Comp.3** | **Comp.4** | **Comp.5** | **Comp.6** | **Comp.7** | **Comp.8** |
| Standard deviation | 1.61 | 1.52 | 1.12 | 0.85 | 0.72 | 0.68 | 0.37 | 0.17 |
| Proportion of Variance | 0.32 | 0.29 | 0.16 | 0.09 | 0.06 | 0.06 | 0.02 | 0.00 |
| Cumulative Proportion | 0.32 | 0.61 | 0.77 | 0.86 | 0.92 | 0.98 | 1.00 | 1.00 |

Si:MS = ratio of total silt (2-63 µm) to medium sand (250-500 µm); Csi:Si = ratio of coarse silt (30-63 µm) to total silt; Ti:Zr = ratio of titanium to zirconium.

Samples cluster according to parent material and aspect when plotting PC1 against PC2 (Figure 2.17). Samples collected within bedrock residuum (i.e. at greater depth), tend to fall in the lower right quadrant regardless of aspect indicating these samples tend to have coarser textures, less titanium, higher pH, and more feldspar. Near-surface samples tend to plot farther to the left because of finer median PSD and more titanium and silt contents, but largely separate out based on texture/aspect. Leeward solum samples cluster in the lower left quadrants of Figure 2.17A and B, reflecting finer textures and higher Ti contents. Samples from L48, horizons 5Ab and 5Eb appear to be clear outliers that are especially fine-grained and Ti-rich. Windward samples cluster strongly towards the upper right quadrant suggesting that these samples are coarser and become more quartz-rich with decreasing pH. Some of the windward

samples extend towards the top center-left of the chart; these samples tend to be very acidic surface horizons that are finer and more Ti-rich compared to other windward samples.

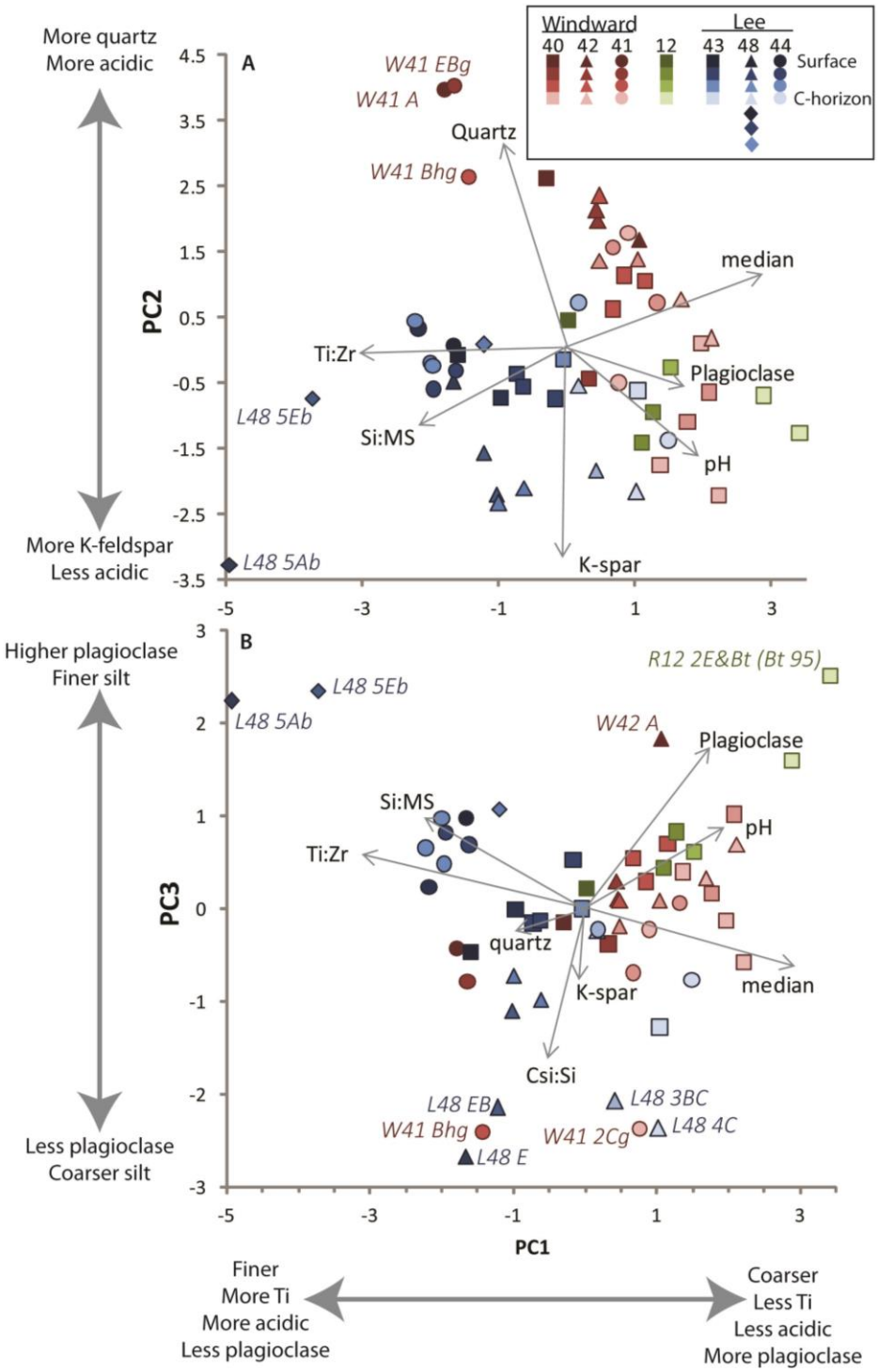


**Figure 2.17:** Biplot showing principal components for SOM analysis**. A:** PC 1on the X-axis and PC2 on the Y-axis. **B**: PC1 on the X-axis and PC3 on the Y-axis. Blue represents samples collected on the lee side of Wildcat Ridge; red represents those from the windward side; green represents samples collected from the lower backslope within the Wildcat Ridge complex. Shades within each of these hues represent the relative depth of the samples; dark shades represent surface samples with shades becoming lighter with increasing depth.

When plotting PC1 against PC3, a depth gradient is more apparent with surface samples occurring on the left transitioning to deeper samples towards the right. Again, this trend reflects more eolian additions to surface samples (higher Ti and generally finer) to coarser Ti-poor samples bedrock residuum samples on the right on PC1. Vertically, PC3 separates largely based on the ratio of coarse silt to total silt and plagioclase contents. Samples near the bottom of the chart such as, L48 E, EB, 3BC, and 4C tend to have relatively more coarse silt that is plagioclase-poor and might have slightly more quartz or K-feldspar. These samples are interpreted to be largely influenced by local Tunnel City Group colluvium according to their laser PSD (Figure 2.17). Many of the samples from the poorly drained windward profile (W41) tend to have less fine silt and plagioclase compared to most other windward samples, perhaps because this profile is more acidic than the other profiles. Plagioclase contents tend to be highest in lower, bedrock residuum samples as well as some of the fine grained eolian sediment-rich samples towards the upper left quadrant.

Principle component analysis suggests that the overwhelming majority (77%) of the variance within the data set can be explained by variables dominated by particle size and titanium content. Lee samples from the solum of profiles consistently are finer grained and contain more coarse silt and titanium compred to windward samples and those interpreted as bedrock residuum. Because the titanium contents are so much higher in all surface samples, which all have relatively high amounts of fine silt, it is likely at least some portion of these finer silts are derived from somewhere other than the local bedrock.

## *Discussion*

### Geomorphic response to climate change and implications for land use

Overall, the patterns revealed by particle size, mineralogy, and geochemistry are best explained by the interaction of eolian processes, bedrock-controlled topography, and weathering. While deeper samples from bedrock residuum share some characteristics such as low titanium across both windward and lee sites, the upper horizons interpreted as an eolian mantle clearly differ in silt content between windward and lee aspects. This contrast reflects the effect of topography in limiting saltating sand

mobility and allowing accumulation of silt-rich dust in the profile. Titanium content is greater in the more silt-rich eolian mantle at lee sites, but increases upward across all sites, probably reflecting addition of farther-traveled dust across the study area after eolian sand movement had largely ceased.

This conclusion does not rule out a role for Late Pleistocene periglacial slope processes in shaping the landscape of the study area. In fact, most of the colluvial deposits found in this study are likely the result periglacial processes, which may have had an influence on eolian activity. In areas of Wisconsin and adjacent states that were outside limits of Late Pleistocene glaciation, lower portions of steep slopes are commonly covered with poorly sorted, silty angular-cobble diamicton that is interpreted to be solifluction rubble (Mason 1995; Mason and Knox 1997; Clayton et al. 2001). A similar colluvial deposit is commonly found at the base of the silty or sandy mantle in footslope positions within Jackson County. The period of active solifluction associated with permafrost is estimated to have ended around 15 ka, based on radiocarbon dating of slope deposits (Mason 1995; Mason and Knox 1997; Loope in preparation). Optically stimulated luminescence (OSL) age estimates collected from within and near the study area suggest active dune formation largely occurred from 18 to 14 ka (Loope in preparation), postdating the period of rapid landscape change as a result of glacial retreat and permafrost degradation (Clayton et al. 2001; Loope in preparation). The stratigraphy of parent materials in central Jackson County largely supports this sequence because colluvium underlies eolian mantles on most slopes. Solifluction lobes were probably active on steeper slopes, particularly when permafrost began to thaw. Sand from local streams and potentially from exposed colluvium migrated across the low-relief terrain and ramped onto the windward aspects of bedrock hills. The eolian sand mantle is relatively thin and dune forms are relatively small and have low relief, all suggesting limited sand availability. Although the limitation of sand can result from partial vegetation cover, if permafrost was still present then it probably reduced sediment availability due to cementation by ice or perched water within the active layer. With or without permafrost, in low areas, sand was likely trapped by wet conditions and/or vegetation, limiting dune development there. LiDAR data from adjacent counties suggests that most dunes developed on areas with slightly more relief as dune forms are absent where low lying Histosols are mapped.

Within the eolian mantle, much of the sand and at least part of the coarse silt component are derived locally from weathered local Cambrian bedrock; however, the silt fraction is at least in part derived from external sources, as indicated by titanium content. Local bedrock-derived silt would have become dust through bombardment by saltating sand. This local dust and dust from more distant sources would have been deposited on the eolian mantle, but would have been quickly re-entrained from barren surfaces where saltation was active (Mason et al., 1999). Under these conditions, silt would not have accumulated unless it was deposited on landscape positions where saltation was limited—the east and southeast aspects of tall bedrock ridges, which are shielded from westerly to northwesterly winds as well as influx of sand from those directions. Much of this silt was likely reworked by slope processes and pedogenic processes, forming a silty mantle with a bimodal PSD in the silt and medium sand fractions.

After the eolian mantle had largely stabilized, fine-grained dust probably blanketed the landscape relatively evenly, as evident in the increase of fine silt towards the tops of the soil profiles both on the lee side and on the windward aspects of the bedrock topography. Because this silt has a higher concentration of titanium than the bedrock residuum, it is unlikely the fine silt is a result of weathering *in situ*. Slow additions, in combination with bioturbation, allowed mixing of this fine silty sediment between 25 and 60 cm deep, depending on the drainage conditions in windward locations, and > 80 cm in lee locations.

Little evidence was found suggesting that massive slope failure was common during the Holocene. Most of the colluvial deposits were found beneath the eolian mantle. The exception is site L48, where a colluvial apron was apparent from the surface to a depth of 34 cm. A fragipan in the soil profile at L48 begins at 34cm (see chapter 3). The 2Ex horizon is interpreted to be part of the eolian mantle based on its PSD; however, it does show some mixing with the Lone Rock colluvium from above. The evidence of mixing suggests the fragipan formed after the colluvium was deposited.

Although bioturbation cannot be ruled out as a factor in the development of sand and silt mantles found within the study area, eolian processes from the late Pleistocene are favored for the initial development of these mantles for several reasons. First, regional LiDAR data shows dune forms are a ubiquitous feature across very similar landscapes nearby, both in open areas, and in somewhat protected

areas. Therefore, it is likely the upper sand mantle at sites W40 and W42 are low sand dunes. Second, silt, especially coarse silt, is more abundant in protected sites on the lee sides of steep bedrock ridges. Therefore, the silty mantles found within lee profiles are likely due to deposition of eolian silt—loess—and reworked loess in areas protected from saltating sands by the barriers formed by prominent bedrock ridges.

### *Summary and conclusions*

Dune forms evident in LiDAR data from Monroe and Juneau Counties suggest widespread eolian activity resulted in an eolian mantle covering the low relief terrain associated with the Central Sand Plains of Wisconsin. This likely occurred between 18 and 14 ka based on OSL ages collected from regional sand dunes (Loope in preparation). Holocene reactivation of dune surfaces (e.g., Rawling et al. 2008; Loope in preparation) cannot be excluded because the sandy mantle rarely exceeds 2 m and the effects of bioturbation cannot be differentiated from reactivation bleaching for OSL age estimates (Hanson et al. 2014). Profile PSDs suggest the eolian sand sheet is mostly between 30 and 100 cm thick and covers much of the landscape in central Jackson County and the surrounding low-relief terrain of the Central Sand Plain; however, in places with larger parabolic dunes, the eolian sand may be up to 5 m thick. Eolian silt associated with the period of deglaciation is only preserved in the most protected landscape positions along the east and southeast aspects of large bedrock ridges; whereas fine silt that occurs in the surface horizons may have been deposited after the time of most intense eolian activity. Therefore, using fine silt variation within a thin loess mantle to identify loess source areas should also use corroborating geochemical or mineralogical evidence.

The abundance of dune forms and the absence of silt deposits across the majority of the sandy terrain suggest this landscape acted largely as a surface of transport where fine materials deposited were entrained by saltating sands across the surface. Most of the silt and finer material was carried farther downwind, perhaps into the Glacial Lake Wisconsin basin, only to be redistributed even farther downwind, presumably onto the Oneota Cuesta. If this is the case, loess on the Green Bay Lobe is a

mixture of fine sediments from multiple sources including the Cambrian landscape of west-central Wisconsin, outwash and valley train deposits associated with the Upper Mississippi River Valley, and very fine materials from distant west sources. Future work will need to confirm that silt and clay fractions are derived from different provenances. Future work is also necessary to explore the role of bioturbation in this landscape.

# CHAPTER 3 : PEDOGENESIS AND WEATHERING


## *Abstract*

Silt additions change the pedogenic pathway of otherwise sandy soils in central Jackson County. Without these silty additions, the sandy residuum and sandy colluvial soils would likely fall on the continuum of podzolization based on drainage from Entisols in higher positions to aquic Spodosols on toeslopes. Siltier soils found in protected lee areas of topographic barriers, with greater inputs of reworked loess, are highly acidic and generally unproductive; however, the pedogenic pathway is shifted from podzolization to lessivage. Bisequal soils with an upper E-Bt and lower Ex-Btx are common in these settings. The increased fine material improves soil water holding capacity, yet at the same time processes associated with lessivage (and perhaps silica translocation) formed fragipans that limit root growth. Comparisons of lower sequa characteristics between catena positions suggest lateral translocation through both silty and sandy catenas is an important process in this landscape.


## *Introduction*

The state factor model (Jenny 1941) of soil development remains an important framework within which soil morphology can be understood, and is often used by soil mappers to predict soil boundaries (Scull et al. 2003). Soil variation is explained by changes in one of the five factors in soil formation—climate, organisms (flora and fauna), relief, parent material, or time. In many locations, however, strict application of the state factor model is difficult or impossible due to the presence of lithologic discontinuities, vegetation and hydrology changes with slope, and hillslope processes that not only change parent material characteristics, but also the time factor. In these situations, the catena concept is a better framework in which to understand pedogenesis on topography with moderate relief (Sommer and Schlichting 1997). The catena concept combines the basic tenets of the state factor model with the process-systems model (Simonson 1959) that better explains intra-profile changes in horizonation, in conjunction with the idea that soils on slopes are genetically linked (Hall 1983).

In the mid-latitudes, many hillslopes were affected by Pleistocene periglacial solifluction that imparts lithologic discontinuities to soils forming the catenas present on those slopes today (Mason and Knox 1997; Semmel and Terhorst 2010). Particularly in the low mountain areas of central Europe, cover beds—solifluction sediment composed of weathered bedrock residuum mixed with varying amounts of loess—have been the focus of several studies recently (Kleber 1992, 1997; Mailänder and Veit 2001; Dietze and Kleber 2010; Waroszewski et al. 2013; Waroszewski et al. 2015). Although the effects of eolian dust additions on pedogenesis (Reheis 1990; Jacobs and Mason 2005, 2007; Jacobs et al. 2012) and biogeochemical cycling (e.g., Kennedy et al. 1998; Reynolds et al. 2001; Reynolds et al. 2006) have been the focus of many studies, the contribution of relatively minor additions of eolian silt to pedogenesis, particularly in an otherwise sandy landscape associated, has received little attention.

Therefore, the objective of this study is to investigate the effects of relatively small amounts of eolian fine grained sediments on soil development in an otherwise sandy landscape. The landscape in central Jackson County Wisconsin presents a good opportunity for a case study since it lies just beyond the limits of the Laurentide Ice Sheet during the most recent glacial episode and was prone to active solifluction and eolian activity (Mason and Knox 1997; Chapter 2 this study).

## *Methods*

### Field methods

Seven profiles were excavated for detailed morphological description and analysis of particle size distribution, clay mineralogy, and pH. General locations for soil profile excavations were targeted prior to fieldwork based on digital soil survey (SSURGO) and elevation data. Targeted locations aimed to represent 1) an Entisol formed into a sandy mantle located in a lower backslope position of a relatively isolated windward hillslope (site W40), 2) Spodosols with increasing Bhs thickness in footslope and toe slope positions, respectively, formed into the sandy mantle west of Wildcat Ridge (W42 and W41), 3) an Entisol formed into the sandy or silty mantle in a lower backslope position within the Wildcat Ridge complex (R12), 4) an Alfisol in the silty mantle of a protected footslope position on the lee side (east

aspect) of Wildcat Ridge (L48), and 5) Alfisols in the silty mantle of slightly less-protected footslope and toeslope positions on the lee side of Wildcat Ridge (L43 and L44) (Figure 1.3).

Because Wildcat Ridge and other ridges in the area are narrow and have little (< 30 cm) loose sediment overlying consolidated bedrock, summit and shoulder positions were avoided. Once in the field, five to ten test holes were inspected using a bucket auger within a ~50 $m^2$ area of each target location, making sure to avoid evidence of disturbance. Each test hole was numbered and latitude/longitude coordinates were recorded along with soil characteristics such as approximate depth to horizons encountered, texture, and coarse fragments. Based on these qualitative data, the test hole deemed to represent a typical soil profile for the local area was selected for soil pit excavations. Based on the test hole data, soil profiles were excavated, described, and sampled according to NRCS guidelines (Schoeneberger et al. 2002) at positions deemed representative of the average morphology of the pedon.

**Clay Mineralogy**

Clay mineralogy was determined using a Rigaku MiniFlex X-ray diffractometer employing Cu Kα radiation. Clay smears on glass slides were analyzed within the 5–31.5 2θ range with a scan speed of 2° per minute and a 0.02 step. Sample treatments include Mg saturation and ethylene glycol solvation as well as K saturation with air dry and progressive heat treatments at 300 and 550°C (Moore and Reynolds 1989). After adjusting the resulting diffractograms by aligning the quartz peak to 3.34 Å, peak heights and background values were quantified using JADE software (Materials Data, Inc.). Net peak intensities were calculated for each mineral by subtracting the background value from the peak intensity value. Clay mineral percentages were quantified following the Illinois State Geological Survey (Method 1 of Hughes and Warren 1989).

**pH**

Soil pH was measured using 1:1 soil-water and 1:2 $CaCl_2$ solutions using a SB801PI SympHony benchtop pH meter (VWR International, LLC).

## *Results*

Soil morphology and horizon characteristics in the following sections are based on soil profile descriptions as well as field note data from test holes. Test hole data recorded colors, thicknesses, and hand textures of A, E, and B horizons as well solum depth and depth to water table. O horizon characteristics were also included in field note data.

### Epipedon properties

Most of the soil profiles observed in central Jackson County have ochric epipedons (Figure 3.1-Figure 3.4). Total O-horizon thickness tends to vary both by geomorphic position on the landscape and also by aspect east or west of Wildcat Ridge. Generally, O horizons are thicker on the lee side (4-11 cm) as compared to windward locations (1-5 cm). In both geomorphic settings, the ratio of hemic to fibric material tends to increase downslope. On the windward side, fibric materials tend to be composed of pine needles, some deciduous leaves, stems, bark, and roots; hemic material is thickest where moss is common

ground cover. On the lee side, fibric material tends to be dominantly composed of fresh and year-old oak leaves with twigs, grasses, and other deciduous leaves.

Conversely, A horizons are thickest and darkest in windward profiles (6-11 cm) as compared to lower lee profiles, where they are thin (< 3 cm) or nonexistent despite the soils being mapped as Mollic Hapludalfs (Figure 3.1). Higher lee positions, e.g. R12, have slightly thicker A horizons (~5 cm) that are very dark grayish brown (10YR 3/2) and lack well-developed albic horizons. Windward A horizons are

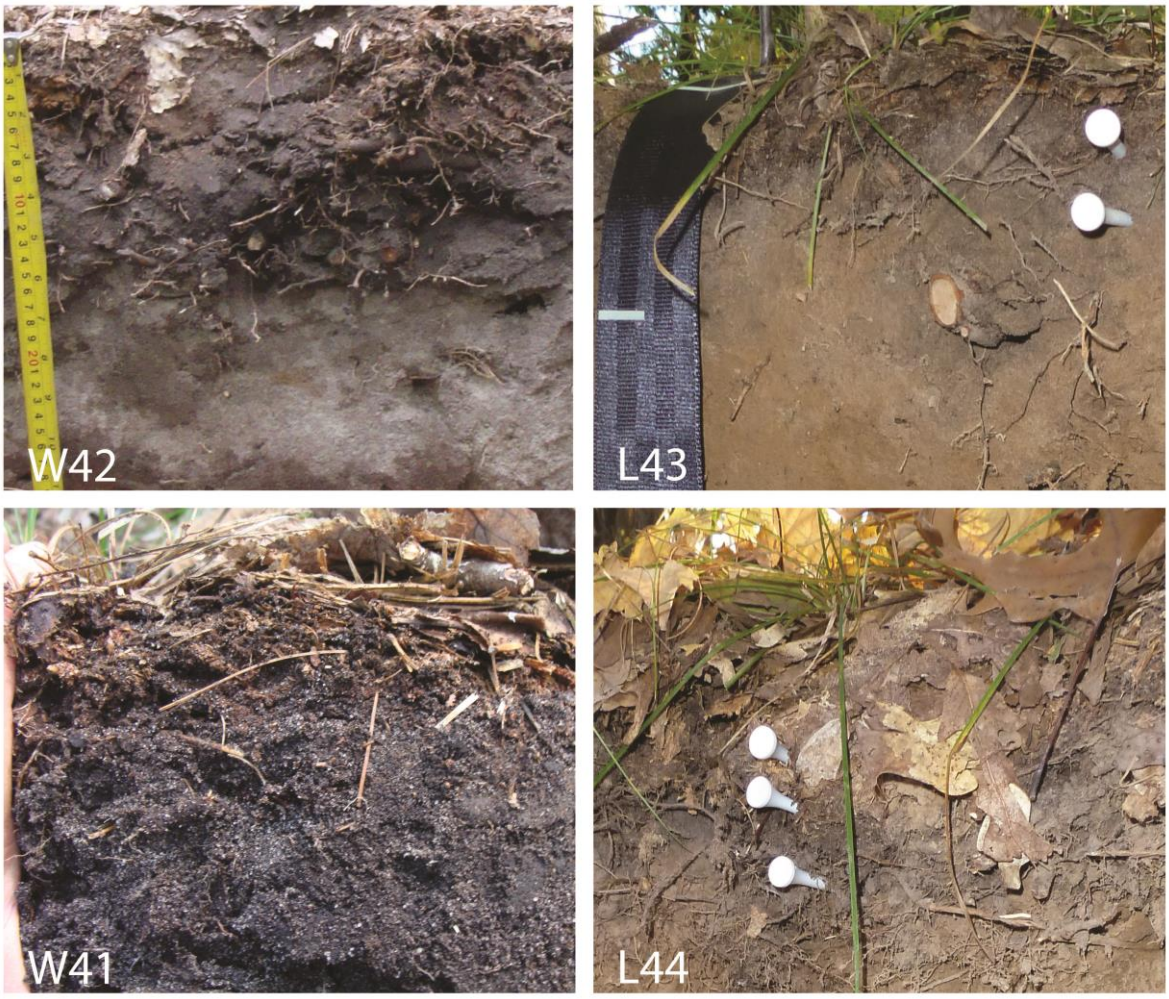


**Figure 3.1:** Photographs of epipedons in foot and toeslope positions for sandy windward and silty leeward profiles in central Jackson County, WI. Note relatively thick A horizons in windward profiles W42 andW41 compared to relatively thin/non-existent A horizons in leeward profiles.

typically black (10 YR 2/1) or very dark brown (10YR 2/2) and have abundant uncoated quartz sand grains (Figure 3.2), which are indicative of the stripping of humus coatings in eluvial horizons that can be translocated as DOM into illuvial horizons, and may possibly reflect bioturbation processes acting to

incorporate highly decomposed (Oa) material with more acidified E horizon material. These A horizons tend to have weak granular structure. The weakness of this structure is at least partially due to the lack of fine-grained material, but may also be the result of the absence of worm bioturbation in these coarse soils. The slow incorporation of humus into the mineral soil in lower slopes of lee profiles results in better developed E horizons (Figure 3.3), which tend to be lighter in color (grayish brown, 10 YR 5/2) on lee locations as compared to darker/browner E horizons (dark brown 10 YR 4/3 or dark gray, 7.5 YR 4/1) of windward profiles.

**B horizon properties**

The thickness and type of B horizons in central Jackson County are variable depending on the texture of the parent material and drainage conditions. Lower backslope positions show similar horizonation corresponding with the general geomorphology of the profile (Figure 3.4). Profiles R12 and W40 are both developed into ~60 cm of an eolian mantle, ~ 20 cm of colluvial material, and the underlying Wonewoc sandstone residuum. These backslope soils exhibit minimal soil development in the upper ~80 cm, but have several lamellae occurring at base of the colluvium and into the underlying residuum despite differing textures of fine sandy loam (R12) and loamy sand (W40). Lamellae in both profiles appear to have discrete upper boundaries, diffuse bottom boundaries, are brownish yellow (10 YR 6/6) and tend to occur where the sandstone laminae are coarser and more poorly sorted than surrounding E horizons (Appendix 3). Lamellae in siltier parent eolian and colluvial mantles (e.g., R12) are thicker and better developed than in sandier windward profiles, presumably because of greater amounts of inherited clay.

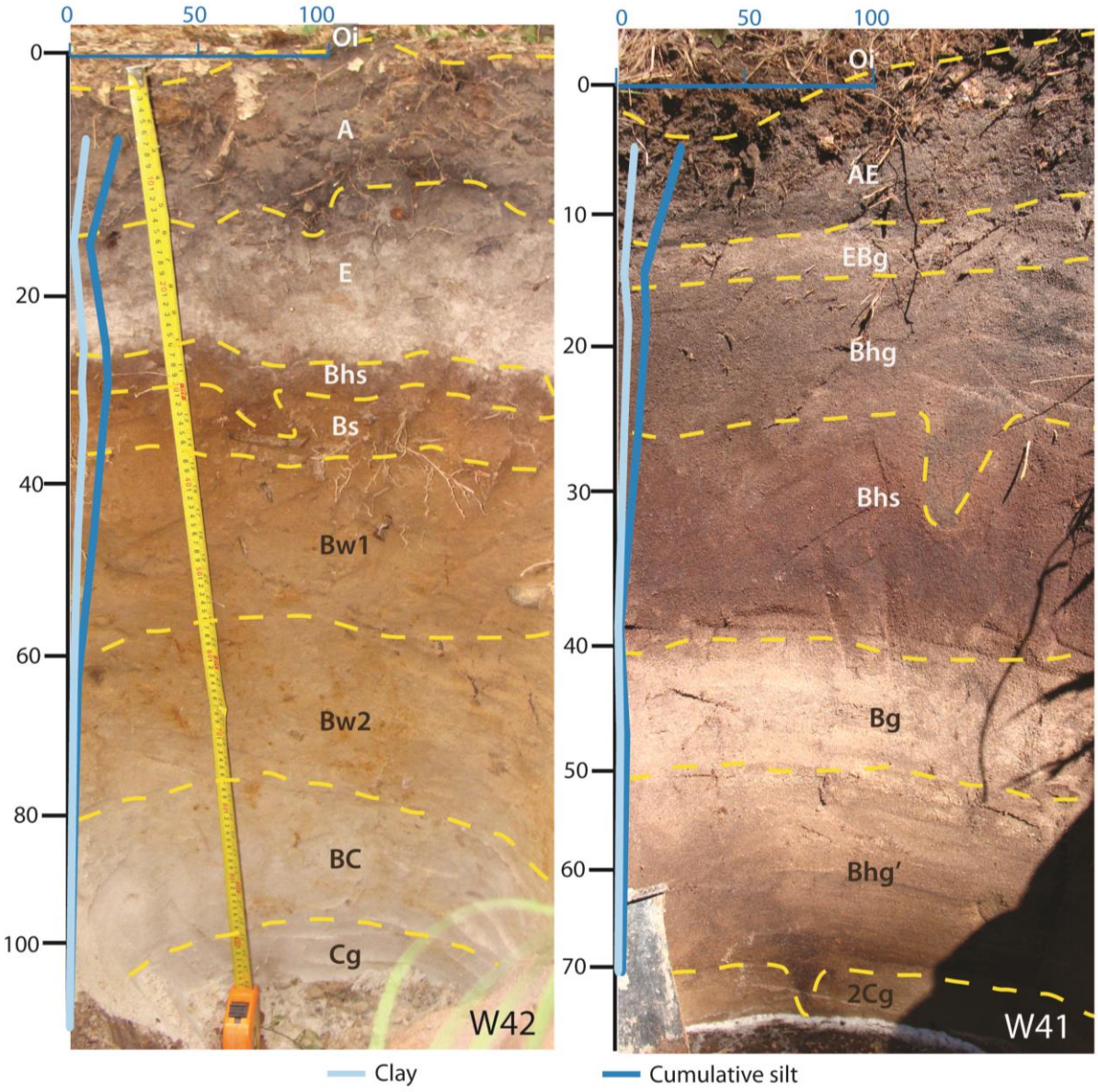


**Figure 3.2:** Photographs of footslope (W42) and toeslope (W41) profiles on the windward side of Wildcat Ridge. Cumulative particle size data with depth is overlain to approximately coincide with the depth shown in the photo. Lighter blue represents clay contents and dark blue represents cumulative silt contents with depth. Both profiles display spodic morphology with subsurface accumulations of carbon and either redox and gleyed

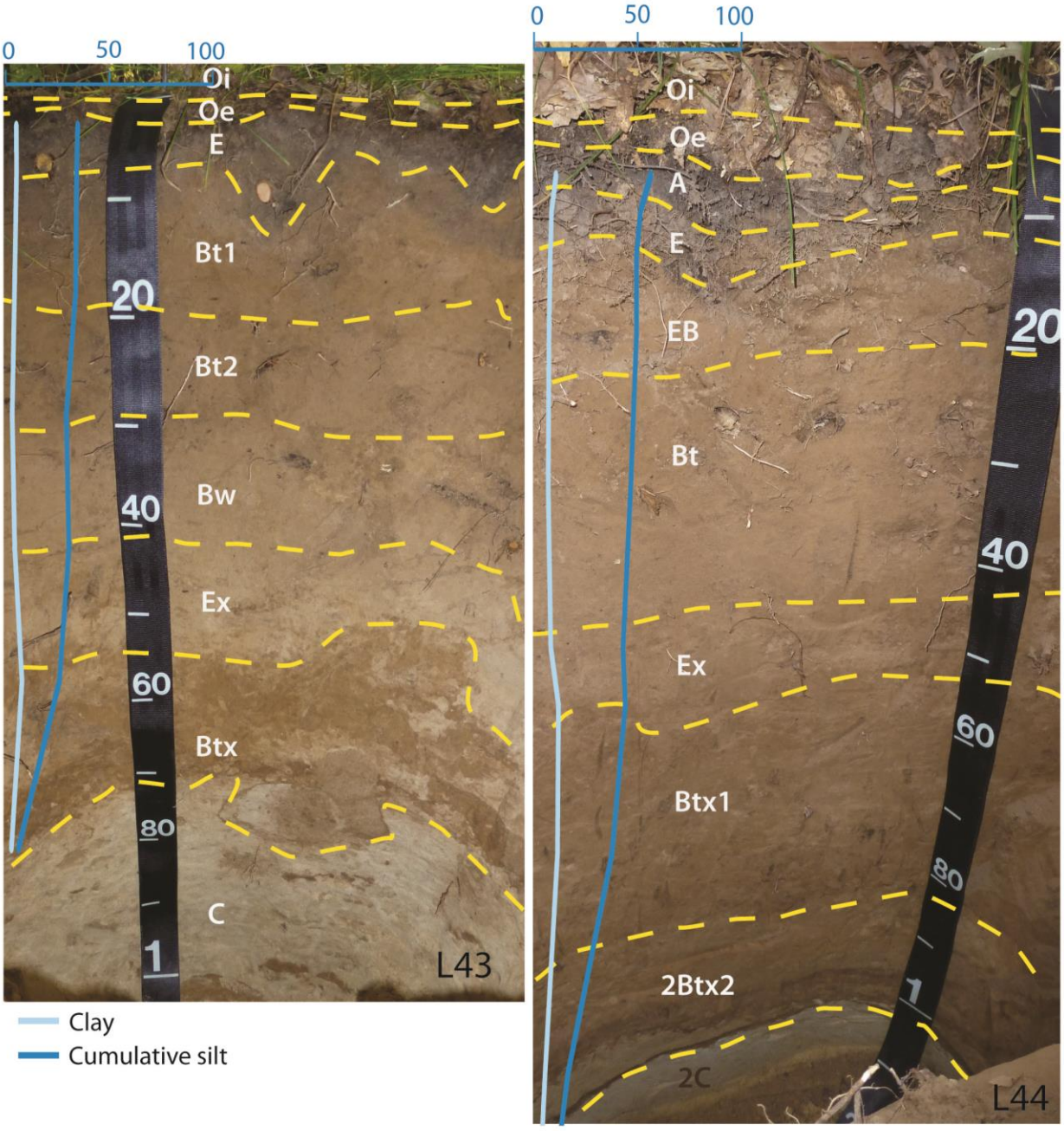


**Figure 3.3:** Photographs of upper footslope (L43) and toeslope (L44) profiles on the lee side of Wildcat Ridge. Cumulative particle size data with depth is overlaid to approximately coincide with the depth shown in the photo. Lighter blue represents clay contents and dark blue represents cumulative silt contents with depth. Both profiles have fragic horizons starting at ~40 cm. Clay and silt are significantly higher in these profiles than in windward profiles. Photos by K. Gruley 2009.

B horizons in lower landscape positions, however, differ based on texture of the parent material. In windward foot and toe slopes, soil profiles in the catena take on a spodic morphology (Figure 3.2), whereas those of lee profiles take on bisequal morphology with an upper E-Bt or E-Bw and lower Ex-Btx sequum in addition to lamellae extending into the upper sandstone residuum (Figure 3.3). Upper Bt horizons in these lower lee profiles tend to be dark yellowish brown (10 YR 4/4) and are 20-30 cm thick out of the 38 cm thick E-Bt sequum thickness. Peds from the upper sequa are often friable. Underlying fragipan horizons have firm, but brittle moist consistence, shattering under pressure. Peds from fragipan horizons often have strong, medium subangular blocky or blocky structure that slake in water. Ex horizons tend to be 5-17 cm thick with light yellowish brown (10 YR 6/4) or pale brown (10 YR 6/3) ped exteriors and dark yellowish brown (10 YR 4/4) ped interiors. Btx horizons are usually yellowish brown (10 YR 5/6) and range between 15 and 35 cm thick in footslope positions and can reach 52 cm thick in toeslope positions. Fragic horizons mostly lack prismatic structure that is commonly noted in fragipans elsewhere (West et al. 1980; Bryant 1989; Habecker et al. 1990; Weisenborn and Schaetzl 2005). Distinct very dark gray or dark brown (7.5 YR 3/3-4) clay films are present in all Btx horizons with flecks of black (7.5 YR 2/1) additionally noted in L44. A thin (1 cm, but can be up to 4 cm) beta Bt lamella occurs at the base of the Btx horizon. Interestingly, Ex horizons are often thicker and better developed in footslope locations (e.g. L43) compared to that of toeslope locations, and conversely, Btx horizons are often thicker and better developed in toeslope positions compared to footslope locations (e.g. L44).

In windward locations, soils show increasing illuvial accumulations of humus and sesquioxides with decreasing drainage. In lower backslope positions e.g. W40, coarse textured soils typically have 6 cm of a Bs horizon underlying a 6 cm AE horizon, approximately 50% of which is clean quartz grains. However, in footslope positions, like site W42, E horizons tend to be approximately 11 cm thick, and can exceed 25 cm in microlows. Although epipedon horizons and underlying B horizons are distinguishable, A, E, and sometimes Bhs horizons have the appearance of bioturbation, likely by citronella ants (*Lasius interjectus*), which are commonly noted in field descriptions. Horizons tend to have a blotchy appearance and boundaries have micro-irregular topography. Bhs and Bs horizons tend to be relatively thin

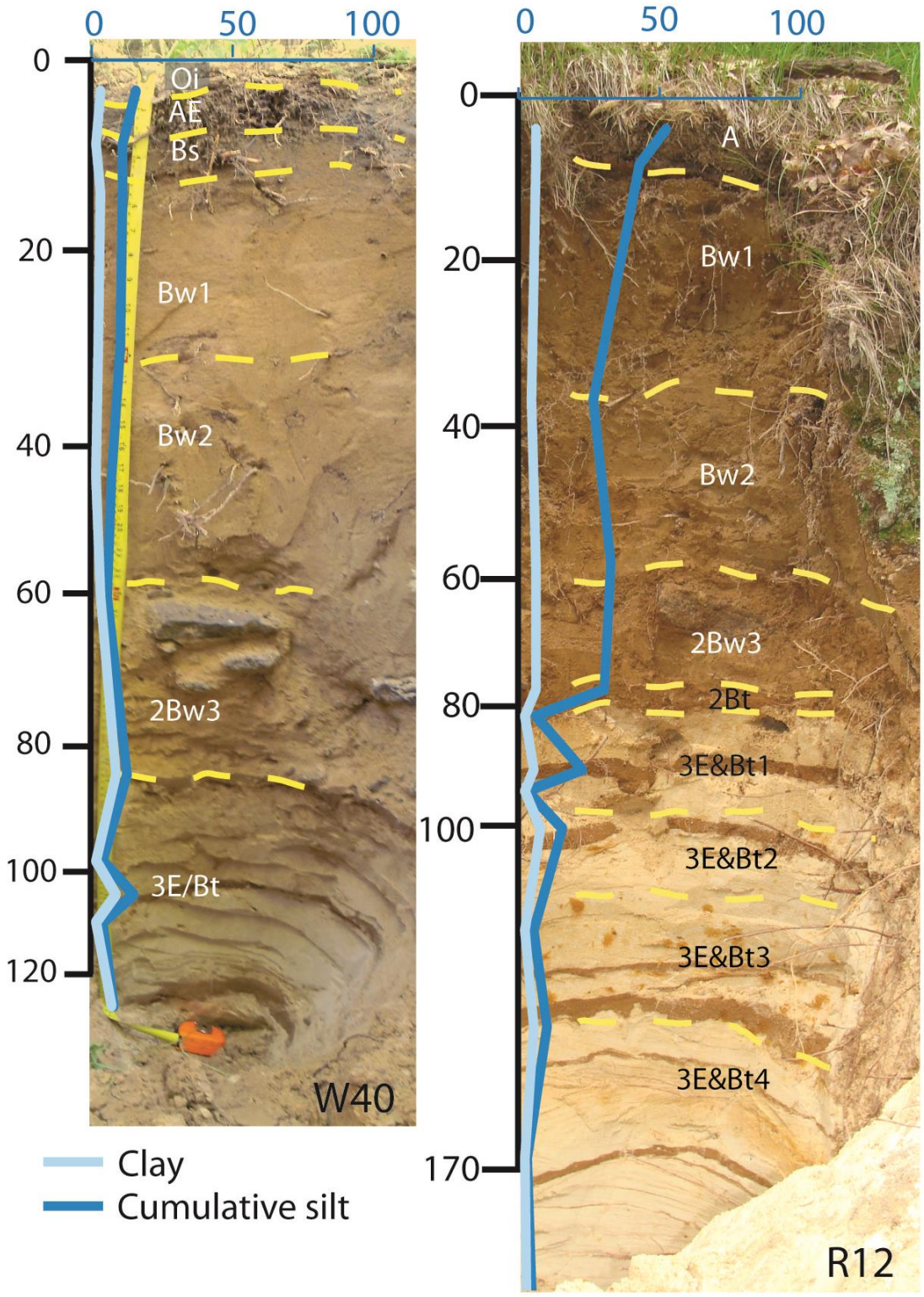


**Figure 3.4:** Photographs of lower backslope profiles in a windward locations (W40) and in a lee position (R12). Cumulative particle size data with depth is overlaid to approximately coincide with the depth shown in the photo. In both profiles, ochric epipedons, cambic horizons, and argillic horizons (lamellae) are present. Lamellae are thicker and better expressed in R12, which has more silt and clay from eolian additions. Photo by K. Gruley 2009.

(approximately 4 cm each), below which is approximately 30 cm of weakly developed B horizons with increasingly prominent and common redoximorphic features. In poorly drained conditions, E horizons exhibit gleyed colors and are relatively thin compared to soils with slightly better drainage. Prominent illuvial accumulations of humus and sesquioxides extend to a depth of approximately 40 cm, and a Bhg' horizon accounts for a secondary accumulation of illuvial humus perched just above gleyed sandstone residuum with shale partings. Relatively thick (16 cm) Bhsm horizons are black to very dusky red (2.5 YR 2.5/1) with firm, large subangular blocky to massive structure, and likely perch water in the upper solum.

**Buried soil**

In one location, L48 a buried soil was described in very firm silt loam between 125 and 131 cm depth underlying friable stratified sand (see Chapter 2 for stratigraphy; ). The matrix of the 5Ab horizon was dominantly dark brown (10YR 4/3), although some areas were dark grayish brown (10YR 4/2). Distinct, coarse light gray (10 YR 7/2) mottles are common. Flecks of organic matter are common throughout buried A and E horizons, which appear to be charcoal and/or coniferous leaves. The underlying E was clear-gradual because of the lighter (light brownish gray, 10 YR 6/2) matrix; however, some areas of dark grayish brown (10YR 4/2) are also visible. Distinct, medium yellowish red (5YR 5/8) iron concentrations were noted in the buried E horizon. Structure in the 5Ab horizon was weak, moderate granular that graded to massive, and in the 5Eb horizon, peds were described as strong, medium angular blocky. Underlying the 5Eb horizon is interpreted to be a 5Bsb horizon between 142 and 153 cm depth in a fine sandy loam strata. The buried B horizon is rich in iron oxides and is dominantly yellowish red (5YR 4/6). Dark reddish brown (5YR 3/3) iron concentrations are medium to coarse and are common. Many fine to medium, spherical black (5YR 2.1/1) Fe-Mn concretions are common in the 5Bsb horizon; a few could also be found in the lower 5Eb horizon. These concretions violently effervesced in the presence of $H_2O_2$. It was difficult to ascertain the structure of the 5Bsb horizon, but it appeared to be

medium, moderate platy structure grading to massive.

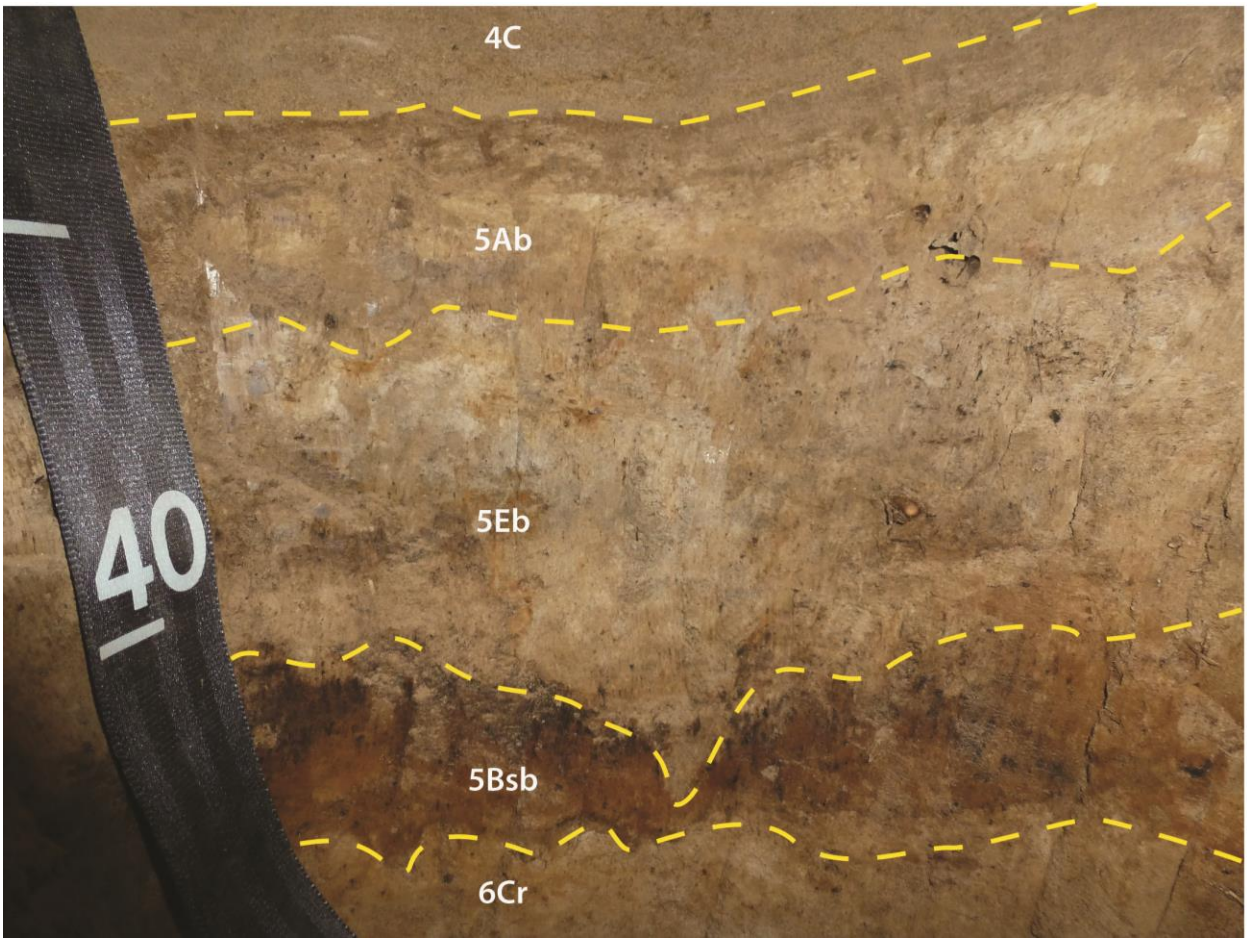


**Figure 3.5:** Close up photograph of the buried soil identified in site L48. Photo by K. Gruley 2012.

The boundary between the stratified sands and the underlying silty buried soil is abrupt. Interestingly, soft sediment deformation features appear within the top of the 5Ab horizon (). Horizontal layers seem to be slightly convoluted, yet not mixed with the overlying stratified sand.

## Profile thickness

Solum thicknesses of the two partial catenas also show differences based on windward or lee location. Sola in windward profiles tend to be the thickest in higher landscape positions, where the sandy eolian mantle is thicker. In lower landscape positions with thinner eolian mantles, sola are thinner due to the influence of a relatively shallow water table. Conversely, sola from lee profiles tend to be thickest in toeslope positions, as compared to lower backslope positions.

**pH**

Soil pH ranges between 5.3 and 3.4 with a mean of 4.2 and CaCl pH is slightly lower, ranging between 4.9 and 3.2 with an average of 4.1 (Figure 3.6). Drainage condition appears to have an influence on overall soil acidity. Backslope soils R12 and W40 tend to have the highest overall soil pH, whereas toeslope sites, W41 and L44, have the lowest overall pH. In the upper solum (>30 cm), pH values for W42 are lower than those of L44 and L48, but become higher than either of these profiles from the Bs horizon down, where mottles become increasingly visible. Windward soil pH is not significantly different from that of lee profiles, however, the depth patterns of pH do show slight differences

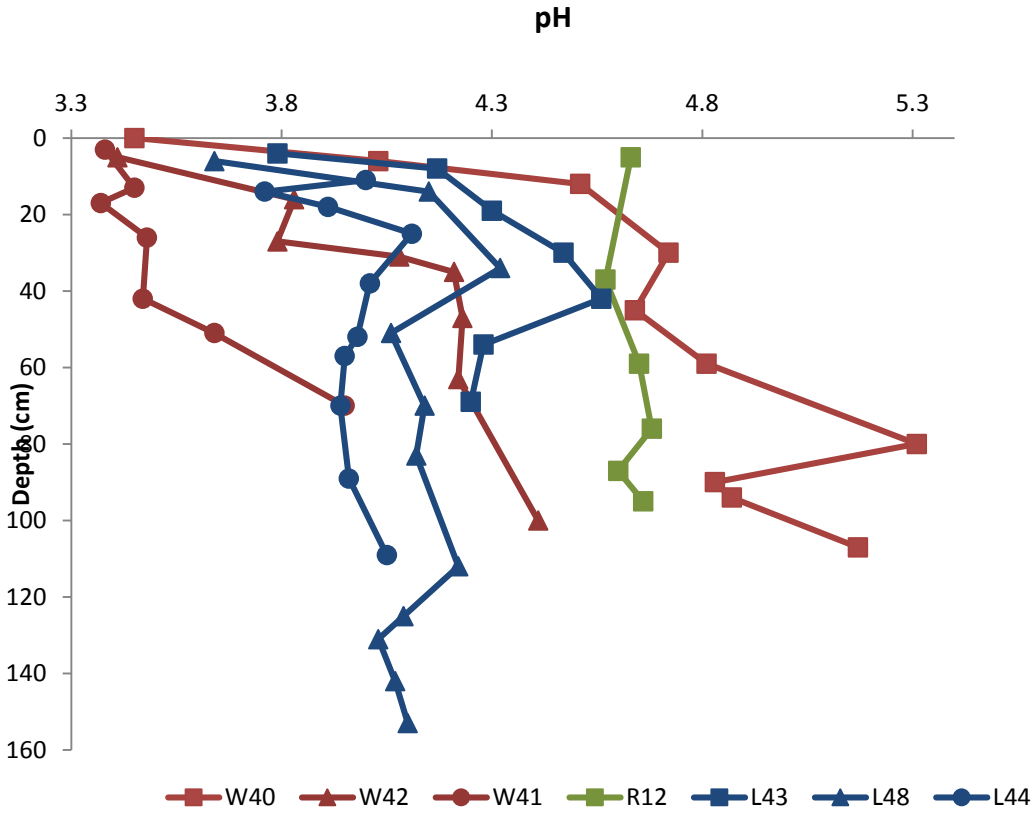


**Figure 3.6:** Depth plot of pH data for windward, ridge, and lee profiles in the study area.

between windward and lee profiles. In windward profiles, pH is generally lowest in the surface (A) horizons, increasing downwards towards the highest measured pH in the bedrock residuum. In lee profiles, the most acidic samples tend to be from E horizons and the least acidic horizons tend to be mid-

profile in an Ex or Bt horizon. For example, L43 shows an increase in pH from 3.79 in the E horizon to 4.56 in the Ex horizon, which is followed by a decrease to 4.25 in the C horizon.

**Clay mineralogy**

Based on X-ray diffraction peaks, the sampled profiles are usually dominated by clays with a 7.2 Å peak (median 40.6%) followed by vermiculite (25.1%) and illite (20.0%) and usually have very low contents of expandable (14.5-18Å) minerals (6.7%) (Figure 3.7). Progressive heat treatments reveal that kaolinite dominates the 7.2 Å peak, with some chlorite present in some samples; kaolinite/chlorite amounts for all samples tend to be the most consistent with depth compared to the other three groups, having the smallest range and standard deviation (data not shown). The majority of expandable clays are interstratified I/S or hydroxy interlayered materials (HIM). Smectite (17.0-18.0 Å) content tends to be a small percentage, averaging 2.6%, with the maximum amounts (24.8%) occurring in sample 5Ab of site L48. Relatively high smectite amounts occur either in the buried soil horizons of site L48, or samples where translocated clay amounts are high, e.g., W40.

Clay mineral percentages between windward and lee profiles are not significantly different (Table 3.1). By far the highest amounts of expandable minerals (14.5-18 Å) occur in poorly drained W41, specifically in Bhg, EBg, and Bhsm horizons (Figure 3.7). Excluding this profile, expandable minerals on average account for less (3.7%) of the total clay mineralogy for windward samples when compared to lee profiles (8.7%) and are highest in the buried soil of profile L48. In most lee profiles, highest concentrations of expandable minerals occur in Bt(x) horizons (~5-10%) with relatively high concentrations also occurring in bedrock residuum samples, particularly in lamellae. Site L44 is an exception, which contains the highest amounts of expandable minerals (17.1%) in the E horizon.

Generally, vermiculite contents are lowest at the base of the profile (~10-20%) and tend to increase towards the surface to ~40-50% in Bw horizons at the expense of illite (Figure 3.7). Illite contents are highest (20-35%) in horizons interpreted to be bedrock residuum. In samples collected from E&Bt horizons, illite is highest in E parts of the horizon and is diluted by relatively increased contents of

vermiculite and expandable clays in Bt lamellae. Most profiles show increased illite content in surface horizons (A and/or E horizons) by ~10-20% compared to underlying Bw horizons. Relatively high illite contents (59.4%) at the surface of L48, however, are probably the result of less-weathered, illite-rich colluvium originating from the Tunnel City group capping Wildcat Ridge.

**Table 3.1:** Difference of means (t-test) and basic statistics for windward vs. lee clay mineralogy.

| | **Exp.** | **V** | **Illite** | **K + C** |
|---|---|---|---|---|
| ***Windward*** | | | | |
| N | 25 | 25 | 25 | 25 |
| Min. | 0.7 | 3.0 | 5.4 | 29.6 |
| Max. | 46.2 | 49.5 | 43.3 | 58.6 |
| Median | 4.3 | 29.7 | 17.2 | 41.6 |
| Mean | 10.6 | 28.7 | 19.0 | 41.6 |
| **SD** | 13.5 | 15.9 | 10.3 | 7.4 |
| ***Lee*** | | | | |
| N | 36 | 36 | 36 | 36 |
| Min. | 0.7 | 4.4 | 8.2 | 26.1 |
| Max. | 20.8 | 53.1 | 59.4 | 49.9 |
| Median | 8.1 | 24.8 | 23.2 | 39.3 |
| Mean | 8.7 | 26.8 | 24.8 | 39.6 |
| **SD** | 5.4 | 10.5 | 11.8 | 6.2 |
| ***t(24)=*** | ***0.907*** | ***-0.235*** | ***-0.677*** | ***0.249*** |
| ***Sig.*** | | | | |

Exp.=expandable clays (14.5-18 Å); V=vermiculite or HI (~14 Å); K=kaolinite, C=chlorite (~7 Å); N= number of samples; min.= minimum value; max.= maximum value, SD = standard deviation; Sig. = significance.
* $p < 0.05$
** $p < 0.01$
*** $p < 0.001$

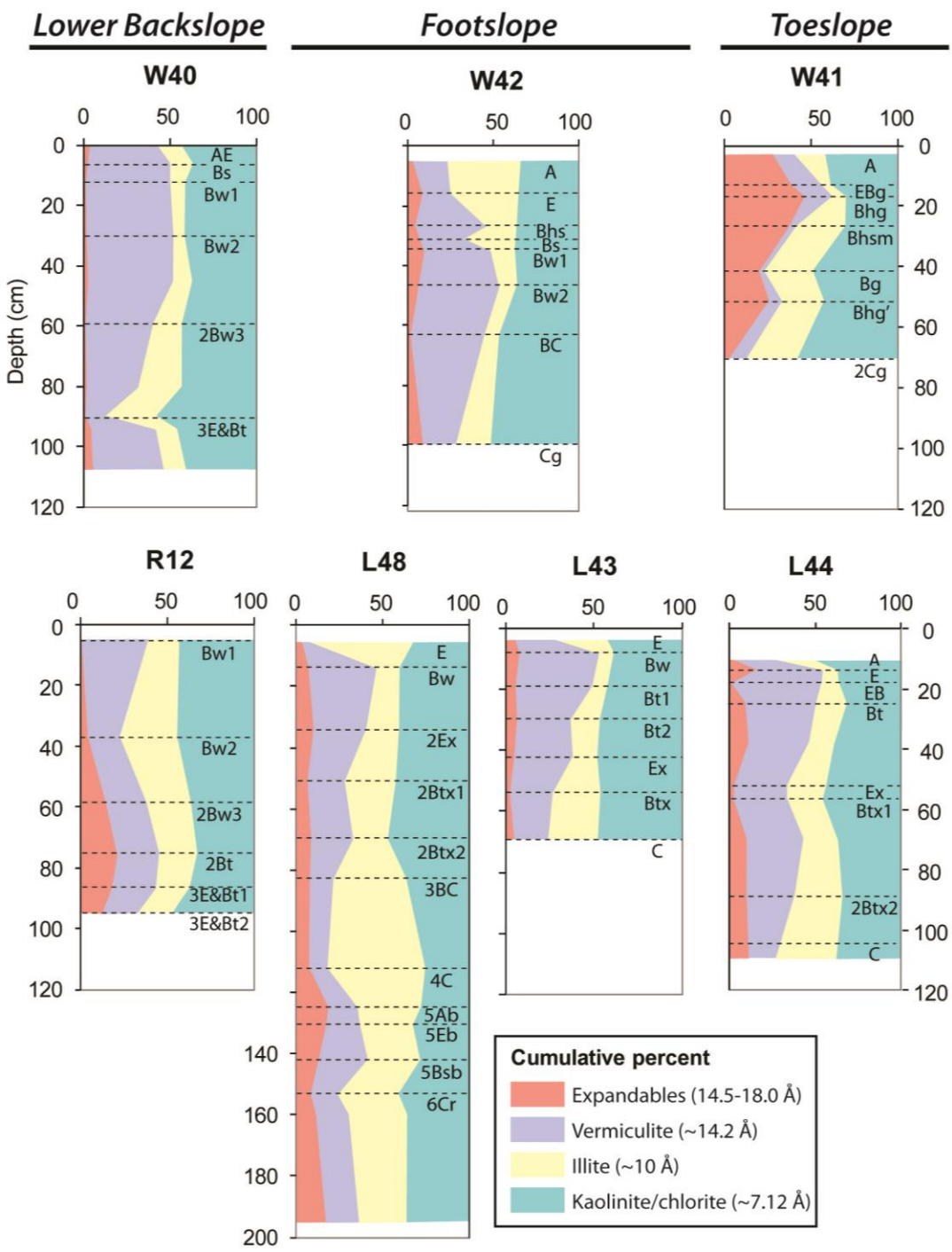


**Figure 3.7:** Semi-quantitative, cumulative XRD clay mineral data with depth for select profiles in central Jackson County. Dark pink colors represent expandable minerals; purple represents vermiculite or HI materials; yellow represents illite contents (~10 Å); greens represent both kaolinite and chlorite contents.

X-ray diffraction reflections with depth suggest clay mineralogy is more complicated than semi-quantitative analysis shows (Figure 3.8). The peak near 10 Å is low and broad, especially in surface horizons, suggesting that most of the illite is poorly crystalized and includes mixed layers. The 10 Å peak tends to increase slightly in height and sharpness with depth, suggesting mixed layer clays increase in illite content with depth. The broad shoulder extending on either side of the 14 Å peak indicates a relatively high amount of randomly interstratified illite/smectite (IS), occurring in varying ratios. Smectite-dominated IS tends to increase with depth; the largest amount occurs in the sample 3E&Bt (Bt lamellae) at a depth of 107-108 cm, which shows a strong, broad peak at ~16.8 Å. In more clay-rich profiles like L44, the >14 Å shoulder increases with depth until it appears as a separate strong, broad peak

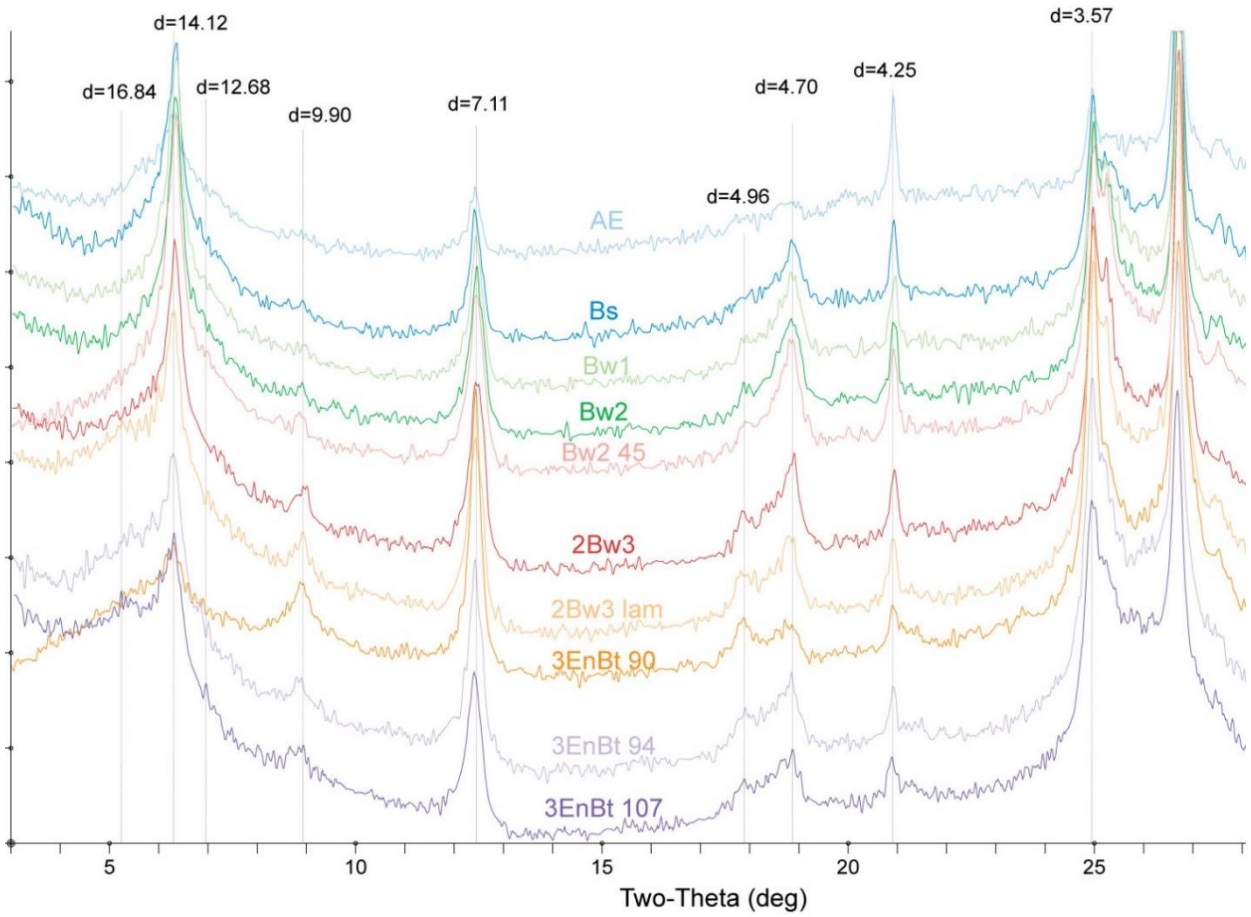


**Figure 3.8:** Stacked XRD scans for profile W40, which contains a relatively low amount of clay. Peak locations are marked in Å.

at ~16.8 Å at 70 cm, which continues to shift towards 17 Å through the 2Btx2 and 2C horizons (not shown).

A very strong, sharp peak at 14 Å occurs in most samples, which remains strong and sharp with K-saturation treatment and shifts towards 13-11 Å with dehydration at 300°C, indicating the presence of a relatively high amount of hydroxyl-interlayered (HI) clays (Figure 3.9). The remaining peak at 14 Å and ~7 Å after the 550 heat treatment reveals that chlorite is present in most well-drained samples, with the exception of surface samples. Chlorite was not identified in any of the samples from W41 (data not shown). Because true chlorite is usually unstable in oxidizing conditions, it is likely peaks identified as chlorite are pedogenically fully hydroxylated HIV minerals.

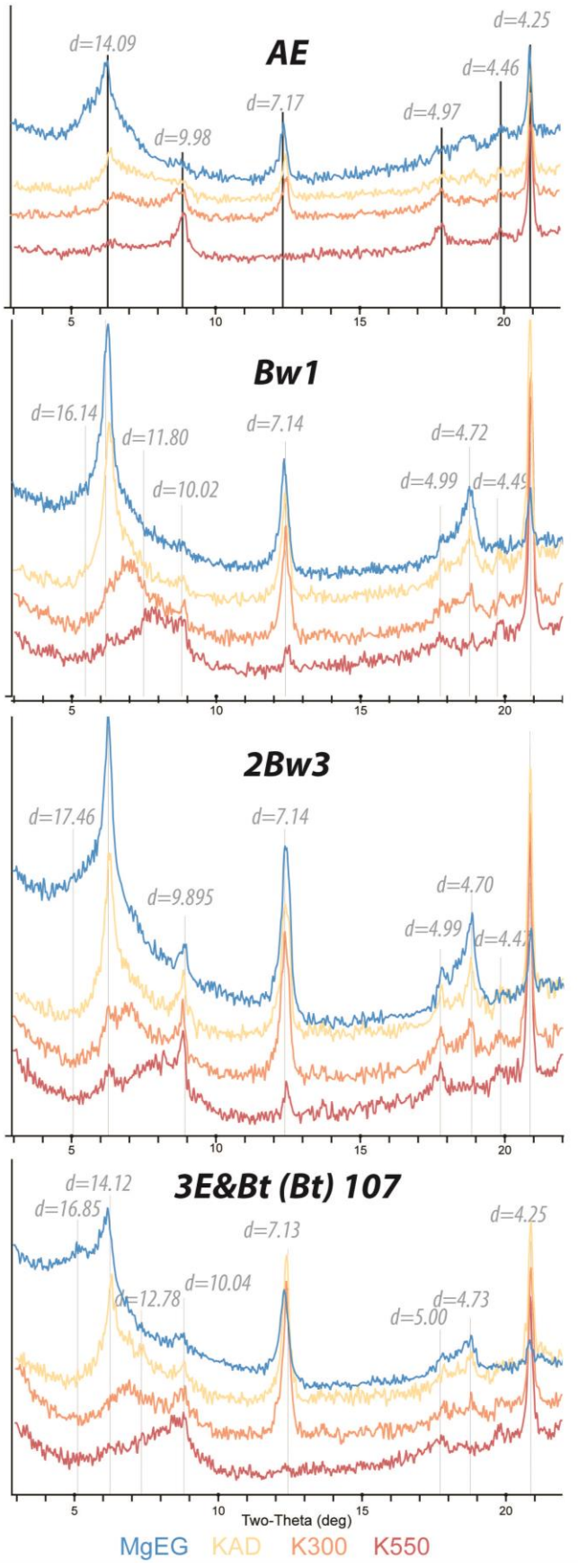


**Figure 3.9:** XRD clay mineralogy scans for four horizons selected from site W40 stacked according to treatment. Blue lines show samples that were Mg-saturate and treated with EG. Yellow lines show K-saturated, air-dry samples; oranges lines show K-saturated samples after 300°C heating for 2 hours; red lines show K-saturated samples after 550°C heating for 2 hours.

### *Discussion*

Both windward and lee epipedons show interesting and unexpected patterns in central Jackson County. First, relatively thick O horizons and thin to absent A horizons are normally associated with coarse textured soils and acidic, coniferous vegetation. It is unclear why coarse textured windward soils with spodic morphology have relatively thin O horizons and thick A horizons when compared with finer textured soils on the lee side of Wildcat Ridge. Bioturbation of the litter layer with top mineral soil by citronella ants, among other soil fauna, is one probable explanation. This bioturbation explanation is supported by C:N data (see chapter 4) that shows A horizons from windward profiles are less decomposed, having higher C:N values (~19-22) compared to surficial mineral horizons from lee profiles (C:N ~ 11-14).

Second, finer textured lee profiles are mapped as Mollic Hapludalfs (Langton and Simonson 1998), which should have relatively thick A horizons, yet profiles and test holes investigated in this study revealed relatively thick O horizons and largely absent A horizons. More work needs to be done to assess the spatial variability of O and A horizon thickness and characteristics in these finer textured soils. The lack of A horizon development suggest little bioturbative mixing between organic and mineral horizons in lee profiles. In addition, the relatively thick O horizons in lower positions on lee aspects may be the result of common deciduous vegetation in lee locations and additional leaves blown in from upland sites (Frolking 1982). The weakly developed A horizons in lee locations are typical of southern xeric forests in Wisconsin (Curtis 1971), because oak leaves are deficient in Mg and Ca, and thus, biocycling of these nutrients is slower compared with that of other deciduous vegetation (e.g. maples).

Although lee profiles appear to increase in thickness downslope, which is consistent with evidence cited in other catena studies to suggest hillslope erosion, the absence of cumulic A horizons argues against that interpretation. The thickness of the litter layer likely absorbs impact of even heavy rain and thus, little long-term erosion is expected in similar lee locations.

The patterns of sequa thickness and development downslope in both coarse windward and silty lee catenas are similar. Footslope positions in both windward and lee catenas show better developed and

thicker E and Ex horizons, respectively, than coupled illuvial horizons downslope. Conversely, toeslope positions exhibit thicker and better developed B horizons with illuvial sesquioxides and humus in windward profiles and Btx horizons in lee profiles.

These results suggest that lateral, i.e., interpedon (Sommer and Schlichting 1997), translocation of soil materials is an important process in this landscape (Figure 3.10). In this process, soil plasma (e.g., water, clays, solutes, organics) is translocated downslope via subsurface throughflow (between pedons) and illuviated in lower slope positions (Sommer et al. 2000; Sommer et al. 2001). Aluminum oxides may also be more common in solution in upslope profiles since pH tends to be higher in these locations implying more Al buffering may occur there. In this case, clay, iron oxides, and presumably soluble silica and aluminum are removed from upper positions in the catena (e.g., L43) and deposited in the B horizons of lower landscape positions (e.g., L44). Conversely, the upper sequum in lee profiles, which

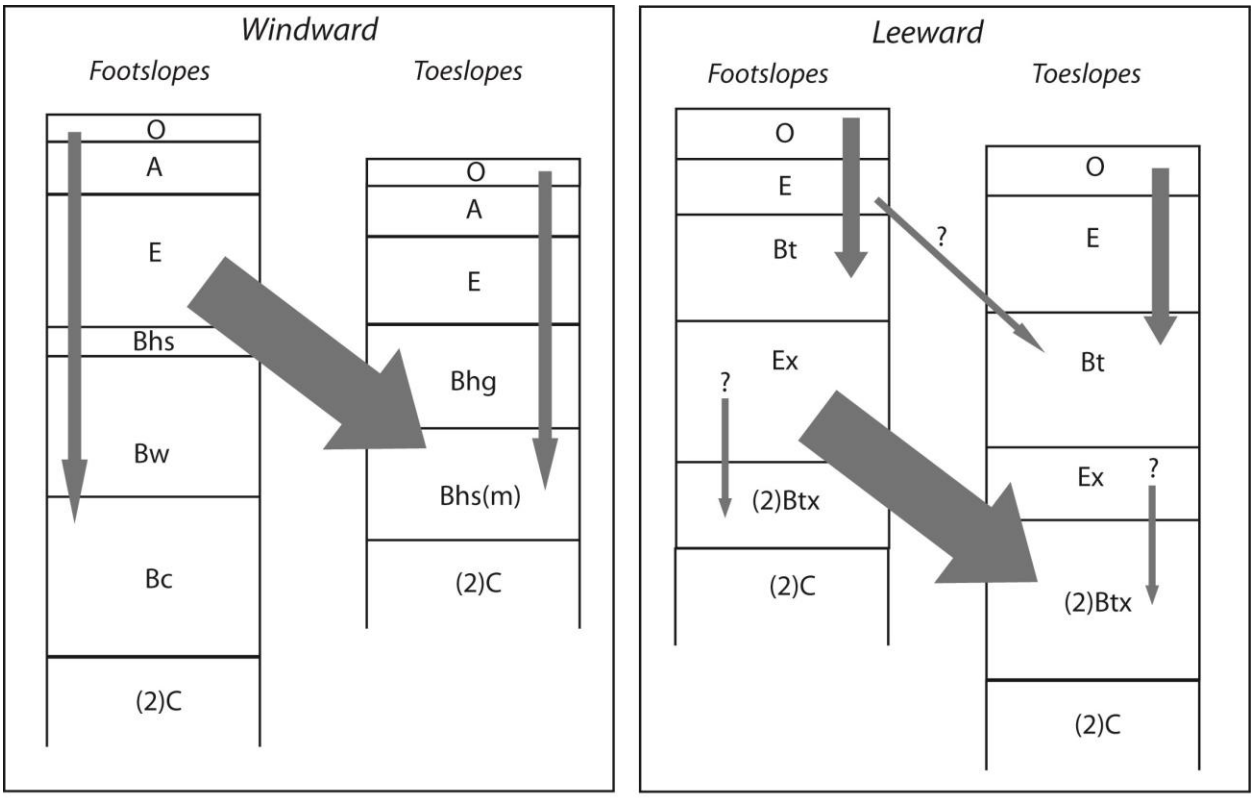


**Figure 3.10:** Conceptual diagram illustrating translocation in lower landscape positions for sandy windward and silty leeward catenas. Gray arrows represent qualitative estimates of vertical and lateral translocation. Translocation arrows are not necessarily representative of synchronous processes, rather processes operational at some point during the entire duration of pedogenesis. Boxes represent thickness estimates for horizons in each catena position shown (not to scale). After Sommer et al. 2001, Sommer et al. 2002).

also consists of E-Bt horizons, is thicker and better developed in toeslope positions (e.g., L44) compared to upslope positions (e.g., L43). This pattern where thinner and less developed E and Bt horizons occur upslope from thicker and more well developed E and Bt horizons on toeslopes suggests this upper sequum is probably formed primarily by vertical (intrapedon) translocation of clay. In other words, the upper solum on lower slopes experiences more vertical percolation of water, which enhances both the eluvial and illuvial horizons compared to upslope positions. This suggests that some water does move downslope as overland flow, even if it does not move much soil with it, resulting in less infiltration and percolation higher in the catena and more in lower catena positions. The depth of an upper Bt horizon is usually coincident with the average depth of infiltration over the course of the year (Schaetzl and Anderson 2005, p. 366).

It is unclear if the Btx horizon in lee profiles formed initially under dominantly vertical or lateral translocation. Btx horizons are consistently just above the lithologic discontinuity between the silty/loamy mantle and the underlying sandy bedrock residuum. This lithologic discontinuity would have initiated Bt development as water moving through the soil would perch in the finer sediment until saturation was achieved allowing gravitational movement of water into the coarser bedrock residuum below. This process is common where vertical translocation is assumed. However, the base of the Btx horizon appears to be darker and thicker (more clay rich) in lower landscape positions compared to just upslope (Figure 3.3), and expandable clay minerals, especially finer and more mobile smectites are more abundant in the lower profiles of lower landscape positions (Figure 3.7). These data suggest that lateral translocation processes may be at least partially responsible for Btx development in this landscape.

Regardless of whether Btx development was primarily via lateral or vertical translocation, the presence of a second E-Bt sequum in these soils is probably due to maximum infiltration events—likely those associated with spring snowmelt (Schaetzl 1992).Soil water containing organic acids moving through these quartz-rich soils would have little to buffer the acidity, i.e., few weatherable minerals could contribute to buffering the soil acidity. This lack of weatherable minerals in combination with organic acids would in effect lower the soil pH (Ross et al. 2008). As a result, soil horizons, especially in the

upper solum, in central Jackson County are highly acidic, which likely means silica and aluminum hydroxides are soluble in this landscape; however, in these sandy soils, Al is mainly complexed to OM rather than being able to buffer acidity, which drives the soil pH even lower (Ross et al. 2008). When arrested, soluble silica, oxides, and clay minerals moving in soil water could precipitate or be deposited at the lithologic discontinuity forming a Btx horizon that grows upward (aggrades) from the discontinuity.

Eventually, a Btx horizon developing in this manner would become thick and well developed enough to begin seasonally perching water, which would then move laterally across the top of the fragipan (Harlan and Franzmeier 1977). In the process, this acidic perched water would leach clays and iron coatings from ped faces leaving an Ex horizon behind. The pronounced degradation of the fragipan in footslope profiles suggest lateral movement of water on the top of the Btx horizons is relatively common in that slope position. Materials removed from Ex horizons in higher slope positions could be deposited in toeslope positions, enhancing the Btx horizon in toeslope soils.

Lateral podzolization appears to be a process that works on windward slopes as well. E horizons of toeslope soils, e.g., W41, are relatively thin whereas E horizons from upslope positions, e.g., W42 are much thicker and better developed. Conversely, illuvial horizons appear to have accumulated far more humus, sesquioxides, and expandable clays on toeslopes as compared to upslope profiles. This pattern is similar to the work of Sommer et al (2001) who found thinner eluvial horizons and thicker spodic horizons in lower catena positions in a sandstone landscape in Germany. The relatively thick litter layer and the presence of relatively thin, poorly developed Entisols occurring on higher slope positions suggest decreased infiltration in these higher slope positions compared to lower (foot and toeslope locations). Where water can infiltrate the surface in these acidic soils, it can strip humus, iron, and aluminum coating to be translocated with percolating water flowing according to gravitation. In some cases, Bhs and Bhsm horizons show evidence of silica cementation that may reduce vertically moving water and enhance lateral percolation. More work needs to be done to assess the relative contribution of vertical to lateral translocation in both windward and lee profiles.

Quartz, illite, and IS (70% illite) are the most abundant of the < 2 µm fraction in Cambrian sandstones of the region, with K-feldspar, chlorite, and kaolinite occurring in minor amounts (Emrich 1966; Distefano 1973). Kaolinite in Mt. Simon and presumably Galesville sandstones is authigenic, whereas, in the Eau Claire Formation it is detrital (Distefano 1973). Sandstone residuum and shale samples collected ~30 km north of the study area have clays dominantly composed of illite (67-100%) with some kaolinite in most samples (Stanley 2008b). Because clay mineral assemblages in central Jackson County tend to have much more kaolinite/chlorite and vermiculite/HIM compared to those Cambrian sandstone samples, it is possible the illite in these soils has been diluted by eolian inputs that carried both pre-weathered soil material (e.g., vermiculite/HIM and some expandable minerals) and smectites from western sources, as well as illite and kaolinite from local Cambrian landscapes. The clay mineral assemblages of central Jackson County are fairly similar to loess samples collected ~30 km north in central Clark County (Stanley 2008b).

## *Conclusions*

Silt additions change the pedogenic pathway of soils in this sandy area. Without these silty additions, the sandy residuum and sandy colluvial soils would likely fall on the continuum of podzolization based on drainage. For example, most sandy soils that lack impeded drainage are Entisols showing little soil development. In lower positions on the landscape, sandy soils develop increasing spodic morphology and contain substantial amounts of humus and sesquioxides in poorly drained toeslope positions.

Siltier soils, with greater inputs of reworked loess are still highly acidic and generally unproductive soils; however the pedogenic pathway is shifted from podzolization to lessivage. Bisequal soils with an upper E-Bt and lower Ex-Btx are common in these settings. The increased fine material improves water holding capacity for soils, yet at the same time processes associated with lessivage (and perhaps silica translocation) formed fragipans that limit root growth. Comparisons of sequa

characteristics downslope suggest lateral flow and translocation through both sandy and silty catenas is an important process in this landscape.

# CHAPTER 4 : THE ROLE OF GEOMORPHOLOGY IN SOIL ORGANIC MATTER DYNAMICS WITH DEPTH


## *Abstract*

To determine how silty eolian additions may affect soil organic matter (SOM) dynamics with depth, samples were collected from sandy and silty eolian mantles in central Jackson County, Wisconsin. Soil organic matter samples collected by horizon to a depth of ~ 60 cm were analyzed for C:N, OC%, N%, $\delta^{13}C$ and $\delta^{15}N$ and compared to particle size and clay mineralogy data. SOM from mineral soil samples was compared to modern OM picked out of mineral soil samples, as well as to litter horizons, large roots, and fresh oak leaves and white pine needles. SOM from horizons within 30 cm depth from the surface show increasingly less negative $\delta^{15}N$ and $\delta^{13}C$ as well as increasing C:N values with depth, which are trends that are consistent with increasing levels of decomposition. In silty profiles below eluvial horizons, decomposition patterns appeared as stepped decreases with depth, where decomposition was similar in sets of Bt, Ex, and/or Btx horizons. In these settings, OM sorption to clay minerals that are translocated may protect OM from further decomposition. In sandy profiles, with impeded drainage, podzolization resulted in less decomposed (fresher) DOM protected by organic-mineral complexes (chelation) that is illuviated into subsurface horizons. Weak correlation between OC and silt in windward samples is not evidence of OC binding mechanisms to silt, but rather indicate that relatively high silt and OC contents occur at the surface of these soils, probably through independent processes. These results point to the importance of understanding the geomorphology and sedimentology of soil parent materials in SOM research. Comparisons of trends for samples collected by horizon and those collected by depth increments are different in both range and in some cases direction. This difference is likely the result of horizon mixing during incremental sampling protocols, which can result in incomplete understanding of SOM dynamics. Therefore, SOM sampling with depth should be based on horizonation, rather than uniform depth increments.

## *Introduction*

Soil organic carbon (SOC) is recognized as a major terrestrial carbon sink, and as a result, understanding soil organic matter (SOM) dynamics is increasingly important. Until recently, most of our understanding of SOC dynamics has overlooked the role of geomorphic processes, both erosional and depositional (Rosenbloom et al. 2006). Recent efforts to link SOC dynamics with landscape-scale geomorphic processes have largely focused on how C is eroded and deposited along with sediment, especially when associated with rapid landscape changes due to anthropogenic disturbances (Harden et al. 2002; Rosenbloom et al. 2006; Yoo et al. 2006).

Not only is much of our understanding about SOC dynamics based on implied static soils/landscapes, it also is primarily based on the dynamics of relatively shallow (surface) accumulations of SOM. This bias ignores relatively large accumulations of SOC at depths >30 cm that are common in some landscapes (Stone et al. 1993; Grand and Lavkulich 2011). Carbon stored at depth may be important for at least three reasons: 1) relatively fresh C can be stabilized when dissolved organic matter (DOM) is translocated and precipitated at depth where microbial processes are impeded (Schwendenmann and Veldkamp 2005), 2) the potential for long-term sequestration is high because mean residence times (MRT) at depth are commonly on the order of millennia (Holzhey et al. 1975; Trumbore 2000), and 3) SOC contents at depth can rival that of surface horizons and if the stabilizing mechanisms are altered, e.g., by human disturbance or climate change, this SOC can cycle on annual or decadal timescales (Chaopricha and Marín-Spiotta 2013). In addition, C with long MRT tends to be common in waterlogged soils with nutrient-poor parent materials resulting in large accumulations of subsurface SOC (Buurman and Jongmans 2005), in which case, SOC in these landscapes may provide insight into past climate or vegetation dynamics.

Predicting future SOC dynamics associated with climate change requires understanding of how complex C stabilization mechanisms, ecosystems, and landscapes respond to change (Trumbore and Czimczik 2008). For this reason, it is important to not only analyze how carbon is stored spatially across the landscape and vertically within the soil profile, but also how modern geomorphic processes affect C

storage in these landscapes. However, research suggests modern hillslope processes are often intimately linked to paleogeomorphic processes under different environmental conditions from the present (Ritter et al. 2011, p. 132).

The landscape in central Jackson County, Wisconsin presents an excellent opportunity to investigate how relatively minor loess accumulation during the Late Pleistocene imparts a control on both surface and subsurface accumulation and stabilization of SOC as well as modern geomorphic processes that further affect SOC dynamics.

## *Background*

### Subsurface SOM in Spodosols

Subsurface accumulations of OM in well-drained Spodosols are due to root additions as well as the illuviation of OM and Fe and/or Al. The latter process occurs by 1) chelation, in which metal-OM complexes form near the surface and are mobilized until OM levels increase and force precipitation, or 2) proto-imogolite formation, in which allophane sols precipitate in the B horizon, and are later coated by OM, forming organs—humus rich cutans (Buurman and Jongmans 2005). Chelation and an acidic soil environment, which retard microbial decomposition, result in SOM that tends to be older and have longer residence times in Spodosols compared to non-Spodosols (Holzhey et al. 1975; Sollins et al. 2006). Subsurface accumulation of OM in waterlogged Spodosols tends to result from the precipitation of illuviated DOC (Farmer et al. 1983; Buurman and Jongmans 2005; Bardy et al. 2008). In waterlogged Spodosols, poor drainage and an acidic soil environment should further reduce decomposition rates, resulting in less-decomposed OM accumulating in subsurface horizons, where OM inputs from roots are also less common (Bardy et al. 2008). Thus, subsurface SOM in waterlogged Spodosols is potentially 1) older and 2) less decomposed (i.e. more closely reflects original litter inputs) than in well-drained Spodsols and may present an opportunity to help us understand past environmental changes. At the very least, subsurface SOM in waterlogged soils may provide insight into SOM turnover, carbon sequestration, and possibly soil resilience to climate change.

**Interpretation of Carbon and Nitrogen Isotopes in SOC**

The $^{13}C/^{12}C$ ratio of SOC, generally expressed as $\delta^{13}C$ relative to the VPDB standard, has been used to assess soil processes as well as to understand paleoenvironmental changes, e.g. SOC turnover (Nadelhoffer and Fry 1988) or a shift between C3 and C4 sources (Balesdent et al. 1993). Several factors can influence $\delta^{13}C$ values of SOC. First, the burning of fossil fuels, which are preferentially depleted in $^{13}C$, has decreased atmospheric $\delta^{13}C$ values by -1.3‰ (more negative) in the last 250 years, referred to as the Suess effect (Ehleringer et al. 2000). Second, a shift in $\delta^{13}C$ values may reflect a change in litter input values, e.g. a change from C3 to C4 plants which will lead to less negative $\delta^{13}C$ (Ehleringer and Cerling 2002). Third, OM compounds with different $\delta^{13}C$ values decay at different rates (Balesdent et al. 1993; Ehleringer et al. 2000). Fourth, microbial decomposition results in further fractionation as plant OM is gradually replaced by microbial carbon with less negative $\delta^{13}C$ (Nadelhoffer and Fry 1988; Balesdent et al. 1993). Fifth, pedoturbation of the upper solum could mix older organic matter from greater depths (less negative $\delta^{13}C$) carbon with younger, organic matter (more negative $\delta^{13}C$) from shallower horizons (Nadelhoffer and Fry 1988). In the absence of vegetation change, it is likely that a combination of the other effects, especially decomposition and the Seuss effect, work in tandem to change $\delta^{13}C$ values of SOC (Ehleringer et al. 2000).

In well drained soils, concentrations of organic N and organic C decrease with depth, which is likely a result of 1) progressive decomposition and mineralization with depth, and 2) increasingly lower inputs with increasing distance from the surface (Melillo et al. 1989). Similarly, C:N ratios are often highest at the soil surface, where they reflect those of litter inputs, and decrease with depth, where they approach those of microbial biomass (Melillo et al. 1989). However, as SOM decreases with depth, both $\delta^{13}C$ and $\delta^{15}N$ values tend to increase; a trend that has been explained by a combination of factors described above - most importantly those involved with decomposition and microbial processing (Nadelhoffer and Fry 1988; Melillo et al. 1989; Balesdent et al. 1993; Baldock et al. 1997; Ehleringer et al. 2000). This depth pattern is evident across many environments and soil types including Spodosols, which contain subsurface accumulations of OM (Balesdent et al. 1993).

Deviations from the trend of increasing $\delta^{13}C$ with depth seem to be more elusive, but might be explained by factors involving both vegetation and edaphic characteristics. For example, wet conditions can slow decomposition, resulting in a constant or decreasing depth trend of $\delta^{13}C$ (Deines 1980). In addition, isotopically heavy organic C from the surface can be illuviated to greater soil depths (Volkoff and Cerri 1987). Changes from C3 to C4 vegetation would cause a shift towards more negative $\delta^{13}C$ values with depth (Ehleringer and Cerling 2002), as would a vegetation shift from hardwood to conifer (Buchmann et al. 1997), albeit much less dramatically.

Change in the relative abundance of $^{15}N$, expressed as $\delta^{15}N$, is often used to assess decomposition in soils. In terrestrial systems, soil nitrogen is largely derived from plant material, and in general, $\delta^{15}N$ values in these plants vary due to fractionation of N as nitrate or ammonia is absorbed by the plant (Letolle 1980). Decomposition tends to result in OM preferentially enriched in $^{15}N$ (higher $\delta^{15}N$ values), which can be accelerated by cultivation and enhanced microbial activity (Shearer et al. 1978; Wada et al. 1984). As organic N contents decrease with depth due to an increasing accumulation of decay products, $\delta^{15}N$ values tend to increase (Letolle 1980; Wada et al. 1984). In other words, $\delta^{15}N$ values tend to be inversely related to organic N contents. Depth profiles of $\delta^{15}N$ in grassland and pine forests soils often exhibit an exponential increase with depth, e.g., $\delta^{15}N$ values are lowest at the surface and rapidly increase (become more positive) before leveling off with greater depth (Hobbie and Ouimette 2009). Alternatively, some soil profiles, especially where N is readily available or those with arbuscular mycorrhizal systems exhibit a $\delta^{15}N$ maximum at intermediate depths, surface $\delta^{15}N$ values are lower (more negative), then increase (become more positive) with depth, and finally decrease again with greater depth (Schuur and Matson 2001; Hobbie and Ouimette 2009). The soils with intermediate maxima are likely Spodosols or Andisols (e.g., Schuur and Matson 2001), where decomposition processes result in lower values near the surface, but $\delta^{15}N$ then increases again in illuvial horizons, where organo-mineral complexes protect precipitated DOM from decomposition.

## *Methods*

### Field

See Chapter 3

### Particle size analysis

See Chapter 2

### Clay mineralogy

See Chapter 3

### Carbon and nitrogen analysis

A subset of samples was chosen for stable isotope analysis based on relatively high organic contents determined by visual inspection or based on horizon and depth (e.g., in Ex and Btx). Modern organic materials (i.e. rootlets, seeds, etc.) were removed using sterile gloves and fine tweezers from bulk mineral soil samples; both organics and remaining mineral soil were analyzed for C and N isotopes separately. Mineral soil samples, modern organic materials removed from mineral soil samples, and O horizon material for six profiles as well as white pine needles, oak leaves, and large roots from two locations were weighed into silver capsules and sent to the Stable Isotope Facility at the University of California Davis for stable C and N isotope analysis using a PDZ Europa ANCA-GSL elemental analyzer interfaced to a PDZ Europa 20-20 isotope ratio mass spectrometer (Sercon Ltd., Cheshire, UK). Delta values are expressed relative to the V-PDB (Vienna PeeDee Belemnite) standard for C and air for N, which have a long term standard deviation of 0.2 ‰ for $^{13}C$ and 0.3 ‰ for $^{15}N$.

### pH

Soil pH was measured using 1:1 soil-water and 1:2 $CaCl_2$ solutions using a SB801PI SympHony benchtop pH meter (VWR International, LLC).

### Principle Component Analysis (PCA)

See chapter 2

## *Results*

### Carbon contents and particle size fractions

Relationships between OC[2] contents and particle size fractions including clay, fine silt (2 – 30 µm), coarse silt (30 – 63 µm), and total silt are generally weak, and also differ between windward and lee profiles. For windward profiles, total silt and fine silt were most strongly correlated with OC percentage ($R^2$=0.48) followed by coarse silt ($R^2$=0.36) (Figure 4.1). Clay correlates poorly to OC content ($R^2$ < 0.14), suggesting that sorption of OM to clays is not a dominant control on OC content in these soils. Organic C content of lee profile samples is poorly correlated to all particle size fractions ($R^2$ < 0.2). The correlation of fine silt and total silt with OC contents in

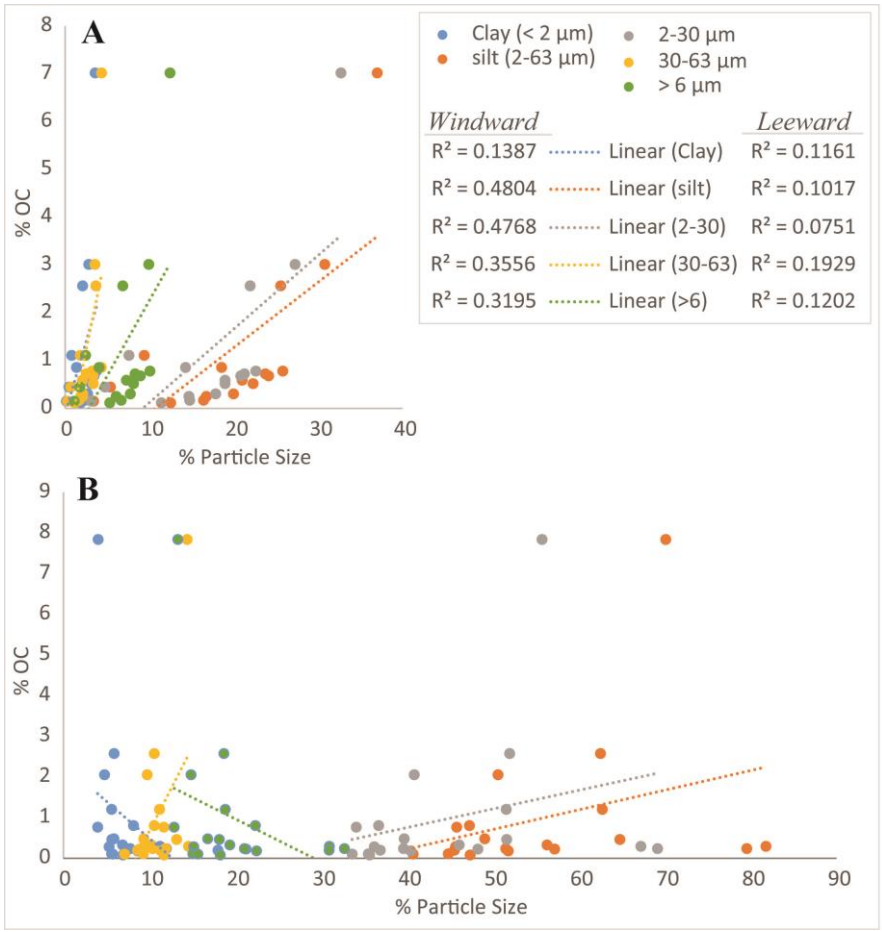


**Figure 4.1:** Organic carbon contents plotted against laser particle size percentage according to particle size factions for **A:** windward samples and **B:** lee samples. Blue dots represent clay (<2 µm); orange dots represent silt (2-63 µm); gray dots represent fine silt (2-30 µm); yellow dots represent coarse silt (30-63 µm), and green dots represent the <6 µm fraction.

[2] Soils in central Jackson county are not calcareous and are acidic (pH generally < 5), thus carbonate pretreatments were not necessary and all carbon contents are interpreted to be organic.

windward profiles may not be related to any direct process link, such as sorption of OM on certain mineral size fractions. Instead, it may be an artifact of the fact that silt in these profiles is greatest at the surface and decreases rapidly with depth, which is what OC content is expected to do in most soil profiles.

### Organic carbon and total nitrogen contents

Organic carbon contents range between 7.84% and 0.08% in mineral soil samples. On average, windward samples tend to have slightly more OC (1.06%) compared to that of lee samples (0.95%); although this difference is not statistically significant, $t(22)=1.067$ (Table 4.1). Depth trends of OC contents do, however, show differences based primarily on soil texture and drainage differences (Figure 4.2). Organic C contents are highest (range 2.5 to 8%) in A horizons, where they presently exist, and generally tend to decrease with depth. Regardless of texture, well-drained soils tend to have OC contents that rapidly decrease from the surface with depth. In silty lee profiles, the depth at which OC contents drop below 0.3% depends on the drainage condition. In toeslope locations, e.g., L44, OC remains above 0.3% at a depth of 52 cm, but in better drained profiles, e.g. L43, OC drops below 0.3 % by 19 cm. L48 has a relatively high amount of OC in the Bw horizon, which may be the result of OC in the silty mantle being mixed with overlying colluvial sediment or translocation of OC in the slightly sandier colluvium. OC contents decrease far less rapidly in silty toe slope positions. The silty buried soil in site L48 also shows increased OC contents between 125 and 142 cm depth (0.29, 0.24, and 0.20% in the 5Ab, 5Eb, and 5Bsb horizons, respectively) compared to 0.08% of the 2Btx2 at 70 cm.

**Table 4.1:** Statistical summary of t-test between windward and lee samples for OC%, N%, C:N, $\delta^{13}C$, and $\delta^{15}N$.

| | **OC%** | **N%** | **C:N** | **$\delta^{13}C$** | **$\delta^{15}N$** |
|---|---|---|---|---|---|
| ***Windward*** | | | | | |
| N of cases | 30 | 30 | 30 | 30 | 30 |
| Minimum | 0.12 | 0.01 | 11.20 | -27.50 | -0.96 |
| Maximum | 7.02 | 0.34 | 31.55 | -25.10 | 6.13 |
| Median | 0.75 | 0.05 | 17.90 | -26.33 | 4.60 |
| Mean | 1.06 | 0.06 | 18.13 | -26.26 | 4.21 |
| Standard Dev | 1.29 | 0.06 | 4.79 | 0.63 | 1.56 |
| Variance | 1.67 | 0.00 | 22.95 | 0.40 | 2.42 |
| ***Lee*** | | | | | |
| N of cases | 23.00 | 23.00 | 23.00 | 23.00 | 23.00 |
| Minimum | 0.08 | 0.01 | 6.06 | -27.27 | 0.45 |
| Maximum | 7.84 | 0.51 | 17.12 | -23.47 | 8.01 |
| Median | 0.38 | 0.04 | 12.20 | -25.05 | 5.78 |
| Mean | 0.95 | 0.07 | 11.36 | -25.29 | 5.56 |
| Standard Dev | 1.63 | 0.10 | 3.25 | 1.07 | 1.88 |
| Variance | 2.66 | 0.01 | 10.54 | 1.13 | 3.52 |
| *t(22)=* | *1.067* | *-0.957* | *5.503* | *-4.434* | *-3.126* |
| *Significance* | | | *** | *** | ** |

OC= organic carbon; N= total nitrogen; C:N=carbon-to-nitrogen ratio; $\delta^{13}C$=relative deviation of $^{13}C$ from standard; $\delta^{15}N$=relative deviation of $^{15}N$ from standard; N= number of samples; min.= minimum value; max.= maximum value, SD = standard deviation; Sig. = significance.
* $p < 0.05$
** $p < 0.01$
*** $p < 0.001$

Sandy profiles with impeded drainage tend to have subsurface accumulations of OC, which is more pronounced with increasingly poor drainage. For example, the Bhs horizon of W42 (Moderately well drained) has 0.78% OC, whereas the Bhsm in the poorly drained W41 has 1.11% OC. Somewhat poorly and poorly drained sandy soils also tend to have a secondary subsurface accumulation of OC near the base of the profile, where OC-rich groundwater saturates the sediment.

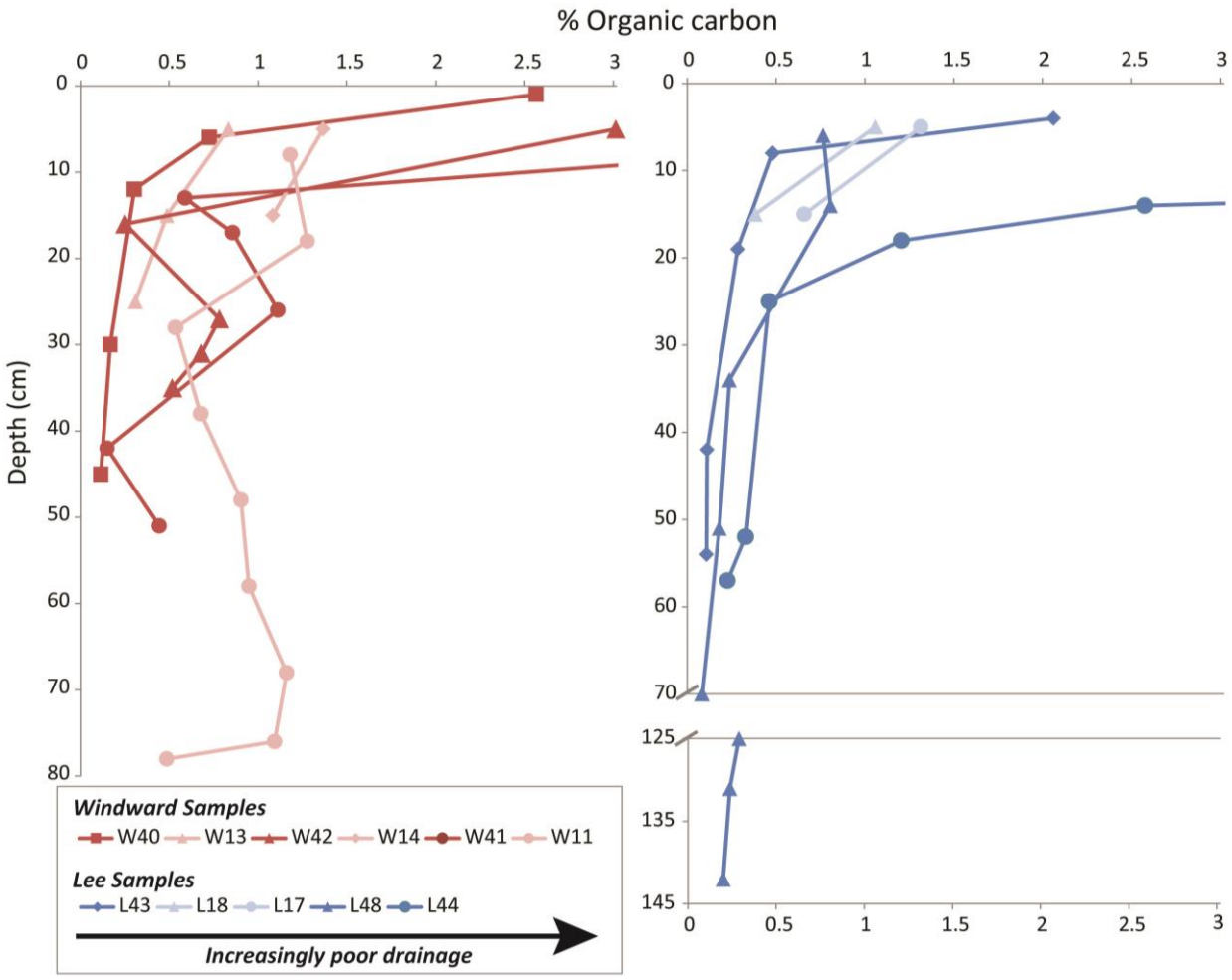


**Figure 4.2:** Graphs showing % OC with depth for windward profiles (left) and lee profiles (right). Red and pink lines represent windward profiles and blue lines represent leeward profiles. Pink and light blue lines illustrate samples collected in 10 cm depth increments using a bucket auger. In order to show more detail with depth, some surface horizon samples have values greater than the graph shows.

Total N contents show similar patterns to OC—highest N contents occur in surface horizons (0.34 – 0.51%), rapidly decreasing with depth (Figure 4.3). Silty lee profiles show nearly identical patterns of differentiation with drainage as OC, as do most windward profiles. The exception to these trends are W11 and W14, which were sampled by auger in 10 cm increments starting at the mineral surface. These

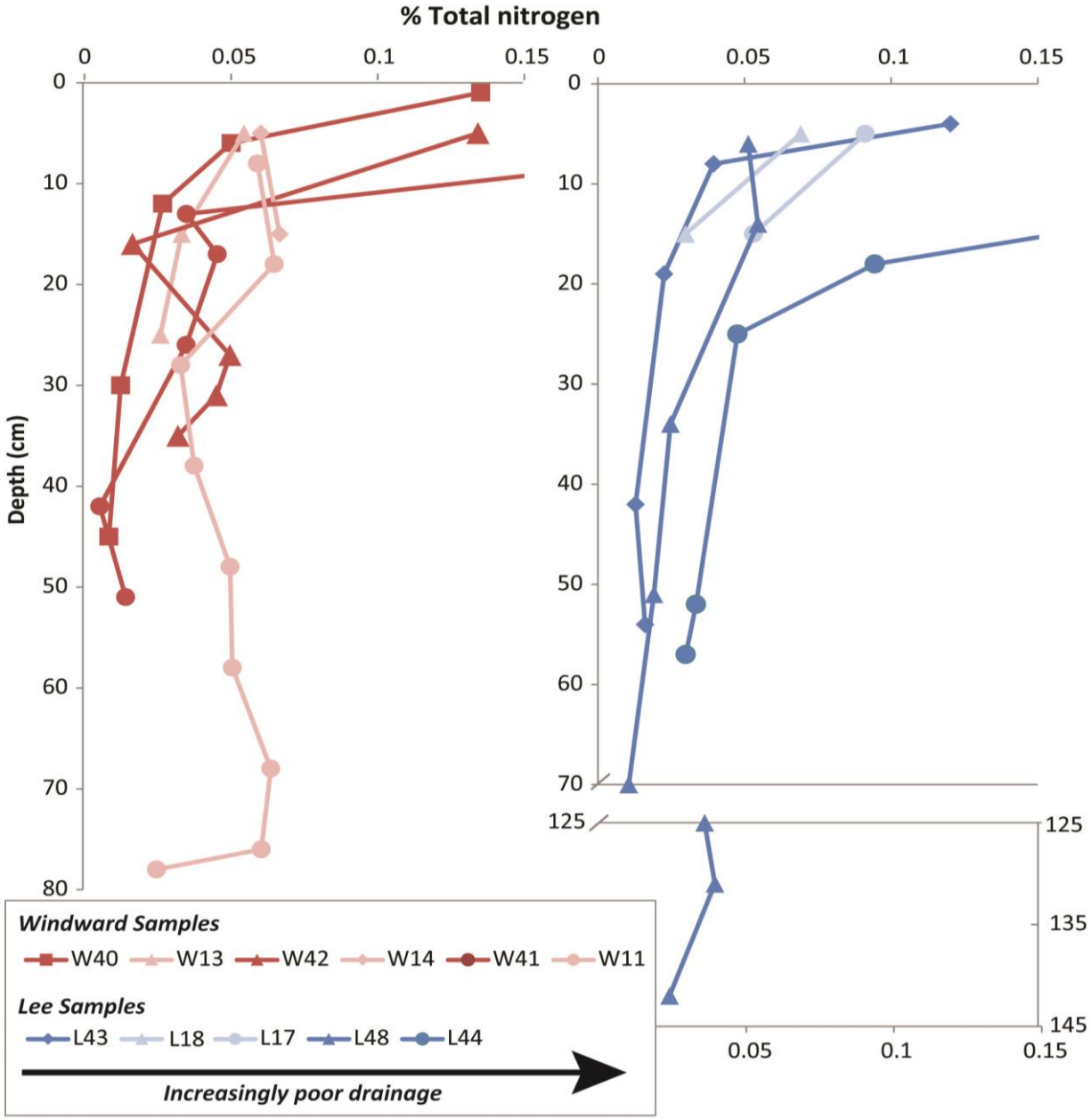


**Figure 4.3:** Graphs showing % total N with depth for windward profiles (left) and lee profiles (right). Pink and light blue lines illustrate samples collected in 10 cm depth increments using a bucket auger. In order to show more detail with depth, some surface horizon samples have values greater than the graph shows.

samples show initial increasing contents from 5 to 15 cm depth, which is probably an artifact of the sampling protocol. These samples likely represent mixed A and E horizons at ~5cm and E and Bhs(m)/Bs horizons at 15 cm.

### Carbon-to-nitrogen ratios

Generally, carbon-to-nitrogen ratios (C:N) are lower for mineral soil samples than for sample OM removed from mineral soil samples[3], litter layer samples, larger roots, and fresh leaves. C:N values for mineral soil samples are significantly lower than those from the litter layer, $t(8)= -2.645$, $p < 0.05$ as well rootlets, $t(30)= -8.47$, $p < 0.001$ (Table 4.2). OM in the mineral fraction would probably be significantly different from larger root samples and possibly fresh leaves if compared with a larger number (n>2) of samples.

**Table 4.2:** Statistical summary for t-test comparing SOM from mineral soil samples to rootlets, O horizon material, larger roots, and fresh leaves.

| | **Mineral soil** | **Sample rootlets** | **O horizons** | **Larger Roots** | **Fresh Leaves** |
|---|---|---|---|---|---|
| N | 53 | 31 | 9 | 2 | 2 |
| Min. | 6.1 | 19.8 | 15.7 | 34.8 | 14.3 |
| Max. | 31.5 | 87.6 | 31.7 | 67.7 | 27.0 |
| Median | 14.9 | 40.8 | 23.8 | 51.2 | 20.7 |
| Mean | 15.2 | 44.0 | 23.8 | 51.2 | 20.7 |
| SD | 5.4 | 15.1 | 5.3 | 23.2 | 9.0 |
| *t=* | | *-8.47* | *-2.645* | *-1.849* | *-0.985* |
| *One-tailed sig.* | | *** | * | | |

N= number of samples; min.= minimum value; max.= maximum value, SD = standard deviation; Sig. = significance.
* $p < 0.05$
** $p < 0.01$
*** $p < 0.001$

[3] Most, but not all, of the modern OM removed from the mineral soil samples were rootlets, for the sake of simplicity in presenting and discussing, these samples will be referred to as 'rootlets' and SOM remaining in the soil sample will be referred to as 'mineral soil samples' for the remainder of this document.

As expected, these data suggest OM associated with the mineral soil samples is more decomposed than the OM of modern rootlets, litter, and other fresh potential OM sources. In comparing C:N values between windward and lee samples, modern rootlets from windward samples are not significantly different from those of lee samples. However, SOM from mineral soil samples from windward locations has significantly higher C:N than that of lee samples, $t(21)= 5.875$, $p < 0.001$, which suggests mineral soil OM in lee profiles is more decomposed than that of windward profiles (Table 4.3).

**Table 4.3:** Statistical summary of t-tests of mineral-associated SOM and picked out SOM between windward and lee profiles.

| | **Mineral soil** | **Sample rootlets** |
|---|---|---|
| ***Windward*** | | |
| N of cases | 30 | 16 |
| Minimum | 11.2 | 29.7 |
| Maximum | 31.5 | 72.7 |
| Median | 17.9 | 36.6 |
| Mean | 18.1 | 40.1 |
| Standard Dev | 4.8 | 10.9 |
| ***Lee*** | | |
| N of cases | 22 | 15 |
| Minimum | 6.1 | 19.8 |
| Maximum | 17.1 | 87.6 |
| Median | 11.0 | 46.6 |
| Mean | 11.2 | 48.3 |
| Standard Dev | 3.3 | 18.0 |
| *t=* | *5.875* | *-1.512* |
| *df* | *21* | *14* |
| *Significance* | *** | |

N= number of samples.
* $p < 0.05$
** $p < 0.01$
*** $p < 0.001$

C:N ratios for SOM from mineral soil samples tend to be highest in the surface horizons (17.1 – 22.4), which is slightly lower than C:N values in overlying organic horizons (15.7 – 31.5). Soil C:N decreases with depth in near-surface horizons (< 15 cm depth), regardless of windward vs. lee location,

reflecting a transition from less decomposed to more decomposed OM (, Figure 4.4). However, distinct differences between windward profiles and lee profiles are readily apparent in subsurface horizons. After the initial rapid surficial decrease in C:N, lee profiles tend to have at least one or two stepped decreases separating sets of horizons with similar values. For example, C:N values are approximately the same (~12.5) for the Bt1 and Bt2 of L43 and ~9.7 for the Bt and Ex horizons of L44. Similarly in profile L48, C:N is ~14.8 for the E and Bw horizons before decreasing to ~9.5 in the 2Ex and 2Btx1 horizons. The lowest C:N values (~7) in lee profiles occur in the deepest samples analyzed, from the lowermost Btx horizons. Interestingly, the buried soil of L48 has C:N values that are slightly higher (~8.2) in the 5Ab and (8.35) in the 5Bsb horizons compared to 7.8 in the 2Btx2 (70 cm) and 6.1 in the 5Eb horizons.

C:N ratios in windward profiles decrease rapidly from the surface until the E (or Bw1) horizon, where they are lowest (between ~11 and 16). Below these eluvial horizons, C:N values increase slightly (by ~2) with depth in better drained profiles, e.g., W 40 and W42 (Figure 4.4). In poorly drained soils, i.e., W41 and W11, C:N values increase to at least the same as the surface values, if not even higher. The apparent difference between site W11 and W41 is probably the result of different sampling strategies. Because W11 was sampled in 10 cm increments, many of the distinctions apparent in horizon-based sampling of W41 are blurred. Regardless, the relatively high C:N values in these subsurface horizons represent less decomposed OM stored there.

In contrast to the overall decreasing values of C:N in most profiles, rootlets and other coarse organics picked out of soil samples increase in C:N value with depth, which is in part, a function of decreasing inputs of surface litter with depth and increasing fine rootlets/hairs (Figure 4.5). Only in the poorly drained windward W41 site do C:N values increase with depth and become closer or equal to rootlet C:N values for the horizon. In fact, the C:N values of mineral soil samples for horizons below 26 cm depth (Bhsm – Bhg′) are higher than the C:N values for horizons above 26 cm, which suggest OM at depth is fresher (less decomposed) than surface OM.

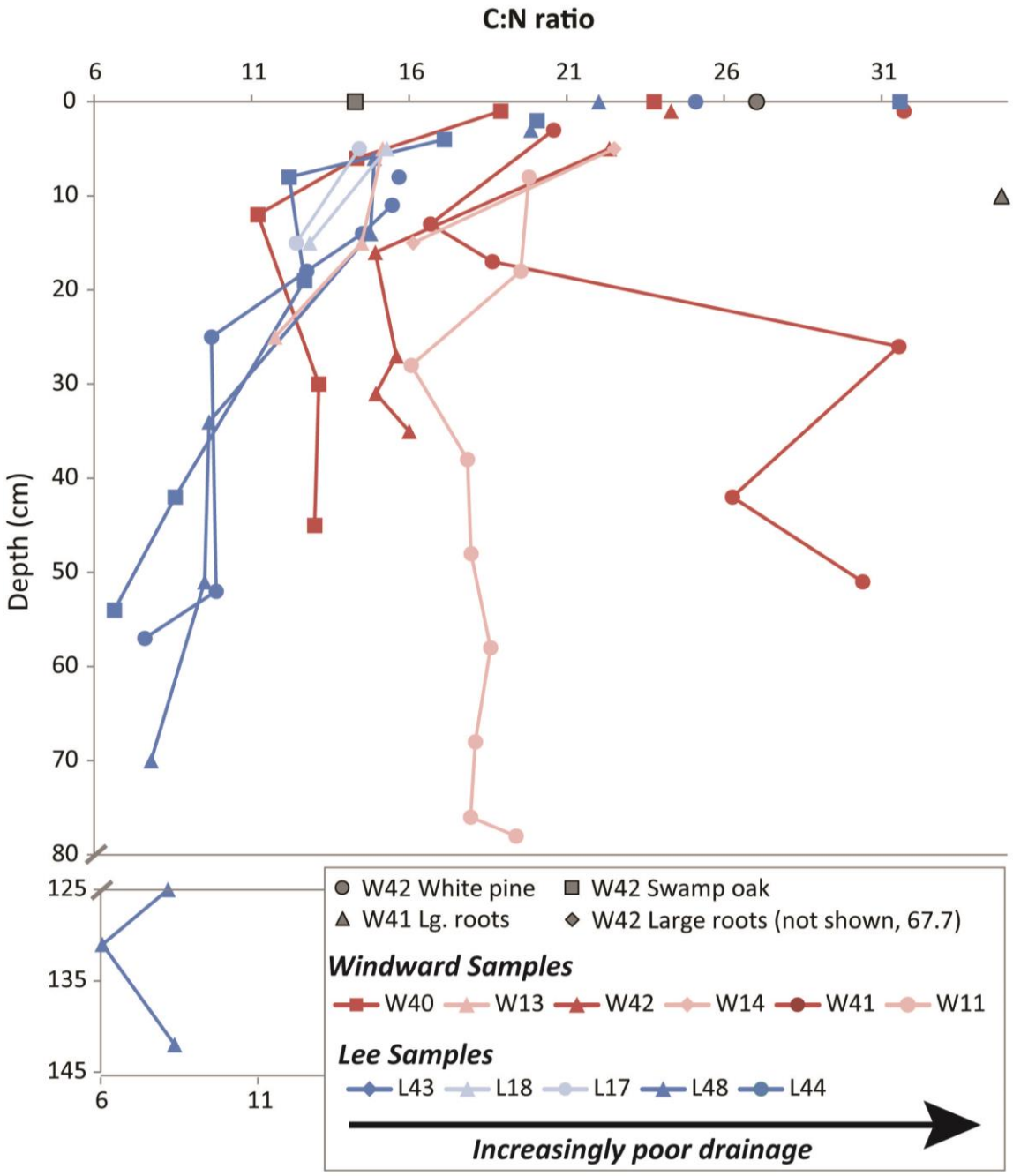


**Figure 4.4:** Depth trends of C:N values for windward profiles (red) and lee profiles (blue). Connected lines signify SOM from mineral soil samples, whereas disconnected points signify O horizon samples. Fresh organic matter samples are shown by gray circles (white pine leaves), gray squares (oak leaves), gray triangles (large roots from W41), and gray diamonds (large roots from W42). The pink and light blue lines show samples that were collected in 10 cm increments using a bucket auger.

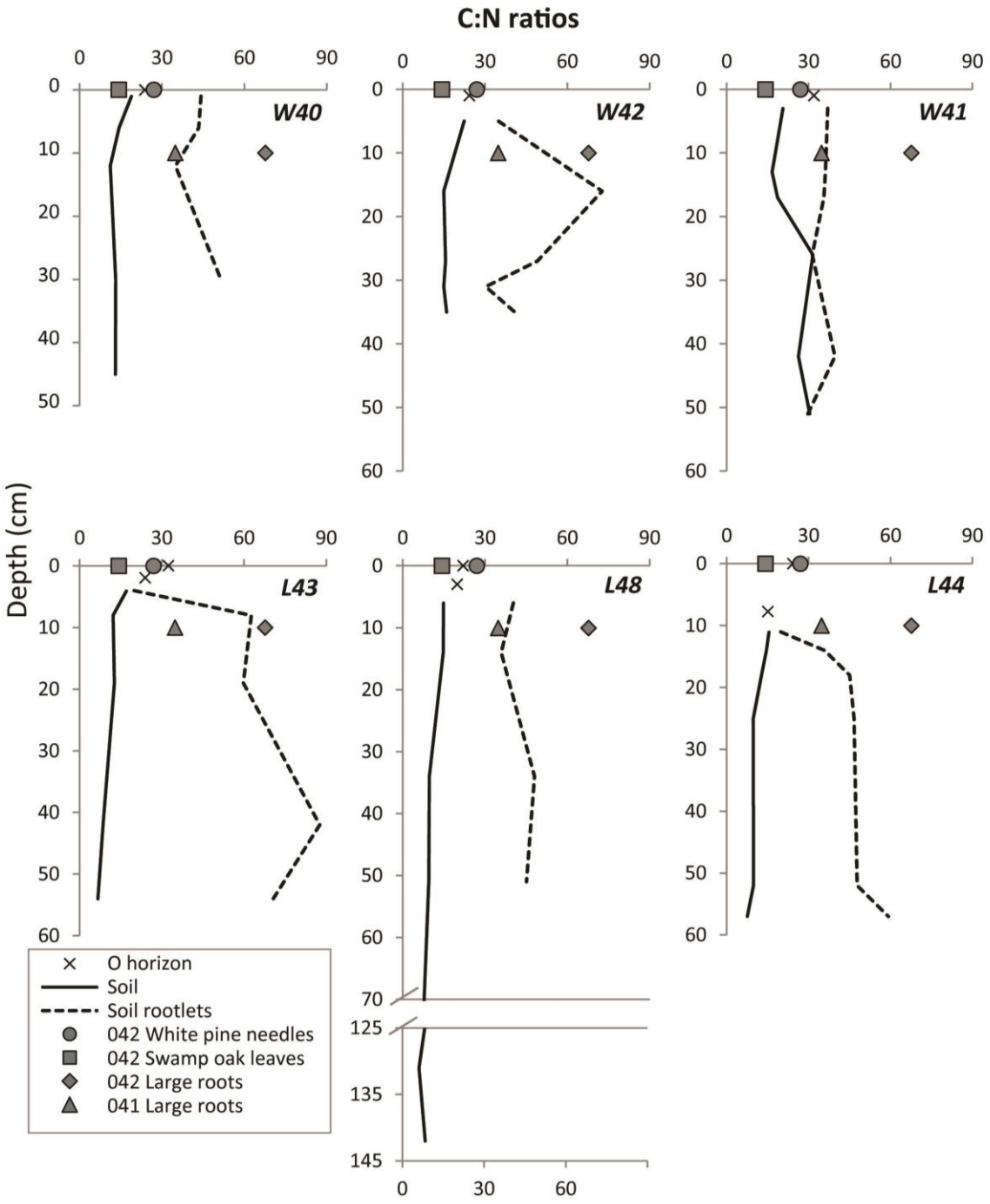


**Figure 4.5:** Depth trends of C:N values for SOM from mineral soil samples (solid line) as well as (dashed line). Disconnected X symbols points signify O horizon samples. Fresh organic matter samples are shown by gray circles (white pine leaves), gray squares (oak leaves), gray triangles (large roots from W41), and gray diamonds (large roots from W42).

**Stable isotopes ($\delta C^{13}$ and $\delta N^{15}$)**

All OM samples have $\delta^{13}C$ values between -29.8 and -23.5‰, which fall within the normal range of C3 vegetation and soil OM derived from it. Soil samples with the most negative $\delta C^{13}$ values occur in the litter layer or at the surface of better drained soils regardless of windward vs. lee position on the landscape (Figure 4.6). For example, the $\delta^{13}C$ of Oi and Oe horizons in site L48 are ~ 29.4‰, relatively rapidly increasing with depth to -25.3‰ in the Bw horizon and increasing more slowly with depth to -24.6‰ in the 2Btx2 horizon. Note, these values are slightly more negative (-24.9‰) in the 5Ab horizon at 125 cm, where they relatively rapidly become less negative with depth in the underlying 5Eb (-24.3‰) and 5Bsb (-23.5‰) horizons. Similarly, the $\delta^{13}C$ of site W40 starts off at -28.3‰ in the Oi horizon and increases to -27.1‰ in the AE and -25.4‰ in the Bw2.

Horizons with illuvial accumulations of OM often exhibit more negative $\delta^{13}C$ values in certain subsurface horizons compared to that of overlying horizons. For example, W42 shows a slight decrease from -25.6‰ in the E horizon to -25.3‰ in the Bhs horizon back to -25.6‰ in the Bs horizon. More poorly drained soils, e.g., W41 and W11 exhibit an overall increasingly negative trend with depth (Figure 4.6). Again, a substantial negative shifts occurs within the Bhg horizon, where values abruptly shift to -27.5‰ from -26.6‰ in the EBg horizon. The relative differences between samples within the same profile are often 1 – 1.5‰ for windward soils, but are often 4 – 6‰ for lee soils. In fact, the $\delta^{13}C$ values of all windward soil samples are significantly more negative, $t(22)= -4.434$, $p < 0.001$, when compared to those of lee samples, which suggests OM in lee profiles, particularly subsoil OM, is more highly decomposed than OM in the subsoil of windward profiles (Table 4.1).

Rootlets are more negative than SOM remaining in mineral soil samples (Figure 4.7). In W41, $\delta^{13}C$ values for rootlet, larger roots, and SOM from mineral soil samples are similar to a depth of ~20 cm suggesting these three groups are similarly processed by microbes and may reflect the same source organic material. In horizons below 20 cm, SOM from mineral soil samples remains slightly less negative whereas rootlet becomes more negative with depth, which is probably the

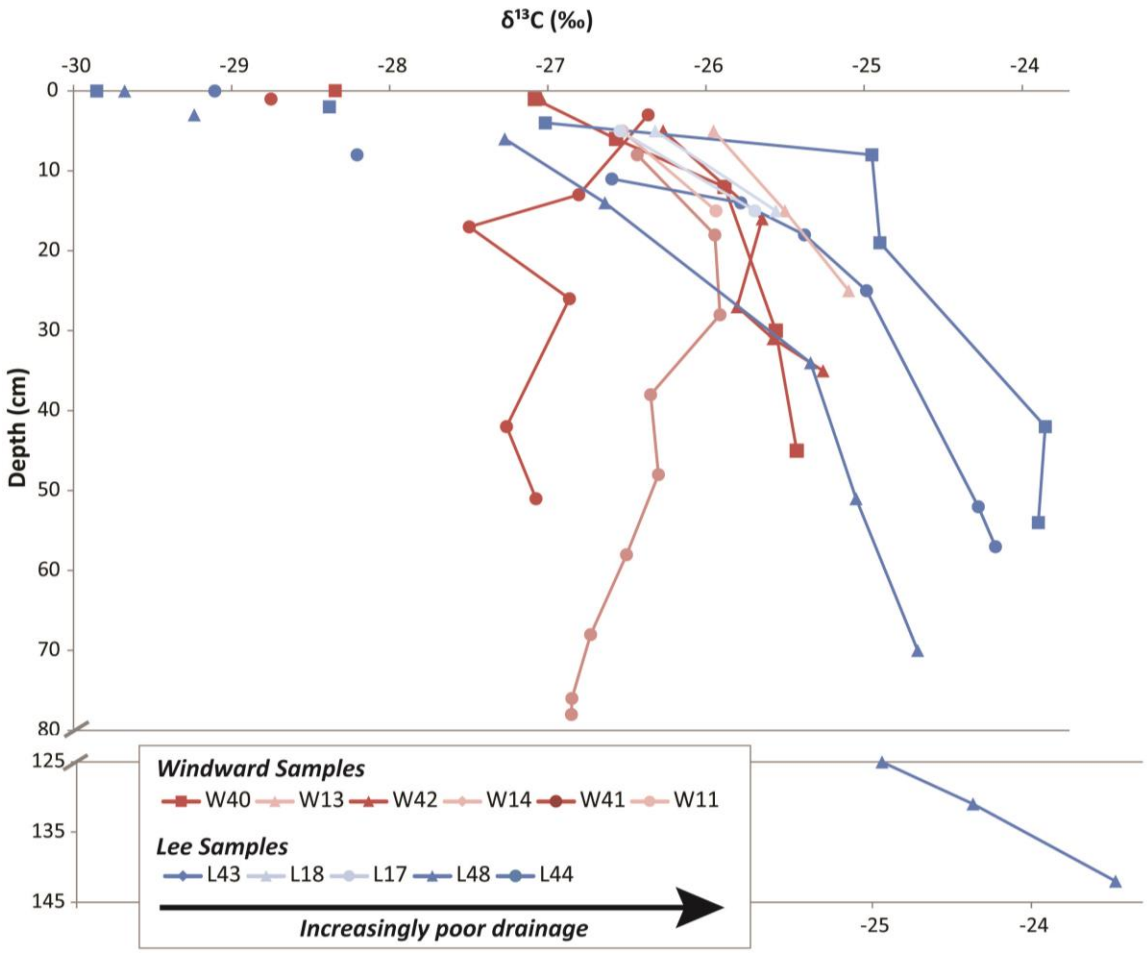


**Figure 4.6:** Depth trends of $\delta^{13}C$ values for windward profiles (red) and lee profiles (blue). Connected lines signify SOM from mineral soil samples, whereas disconnected points signify O horizon samples. The pink and light blue lines show samples that were collected in 10 cm increments using a bucket auger.

result of decreased (more decomposed) surface inputs and relatively more modern (fresh) rootlets with depth. Changes in $\delta^{13}C$ values with depth in these profiles may also reflect changes in rootlet species with depth.

The most negative values for $\delta^{15}N$ occur in litter samples ranging between -5.4 to -0.5 ‰ (Figure 4.8). Values then increase with depth in upper horizons and are mostly positive through the mineral soil. The exceptions to this trend are poorly drained profiles, which have $\delta^{15}N$ values that initially increase with depth until ~15 cm, then decrease again with depth. Notably, W41 shows substantial decreases in

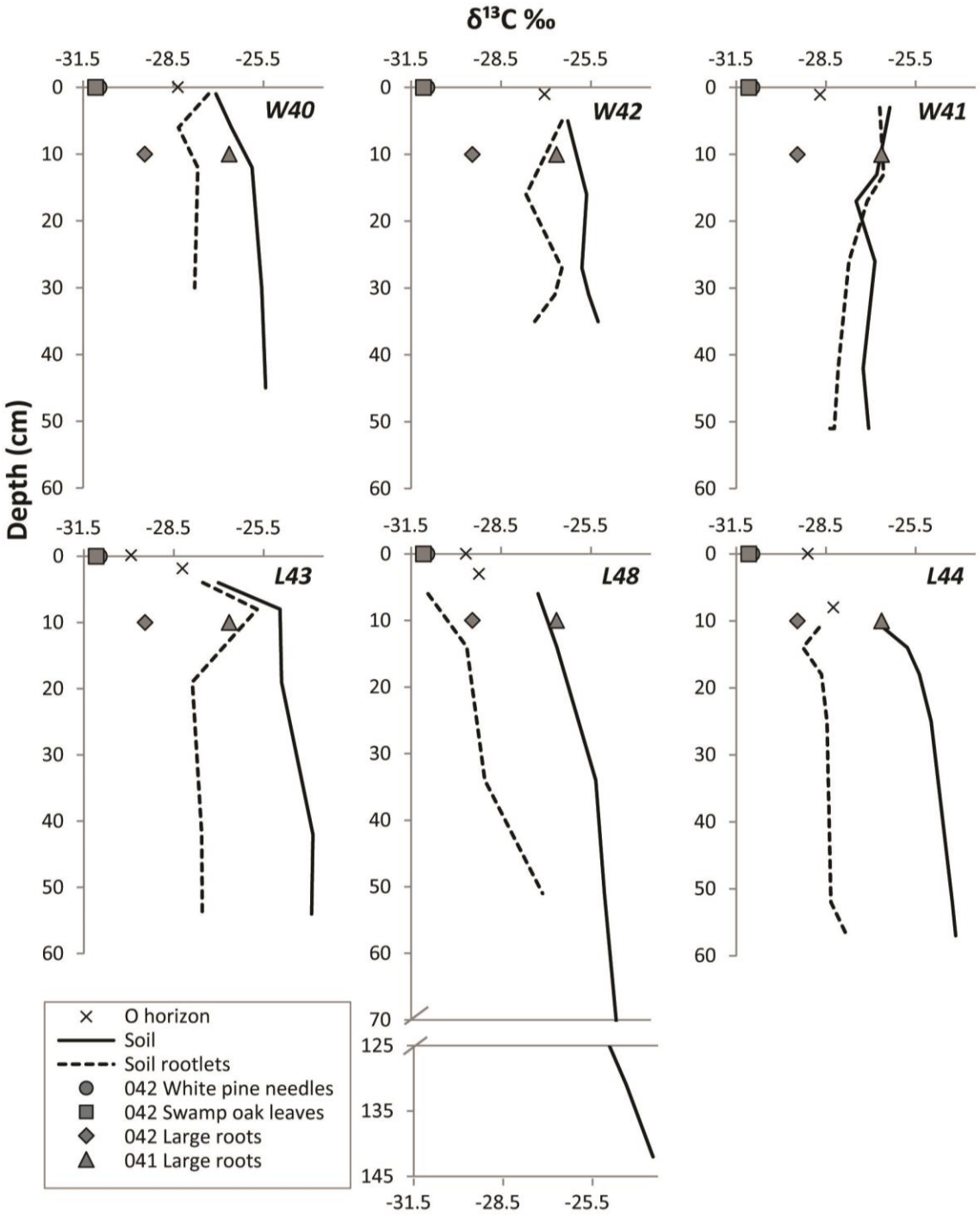


**Figure 4.7:** Depth trends of $\delta^{13}C$ values for SOM from mineral soil samples (solid line) as well as rootlets (dashed line). Disconnected points signify O horizon samples. Fresh organic matter samples are shown by gray circles (white pine leaves), gray squares (oak leaves), gray triangles (large roots from W41), and gray diamonds (large roots from W42).

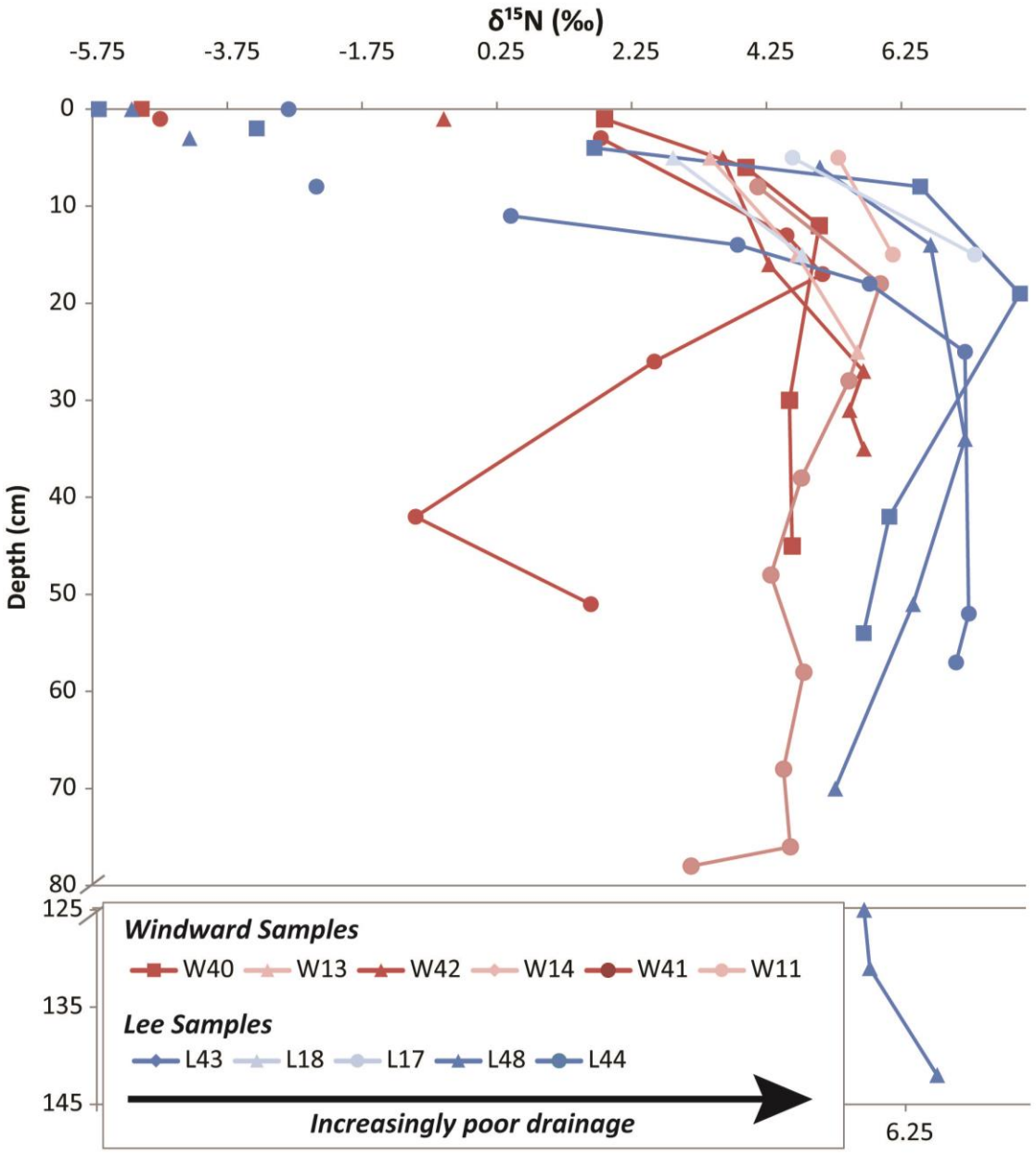


**Figure 4.8:** Depth trends of $\delta^{15}N$ values for windward profiles (red) and lee profiles (blue). Connected lines signify SOM from mineral soil samples, whereas disconnected points signify O horizon samples. The pink and light blue lines show samples that were collected in 10 cm increments using a bucket auger.

$\delta^{15}N$ values with depth, particularly between the Bhg and Bg horizons, where values become negative (-1). The most positive $\delta^{15}N$ values (5 – 5.8‰) for windward profiles occur midway through the profile in the Bw1, Bhs, and Bhg horizons of W40, W42, and W41, respectively. In lee profiles, the highest $\delta^{15}N$ values (7.2 – 8‰) occur in the Ex horizons of sites L48 and L44 and in the Bt2 horizon of L43 before decreasing with depth. However, $\delta^{15}N$ values in site L48 increase slightly from the 2Btx2 horizon (5.3‰) to 5.6‰ and 5.7‰ in the 5Ab and 5Eb horizons, and to 6.7‰ in the 5Bsb.

In all but waterlogged horizons, $\delta^{15}N$ values for rootlets and OM picked out of bulk soil are more negative than that of SOM from the mineral soil samples, indicating the rootlet SOM is less decomposed compared to the remaining SOM in mineral soil samples (Figure 4.9). In waterlogged horizons in W41, however, $\delta^{15}N$ values for rootlets are less negative than SOM from mineral soil samples.

**PCA analysis**

Variables used in PCA analysis include $\delta^{13}C$, $\delta^{15}N$, C:N ratios and logratio transformed clay, silt, sand, and clay mineralogy percentages. Results of PCA performed on 35 samples from six locations within the study area show that PC 1 explains 90% of the variance and the second and third PC explain an additional ~4%; in total, the first three components explain 98% of the variance in the dataset (Table 4.4). C:N ratios load positively and strongly (0.94) on PC 1 with $\delta^{15}N$ loading slightly negatively (-0.25); whereas on PC 2, $\delta^{15}N$ loads negatively and strongly (-0.93) and C:N also loads slightly negatively (-0.26). The first two components, which explain 94% of the variance are interpreted to represent decomposition.

When plotting PC 1 against PC 2, samples are displayed along a continuum from less decomposed samples on the right half of the chart to more decomposed samples clustering in the lower left corner (Figure 4.10). Lee samples dominantly cluster in the lower left having more positive $\delta^{15}N$ values and low C:N values. Surface samples tend to have relatively low $\delta^{15}N$ values and higher C:N values. Samples Bg, Bhg′, and Bhsm from W41 are clear outliers as they are subsurface samples that

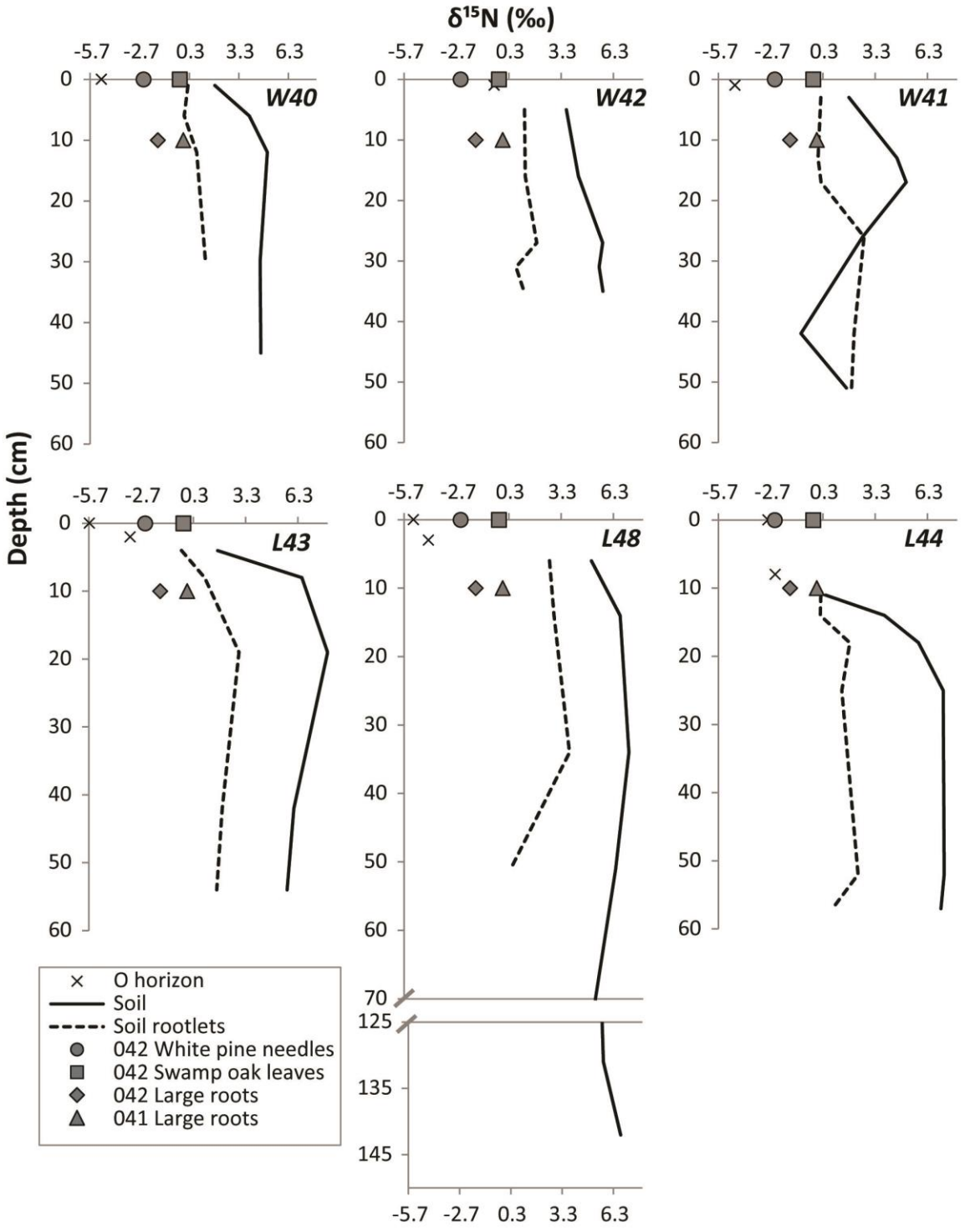


**Figure 4.9:** Depth trends of $\delta^{15}N$ values for mineral-associated SOM (solid line) as well as rootlets and other SOM picked out of bulk soils (dashed line). Disconnected points signify O horizon samples.

**Table 4.4:** Principal component analysis loadings and summary for variables that may be connected to SOM sequestration mechanisms.

| | PC1 | PC.2 | PC.3 | PC.4 | PC.5 | PC.6 | PC.7 | PC.8 | PC.9 | PC.10 |
|---|---|---|---|---|---|---|---|---|---|---|
| **Std. Dev** | 6.43 | 1.44 | 1.05 | 0.76 | 0.71 | 0.59 | 0.32 | 0.25 | 0.15 | 0.10 |
| **Proportion of Variance** | 0.90 | 0.04 | 0.02 | 0.01 | 0.01 | 0.01 | 0.00 | 0.00 | 0.00 | 0.00 |
| **Cumulative Proportion** | 0.90 | 0.94 | 0.96 | 0.98 | 0.99 | 1.00 | 1.00 | 1.00 | 1.00 | 1.00 |
| | **PC1** | **PC.2** | **PC.3** | **PC.4** | **PC.5** | **PC.6** | **PC.7** | **PC.8** | **PC.9** | **PC.10** |
| **$\delta^{13}C$** | | | | | 0.70 | 0.66 | | | | |
| **$\delta^{15}N$** | -0.25 | -0.93 | | | | -0.22 | | | | 0.04 |
| **C:N** | 0.94 | -0.26 | | | | | | | | |
| **% Clay (< 2µm)** | | | | 0.55 | | 0.22 | 0.43 | | 0.58 | 0.21 |
| **% Silt (2-63µm)** | | | | 0.55 | -0.25 | | | 0.38 | | -0.31 |
| **% Sand (63-2000µm)** | | | -0.25 | -0.36 | | | 0.80 | 0.31 | | |
| **Exp. clays** | | | 0.86 | -0.31 | -0.21 | | | | | |
| **Vermiculite** | | | -0.34 | | -0.34 | 0.52 | | -0.63 | -0.26 | |
| **Illite** | | | | 0.39 | 0.50 | -0.37 | 0.33 | -0.51 | -0.26 | |
| **Kaolinite/Chlorite** | | | | | | | | 0.25 | -0.34 | 0.90 |

have the highest C:N values, which suggests these samples contain relatively fresh OM. Interestingly, the Bg sample from W41 has a very low $\delta^{15}N$ value, whereas the Bhsm and Bhg′ horizons from the W41 have higher $\delta^{15}N$. Expandable clays load most strongly (0.86) on PC 3 with vermiculite and sand loading negatively (-0.34 and -0.25, respectively). Thus, PC 3 is interpreted to represent parent materials/weathering. Because variables related to carbon, e.g., C:N, $\delta^{13}C$, and $\delta^{15}N$ exclusively load on PC 1 and 2 and those related to parent material and/or weathering load exclusively on PC 3, this adds to other evidence that particle size and clay mineralogy do not have a direct influence on OM storage or degradation.

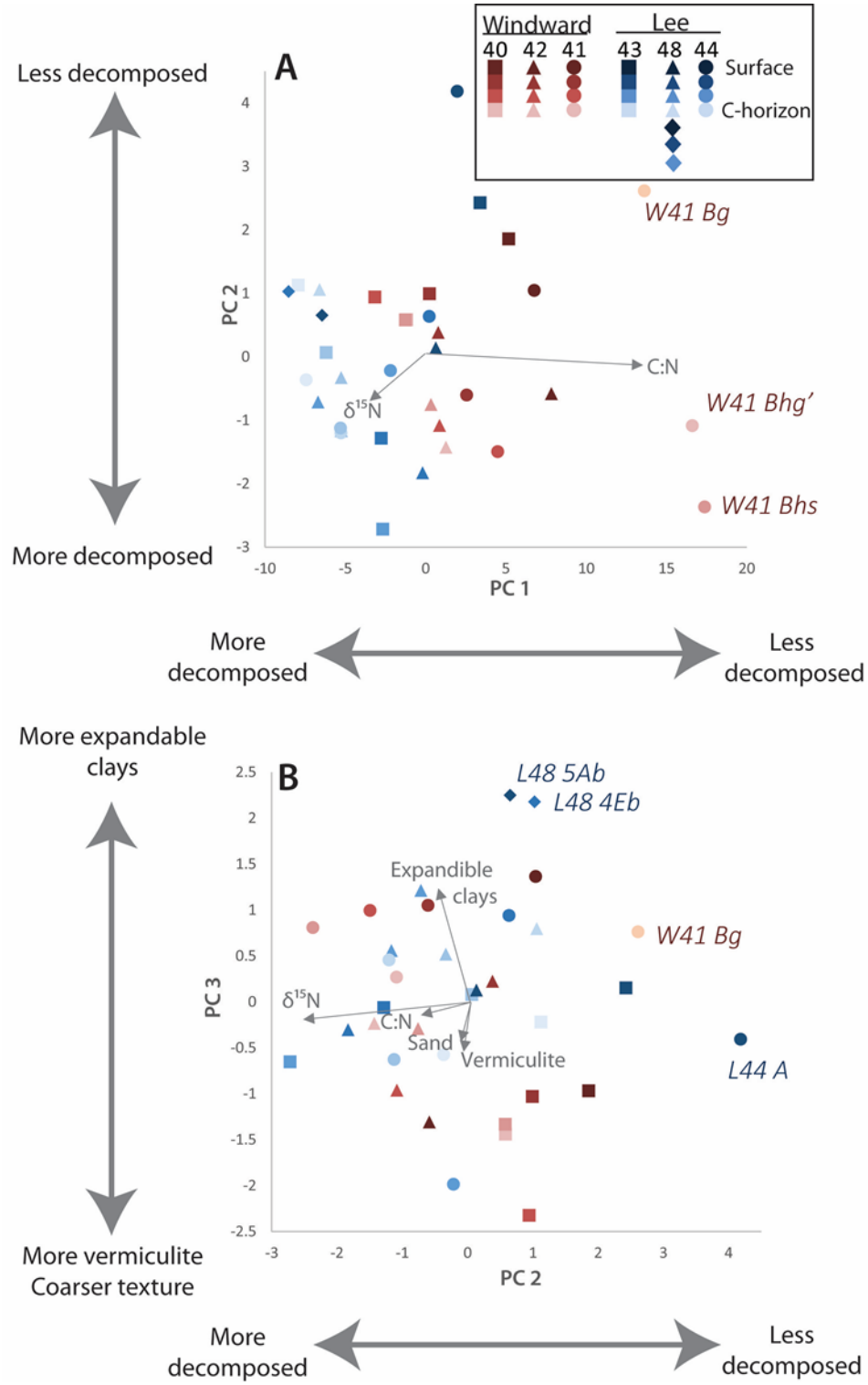


**Figure 4.10:** Biplot showing principal components for SOM analysis. A: PC 1on the X-axis and PC2 on the Y-axis. B: PC2 on the X-axis and PC3 on the Y-axis. Blue represents samples collected on the lee side of Wildcat Ridge; red represents those from the windward side; green represents samples collected from the lower backslope within the Wildcat Ridge complex. Shades within each of these hues represent the relative depth of the samples; dark shades represent surface samples with shades becoming lighter with increasing depth.

## Discussion

A strong understanding of the geomorphology and sedimentology of parent materials and their influence on soil texture and pedogenesis is highly important in OM research. Organic C is commonly associated with the < 6 μm fraction, especially the clay fraction, which based on C:N ratios, tends to be more microbially processed than OM associated with coarser fractions (Kahle et al. 2002; Kiem et al. 2002; Kiem and Kögel-Knabner 2002). Exceptions occur in soils with relatively high clay contents, where microaggregation physically protects OM from degradation (Kölbl and Kögel-Knabner 2004). However, in the sandy and loamy soils of central Jackson County, clay and fine silt contents generally correlate poorly with OC content. Fine silt and clay were weakly correlated with OC content in the subset of windward soil horizons, probably not because of potential protection based on particle size fractions or mineralogy, but because in the windward soils, silt and often clay are highest in surface horizons, where OM is also highest. These results may also diverge from other studies because of the depth of samples included in analysis. Most samples collected for SOM analysis are from shallow surface horizons that compare soils that generally contain the highest amounts of SOM. However, when analyzing SOM samples from > 20 cm depth, these trends likely break down because SOM contents decrease whereas particle size characteristics change little, or contain more clay and silt due to lessivage.

The uppermost horizons in most soil profiles show increasing $^{13}C$ and $^{15}N$ values, as well as increasing C:N values with depth, which fits well with our understanding of $^{13}C$ and $^{15}N$ depth trends in well drained settings (Nadelhoffer and Fry 1988; Balesdent et al. 1993). This depth trend is likely due to increased decomposition of OM. Below eluvial horizons, sandy windward profiles and silty lee profiles diverge in decomposition patterns.

In silty profiles, C:N decreases in steps with depth, and in some profiles, decreasing $\delta^{13}C$ with depth exhibits the same stepped pattern, suggesting little change in degree of decomposition within the sets of Bt, Ex, and/or Btx horizons that are separated by decreases. It is possible that sorption of OC on clay minerals is similar through these sets of horizons. Peds from Ex horizons contain Bt material including illuvial clay, and some cutans in Btx horizons are dark in color (7.5 YR 2/1) indicating the

presence of OM. Soil OM tends to be more decomposed in subsurface horizons of silty soils compared to sandy soils. This trend probably is at least partially due to the capacity of silty sediments to hold more plant available water, which maintains a relatively stable supply of water and oxygen needed for microbes to efficiently decompose OM, compared to sandy soils that may fluctuate more frequently between aquic and xeric conditions.

Windward profiles with impeded drainage and illuvial accumulations of humus, on the other hand, show trends of decreased OM decomposition with depth in illuvial horizons. In poorly drained soils, subsurface OM tends to have high C:N values and more negative $\delta^{13}C$ —sometimes more so than O horizon material for the profile. These results are similar to the slight increase seen in the Cg horizon of an aquic, tropical Spodosol reported by Grand and Lavkulich (2011). Organic C accumulation in these subsurface horizons may be primarily in the form of organo-mineral complexes between Al and Fe colloids and DOM rather than being sorbed on phyllosilicate clay minerals (Kaiser and Zech 2000; Riise et al. 2000). Scheel et al. (2007) suggested dissolved Al preferentially precipitates larger, aromatic C that was largely depleted in N contents from DOM, and furthermore, that DOM from the Oa horizons of spruce (*Picea abies*) contains larger proportions of aromatic compounds than DOM from the Oi horizons of spruce, beech (*Fagus sylvatica*), or beech Oa horizons. Regardless of the specific form of OM translocation and immobilization in illuvial horizons, illuviation of less-decomposed OM is a likely explanation for the occurrence of this form of OM deep in the profile (Marin-Spiotta et al. 2011). Future work could address this hypothesis by studying the micromorphology of OM in the upper Bhsm horizon, which is suspected to include pellets, and polymorphic decomposed OM; whereas, lower spodic horizons would contain primarily monomorphic, cracked OM coatings derived from precipitation of DOM (Scheel et al. 2007; Bardy et al. 2008).

In general, $\delta^{15}N$ values seem to support the hypothesis that the subsurface OM in wet windward profiles is less decomposed, as they are either roughly equivalent to the surface horizons or even more negative. However, in well drained silty soils (e.g., L43, L48), $\delta^{15}N$ decreases slightly in the lower horizons, while $\delta^{13}C$ values increase and C:N decreases. In these soils, $^{15}N$-rich microbial products are

likely mineralized through nitrification, which is not associated with fractionation, and either lost by leaching or taken up by plants in this nutrient limited landscape (Hobbie and Ouimette 2009).

It is important to point out the differences between poorly drained profiles at sites W11 and W41. These profiles were collected in the same general area and are both Humaqueptic Aquods, yet C:N, $\delta^{13}C$, and $\delta^{15}N$ values and trends differ with depth. The soils in this part of the study area are extremely heterogeneous, so some of the difference may be the result of natural soil variability. Another possibility is the difference in sampling protocol for these two sites. Site W41 was collected by horizons, whereas W11 was collected in 10 cm increments. In several profiles, but especially in W41, horizon data shows more variable trends with depth; whereas W11 trends seem to be more muted. These data suggest SOM research should be conducted by collecting soil samples by horizon rather than in set increments. Additionally, future research is needed to explore SOM dynamics and stabilization mechanisms deeper than 20 cm below the surface.

## *Summary and Conclusions*

SOM in surface horizons shows decreasing negative $\delta^{15}N$ and $\delta^{13}C$ as well as increasing C:N values, which is consistent with increasing levels of decomposition with depth. However, below eluvial horizons, sandy windward profiles and silty lee profiles diverge in decomposition patterns. In silty profiles, decomposition patterns appeared as stepped decreases with depth, where decomposition was similar in sets of Bt, Ex, and/or Btx horizons. In these settings, OM sorption to clay minerals that are translocated may protect OM from further decomposition. In sandy profiles, with impeded drainage, podzolization resulted in less decomposed (fresher) DOM protected by organic-mineral complexes (chelation) that is illuviated into subsurface horizons.

Weak positive correlation between OC and silt from some windward samples us not evidence of OC binding mechanisms to silt, but rather reflects relatively high silt and OC contents occurring at the surface of these soils for independent reasons. These results point to the importance of understanding the geomorphology and sedimentology of soil parent materials in SOM research. Furthermore, samples

collected by horizon and those collected by depth increments show different ranges and in some cases direction of C and N isotope values with depth. This difference is likely the result of horizon mixing during incremental sampling protocols, which can result in incomplete understanding of SOM dynamics. Therefore, SOM sampling with depth should be based on horizon boundaries, rather than fixed increments.

# CHAPTER 5 : CONCLUSIONS

Dune forms evident in LiDAR data from Monroe and Juneau Counties suggest widespread eolian activity resulted in an eolian mantle covering the low relief terrain associated with the central sand plains of Wisconsin. Profile PSDs suggest an eolian sand sheet largely between 30 and 100 cm thick, but up to 5 m thick in places, covers much of the low-relief landscape. Eolian silt associated with the period of deglaciation is only preserved in the most protected landscape positions along the east and southeast aspects of large bedrock ridges; conversely, fine silt that occurs in the surface horizons may have been deposited after the time of most intense eolian activity. Thus, using fine silt patterns of thin loess mantles to identify sources without corroborating geochemical or mineralogical evidence may lead to misinterpretation.

The abundance of dune forms and the absence of silt deposits across the majority of the sandy terrain suggest this landscape acted largely as a surface of transport where any fine materials that were deposited from suspension were subsequently re-entrained through bombardment by saltating sands. Most of the silt and finer material was carried farther downwind, perhaps into the Glacial Lake Wisconsin basin, only to be redistributed even farther downwind, presumably onto uplands of the Oneota Cuesta and higher elevation glacial landscapes. If this is the case, loess on the Green Bay lobe is a mixture of fine sediments from multiple sources including the Cambrian landscape of west-central Wisconsin, outwash and valley train deposits associated with the Upper Mississippi River Valley, and very fine materials from distant western sources. Future work will need to confirm that silt and clay fractions are derived from different provenances. Future work is also necessary to explore the role of bioturbation in this landscape.

Silt additions change the pedogenic pathway of soils in lower landscape positions of this sandy area from podzolization to lessivage. Bisequal soils with an upper E-Bt and lower Ex-Btx are common in settings with the silty mantles immediately east of prominent bedrock ridges. Comparisons of sequa characteristics downslope suggest lateral flow and translocation through both sandy and silty catenas is an important process in this landscape.

The weak correlation between OC and silt from some windward samples is not evidence of OC binding mechanisms to silt, but rather a correlation between relatively high silt and OC contents occurring at the surface of these soils. SOM in surface horizons shows increasingly less negative $\delta^{15}N$ and $\delta^{13}C$ as well as increasing C:N values, trends that are consistent with increasing levels of decomposition with depth. However, below eluvial horizons, sandy and silty profiles diverge in decomposition patterns. In silty profiles, decomposition patterns appeared as stepped decreases with depth, where decomposition was similar in sets of Bt, Ex, and/or Btx horizons. In these settings, OM sorption to translocated clay minerals may protect OM from further decomposition. In sandy profiles with impeded drainage, podzolization resulted in less decomposed (fresher) DOM protected by organic-mineral complexes (chelation) that is illuviated into subsurface horizons. Subsurface SOM tended to be more highly decomposed in drier soils compared to that of soils with impeded drainage.

These results point to the importance of understanding the geomorphology and sedimentology of soil parent materials in SOM research. Furthermore, samples collected by horizon and those collected by depth increments show different ranges and in some cases different directions of C and N isotope trends with depth. This difference is likely the result of horizon mixing during incremental sampling protocols, which can result in incomplete understanding of SOM dynamics. Therefore, SOM sampling with depth should be collected according to horizons, rather than incremental depths.

### *Future work*

In order to better assess the contributions and provenance of distant loess compared to more local sources, geochemical (e.g., Ti:Zr ratios) differences between silt fractions should be analyzed. Coarse and fine silt fractions could be compared; however, better analysis would result from identifying differences in modes using detailed laser particle size analysis. More research is also necessary to explore the role of bioturbation in sandy vs. silty mantles. A particularly interesting aspect of this is looking at horizonation processes compared to inter-horizon bioturbation processes. For example, what types of inter-horizon bioturbation processes allow horizon boundaries to remain distinct? Are the timescales of

bioturbative and horizon forming processes different, and how does that influence pedogenesis? How important is bioturbation in soils where geogenic texture contrasts remain distinct?

The interesting stratigraphy and buried soil in site L48 needs to be studied more to answer many unresolved questions. Some of these questions include: What processes deposited the stratified sand and overlying gravelly strata—are they hillslope deposits, or could they possibly be beach sediments associated with a higher stand/iteration of Glacial Lake Wisconsin? When was the stratified sand deposited? What is the age of organic carbon fragments found in the buried soil? What processes are responsible for the deposition of the silt loam that underlie the stratified sand layer? Can similar strata/deposits be found in other lee locations below the silty mantle, and how geographically extensive are these deposits?

The identification of (unmapped) fragipans in this landscape was also a surprise in this research. More work is needed to understand the geographic distribution of fragipans in this landscape. Additionally, soluble silica moving in soil plasma occurs in this landscape as evident from the fragic horizons in silty catenas and Bhsm horizons in low-lying sandy landscape positions. Future work should look in more detail at the role of silica, iron, aluminum, and humus solution, precipitation, and lateral movement in this landscape.

The variations in $\delta^{13}C$, C:N, and $\delta^{15}N$ of SOM with depth can be explained without a role for vegetation change, but a contribution from changes in vegetation sources of OM cannot be ruled out. Therefore, more work is needed to ascertain the contributions of past vegetation sources resulting in $\delta^{13}C$ enrichment of SOM with depth. Nuclear magnetic resonance (NMR) spectroscopy is a method that may help to identify source compounds in order to tease out decomposition effects vs. changes in source vegetation characteristics (Baldock et al. 1997; Kögel-Knabner 1997, 2000, 2002). The potential ability to identify paleovegetation sources in SOM stored at depth speaks not only to the importance of collecting and analyzing SOM samples from depths greater than 20-30 cm, but also may provide a better glimpse into paleoenvironmental conditions for places where appropriate sites for pollen analysis are sparse.

## REFERENCES

Aleinikoff, J. N., D. R. Muhs, R. R. Sauer, and C. M. Fanning. 1999. Late Quaternary Loess in Northeastern Colorado: Part II—Pb Isotopic Evidence for the Variability of Loess Sources. *Geological Society of America Bulletin* 111 (12):1876-1883.

Andrew, J. A. 1965. Size Distribution of the Sand and Heavy Minerals in the Ironton Sandstone (Franconian Stage) of Western Wisconsin. MS Thesis, Geology, University of Wisconsin, Madison, WI.

Asthana, V. 1969. The Mt. Simon Formation (Dresbachian Stage) of Wisconsin. PhD Thesis, University of Wisconsin, Madison.

Baker, R. G., E. A. Bettis, III, R. F. Denniston, L. A. Gonzalez, L. E. Strickland, and J. R. Krieg. 2002. Holocene Paleoenvironments in Southeastern Minnesota - Chasing the Prairie-Forest Ecotone. *Palaeogeography, palaeoclimatology, palaeoecology* 177:103-122.

Baker, R. G., L. J. Maher, C. A. Chumbley, and K. L. Van Zant. 1992. Patterns of Holocene Environmental Change in the Midwestern United States. *Quaternary Research* 37 (3):379-389.

Baldock, J. A., J. M. Oades, P. N. Nelson, T. M. Skene, A. Golchin, and P. Clarke. 1997. Assessing the Extent of Decomposition of Natural Organic Materials Using Solid-State $^{13}C$ NMR Spectroscopy. *Australian Journal of Soil Research* 35 (5):1061-1084.

Balesdent, J., C. Girardin, and A. Mariotti. 1993. Site-Related $^{13}C$ of Tree Leaves and Soil Organic Matter in a Temperate Forest. *Ecology* 74 (6):1713-1721.

Bardy, M., E. Fritsch, S. Derenne, T. Allard, N. R. do Nascimento, and G. T. Bueno. 2008. Micromorphology and Spectroscopic Characteristics of Organic Matter in Waterlogged Podzols of the Upper Amazon Basin. *Geoderma* 145 (3-4):222-230.

Bateman, M. D., and J. V. Huissteden. 1999. The Timing of Last-Glacial Periglacial and Aeolian Events, Twente, Eastern Netherlands. *Journal of Quaternary Science* 14 (3):277-283.

Belby, C. S. 2009. Human Impacts on Sedimentation and Nutrient Sequstrtion in the Upper Mississippi River Floodplain. PhD Thesis, Geography, University of Wisconsin-Madison, Madison, WI.

Berg, R. R. 1954. Franconia Formation of Minnesota and Wisconsin. *Geological Society of America Bulletin* 65 (9):857-882.

Bettis, E. A., III, D. R. Muhs, H. M. Roberts, and A. G. Wintle. 2003. Last Glacial Loess in the Conterminous USA. *Quaternary Science Reviews* 22 (18-19):1907-1946.

Birks, H. J. B. 1976. Late-Wisconsinan Vegetational History at Wolf Creek, Central Minnesota. *Ecological Monographs* 46 (4):395-429.

Black, R. F. 1965. Ice-Wedge Casts of Wisconsin. *Wisconsin Academy of Science, Arts and Letters* 54:187-222.

Bryant, R. B. 1989. Physical Processes of Fragipan Formation. In *Fragipans: Their Occurrence, Classification, and Genesis*, eds. N. E. Smeck and E. J. Ciolkosz, 141-150: Soil Science Society of America.

Buchmann, N., W.-Y. Kao, and J. Ehleringer. 1997. Influence of Stand Structure on $^{13}C$ of Vegetation, Soils, and Canopy Air within Deciduous and Evergreen Forests in Utah, United States. *Oecologia* 110 (1):109-119.

Buurman, P., and A. G. Jongmans. 2005. Podzolisation and Soil Organic Matter Dynamics. *Geoderma* 125 (1-2):71-83.

Camill, P., C. E. Umbanhowar, Jr. , R. Teed, C. E. Geiss, J. Aldinger, L. Dvorak, K. Jon, J. Limmer, and K. Walkup. 2003. Late-Glacial and Holocene Climatic Effects on Fire and Vegetation Dynamics at the Prairie-Forest Ecotone in South-Central Minnesota. *Journal of Ecology* 91 (5):822-836.

Carson, E. C., P. R. Hanson, J. W. Attig, and A. R. Young. 2012. Numeric Control on the Late-Glacial Chronology of the Southern Laurentide Ice Sheet Derived from Ice-Proximal Lacustrine Deposits. *Quaternary Research* 78 (3):583-589.

Carter, L. D., J. A. Heginbottom, and M. K. Woo. 1987. Arctic Lowlands. In *Geomorphic Systems of North America* ed. W. L. Graf, 583-628. Boulder, CO: Geological Society of America

Catt, J. A. 1977. Loess and Coversands. In *British Quaternary Studies: Recent Advances*, ed. F. W. Shotton, 221–229. New York, NY: Oxford University Press.

Chaopricha, N. T., and E. Marín-Spiotta. 2013. Soil Burial Contributes to Deep Soil Organic Carbon Storage. *Soil Biology and Biochemistry* 69 (0):251-264.

Clayton, L., and J. W. Attig. 1987. Lake-Ice Collapse Trenches in Wisconsin, USA. *Earth Surface Processes and Landforms* 12:167-172.

———. 1989. Glacial Lake Wisconsin. Memoir 173. Geological Society of America: Boulder, CO. pp. 80.

Clayton, L., J. W. Attig, and D. M. Mickelson. 2001. Effects of Late Pleistocene Permafrost on the Landscape of Wisconsin, USA. *Boreas* 30 (3):173 - 188.

Clayton, L., and F. Madison. 1983. Pleistocene History of the Black River Falls Area. In *Three Billion Years of Geology: A Field Trip through the Archean, Proterozoic, Paleozoic, and Pleistocene Geology of the Black River Falls Area of Wisconsin*, 10-13. Black River Falls, Wisconsin: Wisconsin Geological and Natural History Survey.

Curtis, J. T. 1971. *The Vegetation of Wisconsin: An Ordination of Plant Communities*. Madison, WI: University of Wisconsin Press.

Davis, A. M. 1977. The Prairie-Decidious Forest Ecotone in the Upper Middle West. *Annals of the Association of American Geographers* 67 (2):204 - 213.

Deines, P. ed. 1980. *The Isotopic Composition of Reduced Organic Carbon*: Elsevier.

Dietze, M., and A. Kleber. 2010. Characterisation and Prediction of Thickness and Material Properties of Periglacial Cover Beds, Tharandter Wald, Germany. *Geoderma* 156 (3–4):346-356.

Distefano, M. 1973. The Mineralogy and Petrology of the Eau Claire Formation, West-Central Wisconsin. MA Thesis, Department of Geology, Northern Illinois University, Dekalb.

Ehleringer, J. R., N. Buchmann, and L. B. Flanagan. 2000. Carbon Isotope Ratios in Belowground Carbon Cycle Processes. *Ecological Applications* 10 (2):412-422.

Ehleringer, J. R., and T. E. Cerling. 2002. C3 and C4 Photosynthesis. In *Encyclopedia of Global Environmental Change*, eds. H. A. Mooney and J. G. Canadell, 186-190. Chichester: John Wiley & Sons.

Emrich, G. H. 1966. Ironton and Galesville (Cambrian) Sandstones in Illinois and Adjacent Areas. Circular 403. 55.

Eoff, J. D. 2008. Sequence-Stratigraphic Context of Cambrian Extinctions: Sedimentary Facies and Trilobite Faunas of the Tunnel City Group, Upper Mississippi Valley. PhD Thesis, ConocoPhillips School of Geology and Geophysics, University of Oklahoma, Norman, OK.

Farmer, V. C., J. O. Skjemstad, and C. H. Thompson. 1983. Genesis of Humus B Horizons in Hydromorphic Humus Podzols. *Nature* 304 (5924):342-344.

Fehrenbacher, J. B., J. L. White, A. H. Beavers, and R. L. Jones. 1965. Loess Composition in Southeastern Illinois and Southwestern Indiana. *Soil Science Society of America Journal* 29 (5):572-579.

Fehrenbacher, J. B., J. L. White, H. P. Ulrich, and R. T. Odell. 1965. Loess Distribution in Southeastern Illinois and Southwestern Indiana. *Soil Science Society of America Journal* 29 (5):566-572.

Finley, R. W. 1976. Original Vegetation Cover of Wisconsin. St. Paul, MN: North Central Forest Experiment Station, USDA Forest

Follmer, L. R. 1996. Loess Studies in Central United States: Evolution of Concepts. *Engineering Geology* 45 (1-4):287-304.

French, H. M. 1996. *The Periglacial Environment*. 2nd ed: Harlow: Longman.

Frolking, T. A. 1982. The Genesis and Distribution of Upland Red Clays in Wisconsin's Driftless Area. *Quaternary History of the Driftless Area. Wisconsin Geological and Natural History Survey Field Trip Guidebook* 5:88-97.

Frye, J. C., H. D. Glass, and H. B. Willman. 1962. Stratigraphy and Mineralogy of the Wisconsinan Loesses of Illinois. Circular 334. 55.

Gee, G. W., and J. W. Bauder. 1986. Particle-Size Analysis. In *Methods of Soil Analysis: Part 1—Physical and Mineralogical Methods*, ed. A. Klute, 383-411. Madison, WI: Soil Science Society of America, American Society of Agronomy.

Grand, S., and L. M. Lavkulich. 2011. Depth Distribution and Predictors of Soil Organic Carbon in Podzols of a Forested Watershed in Southwestern Canada. *Soil Science* 176 (4):164-174 10.1097/SS.0b013e3182128671.

Grimley, D. A. 1996. Stratigraphy, Magnetic Susceptibility, and Mineralogy of Loess - Paleosol Sequences in Southwestern Illinois and Eastern Missouri PhD Thesis, University of Illinois, Urbana-Champaign.

———. 2000. Glacial and Nonglacial Sediment Contributions to Wisconsin Episode Loess in the Central United States. *Geological Society of America Bulletin* 112 (10):1475-1495.

Grimley, D. A., L. R. Follmer, and E. D. McKay. 1998. Magnetic Susceptibility and Mineral Zonations Controlled by Provenance in Loess Along the Illinois and Central Mississippi River Valleys. *Quaternary Research* 49 (1):24-36.

Grimm, E. C. 1984. Fire and Other Factors Controlling the Big Woods Vegetation of Minnesota in the Mid-Nineteenth Century. *Ecological Monographs* 54 (3):291-311.

Habecker, M. A., K. McSweeney, and F. W. Madison. 1990. Identification and Genesis of Fragipans in Ochrepts of North Central Wisconsin. *Soil Science Society of America Journal* 54 (1):139-146.

Hall, G. F., N. E. S. L.P. Wilding, and G. F. Hall. 1983. Pedology and Geomorphology. In *Developments in Soil Science*, 117-140: Elsevier.

Hanson, P. R., J. A. Mason, P. M. Jacobs, and A. R. Young. 2014. Evidence for Bioturbation of Luminescence Signals in Eolian Sand on Upland Ridgetops, Southeastern Minnesota, USA. *Quaternary International*: doi:10.1016/j.quaint.2014.06.039.

Harden, J. W., T. L. Fries, and M. J. Pavich. 2002. Cycling of Beryllium and Carbon through Hillslope Soils in Iowa. *Biogeochemistry* 60 (3):317-336.

Harlan, P. W., and D. P. Franzmeier. 1977. Soil Formation on Loess in Southwestern Indiana .1. Loess Stratigraphy and Soil Morphology. *Soil Science Society of America Journal* 41 (1):93-98.

Heide, K. 1984. Holocene Pollen Stratigraphy from a Lake and Small Hollow in North-Central Wisconsin, USA. *Palynology* 8:3-19.

Hobbie, E., and A. Ouimette. 2009. Controls of Nitrogen Isotope Patterns in Soil Profiles. *Biogeochemistry* 95 (2):355-371.

Hole, F. D. 1950 (reprinted 1968). *Aeolian Silt and Sand Deposits of Wisconsin*. Madison: Wisconsin Geological and Natural History Survey.

Holzhey, C. S., R. B. Daniels, and E. E. Gamble. 1975. Thick Bh Horizons in the North Carolina Coastal Plain: II. Physical and Chemical Properties and Rates of Organic Additions from Surface Sources. *Soil Science Society of America Journal* 39 (6):1182-1187.

Hughes, R. E., and R. Warren. 1989. Evaluation of the Economic Usefulness of Earth Materials by X-Ray Diffraction. Prepared for Proceedings of 23rd Forum on the Geology of Industrial Minerals: Illinois State Geological Survey, Industrial Minerals Notes, 47-57.

Jackson, M. L., and G. D. Sherman. 1953. Chemical Weathering of Minerals in Soils. *Adv. Agron* 5 (22):317.

Jacobs, P. M., J. C. Knox, and J. A. Mason. 1997. Preservation and Recognition of Middle and Early Pleistocene Loess in the Driftless Area, Wisconsin. *Quaternary Research* 47 (2):147-154.

Jacobs, P. M., and J. A. Mason. 2005. Impact of Holocene Dust Aggradation on a Horizon Characteristics and Carbon Storage in Loess-Denived Mollisols of the Great Plains, USA. *Geoderma* 125 (1-2):95-106.

———. 2007. Late Quaternary Climate Change, Loess Sedimentation, and Soil Profile Development in the Central Great Plains: A Pedosedimentary Model. *Geological Society of America Bulletin* 119 (3-4):462-475.

Jacobs, P. M., J. A. Mason, and P. R. Hanson. 2011. Mississippi Valley Regional Source of Loess on the Southern Green Bay Lobe Land Surface, Wisconsin. *Quaternary Research* 75 (3):574-583.

———. 2012. Loess Mantle Spatial Variability and Soil Horizonation, Southern Wisconsin, USA. *Quaternary International* 265 (0):43-53.

Jenny, H. 1941. *Factors of Soil Formation; a System of Quantitative Pedology*. 1st ed. New York, London: McGraw-Hill.

Johnson, M. D. 1986. *Pleistocene Geology of Barron County, Wisconsin*. Madison, WI: Wisconsin Geological and Natural History Survey

Johnson, W. H. 1990. Ice-Wedge Casts and Relict Patterned-Ground in Central Illinois and Their Environmental Significance. *Quaternary Research* 33 (1):51-72.

Johnson, W. H., and L. R. Follmer. 1989. Source and Origin of Roxana Silt and Middle Wisconsinan Midcontinent Glacial Activity. *Quaternary Research* 31:319–331.

Kahle, M., M. Kleber, and R. Jahn. 2002. Carbon Storage in Loess Derived Surface Soils from Central Germany: Influence of Mineral Phase Variables. *Journal of Plant Nutrition and Soil Science* 165 (2):141-149.

Kaiser, K., and W. Zech. 2000. Dissolved Organic Matter Sorption by Mineral Constituents of Subsoil Clay Fractions. *Journal of Plant Nutrition and Soil Science* 163 (5):531-535.

Kasse, C. 1997. Cold-Climate Aeolian Sand-Sheet Formation in North-Western Europe (*C*. 14-12.4 Ka); a Response to Permafrost Degradation and Increased Aridity. *Permafrost and Periglacial Processes* 8 (3):295-311.

———. 2002. Sandy Aeolian Deposits and Environments and Their Relation to Climate During the Last Glacial Maximum and Lateglacial in Northwest and Central Europe. *Progress in Physical Geography* 26 (4):507-532.

Kennedy, M. J., O. A. Chadwick, P. M. Vitousek, L. A. Derry, and D. M. Hendricks. 1998. Changing Sources of Base Cations During Ecosystem Development, Hawaiian Islands. *Geology* 26 (11):1015-1018.

Kiem, R., H. Knicker, and I. Kögel-Knabner. 2002. Refractory Organic Carbon in Particle-Size Fractions of Arable Soils I: Distribution of Refractory Carbon between the Size Fractions. *Organic Geochemistry* 33 (12):1683-1697.

Kiem, R., and I. Kögel-Knabner. 2002. Refractory Organic Carbon in Particle-Size Fractions of Arable Soils II: Organic Carbon in Relation to Mineral Surface Area and Iron Oxides in Fractions <6μm. *Organic Geochemistry* 33 (12):1699-1713.

Kleber, A. 1992. Periglacial Slope Deposits and Their Pedogenic Implications in Germany. *Palaeogeography, palaeoclimatology, palaeoecology* 99 (3–4):361-371.

———. 1997. Cover-Beds as Soil Parent Materials in Midlatitude Regions. *CATENA* 30 (2–3):197-213.

Knox, J. C. 1985. Responses of Floods to Holocene Climatic Change in the Upper Mississippi Valley. *Quaternary Research* 23 (3):287-300.

Knox, J. C., P. J. Bartlein, T. Webb, III, L. Clayton, T. A. Frolking, F. D. Hole, J. W. Attig, M. D. Johnson, L. J. Maher Jr., P. T. McDowell, and D. M. Mickelson. 1982. *Quaternary History of the Driftless Area with Special Papers*. Madison: Wisconsin Geological and Natural History Survey.

Kögel-Knabner, I. 1997. $^{13}C$ and $^{15}N$ NMR Spectroscopy as a Tool in Soil Organic Matter Studies. *Geoderma* 80 (3-4):243-270.

———. 2000. Analytical Approaches for Characterizing Soil Organic Matter. *Organic Geochemistry* 31 (7-8):609-625.

———. 2002. The Macromolecular Organic Composition of Plant and Microbial Residues as Inputs to Soil Organic Matter. *Soil Biology and Biochemistry* 34 (2):139-162.

Kölbl, A., and I. Kögel-Knabner. 2004. Content and Composition of Free and Occluded Particulate Organic Matter in a Differently Textured Arable Cambisol as Revealed by Solid-State $^{13}C$ NMR Spectroscopy. *Journal of Plant Nutrition and Soil Science* 167 (1):45-53.

Koster, E. A. 1988. Ancient and Modern Cold-Climate Aeolian Sand Deposition: A Review. *Journal of Quaternary Science* 3 (1):69-83.

Kucera, M., and B. A. Malmgren. 1998. Logratio Transformation of Compositional Data: A Resolution of the Constant Sum Constraint. *Marine Micropaleontology* 34 (1):117-120.

Langton, J. E., and D. T. Simonson. 1998. *Soil Survey of Jackson County, Wisconsin*. Washington, DC: Soil Conservation Service, U.S. Govt. Printing Office.

Lea, P. D., and C. F. Waythomas. 1990. Late-Pleistocene Eolian Sand Sheets in Alaska. *Quaternary Research* 34 (3):269-281.

Leigh, D. S., and J. C. Knox. 1994. Loess of the Upper Mississippi Valley Driftless Area. *Quaternary Research* 42 (1):30-40.

Letolle, R. ed. 1980. *Nitrogen-15 in the Natural Environment*: Elsevier.

Loope, H. M. in preparation. Chronology and Paleoenvironmental Significance of Eolian Sand Activity South of the Laurentide Ice Sheet During the Last Glacial Period, Upper Mississippi River Basin, USA. PhD Thesis, Geography, University of Wisconsin-Madison, Madison, WI.

Luehmann, M. D., R. J. Schaetzl, B. A. Miller, and M. E. Bigsby. 2013. Thin, Pedoturbated, and Locally Sourced Loess in the Western Upper Peninsula of Michigan. *Aeolian Research* 8 (0):85-100.

Maher, L. J. 1982. The Palynology of Devil's Lake, Sauk County, Wisconsin. In *Quaternary History of the Driftless Area, Field Trip Guide Book No. 5*, 119-135. Madison, WI: Univeristy of Wisconsin Extension, Geological and Natural History Survey.

Mailänder, R., and H. Veit. 2001. Periglacial Cover-Beds on the Swiss Plateau: Indicators of Soil, Climate and Landscape Evolution During the Late Quaternary. *CATENA* 45 (4):251-272.

Marin-Spiotta, E., O. A. Chadwick, M. Kramer, and M. S. Carbone. 2011. Carbon Delivery to Deep Mineral Horizons in Hawaiian Rain Forest Soils. *Journal of Geophysical Research: Biogeosciences* 116 (G3):G03011.

Markewich, H. W., R. J. Litwin, M. J. Pavich, and G. A. Brook. 2009. Late Pleistocene Eolian Features in Southeastern Maryland and Chesapeake Bay Region Indicate Strong WNW–NW Winds Accompanied Growth of the Laurentide Ice Sheet. *Quaternary Research* 71 (3):409-425.

Mason, J. A. 1995. Effects of Glacial-Interglacial Climate Change on Mass Wasting, Southeastern Minnesota. PhD Thesis, University of Wisconsin, Madison.

———. 2001. Transport Direction of Peoria Loess in Nebraska and Implications for Loess Sources on the Central Great Plains. *Quaternary Research* 56 (1):79-86.

Mason, J. A., and P. M. Jacobs. 1998. Chemical and Particle-Size Evidence for Addition of Fine Dust to Soils of the Midwestern United States. *Geology* 26 (12):1135-1135.

Mason, J. A., P. M. Jacobs, R. S. B. Greene, and W. D. Nettleton. 2003. Sedimentary Aggregates in the Peoria Loess of Nebraska, USA. *CATENA* 53 (4):377-397.

Mason, J. A., and J. C. Knox. 1997. Age of Colluvium Indicates Accelerated Late Wisconsinan Hillslope Erosion in the Upper Mississippi Valley. *Geology* 25 (3):267-270.

Mason, J. A., E. A. Nater, and H. C. Hobbs. 1994. Transport Direction of Wisconsinan Loess in Southeastern Minnesota. *Quaternary Research* 41 (1):44-51.

Mason, J. A., E. A. Nater, C. W. Zanner, and J. C. Bell. 1999. A New Model of Topographic Effects on the Distribution of Loess. *Geomorphology* 28 (3-4):223-236.

Melillo, J., J. Aber, A. Linkins, A. Ricca, B. Fry, and K. Nadelhoffer. 1989. Carbon and Nitrogen Dynamics Along the Decay Continuum: Plant Litter to Soil Organic Matter. *Plant and Soil* 115 (2):189-198.

Mickelson, D. M., L. Clayton, D. S. Fullerton, and H. W. Borns Jr. 1983. The Late Wisconsin Glacial Record of the Laurentide Ice Sheet in the United States. In *Late Quaternary Environments of the United States*, ed. H. E. Wright Jr, 3–37. Minneapolis, MN: University of MN press.

Mickelson, D. M., J. C. Knox, and L. Clayton. 1982. Glaciation of the Driftless Area: An Evaluation of the Evidence. In *Quaternary History of the Driftless Area*, 155–169. Madison, Wisconsin: Geological and Natural History Survey, University of Wisconsin-Extension.

Moore, D. M., and R. C. Reynolds. 1989. *X-Ray Diffraction and the Identification and Analysis of Clay Minerals*. Oxford: Oxford University Press.

Morrison, B. C. 1968. Stratigraphy of the Eau Claire Formation of West-Central Wisconsin. MA Thesis, University of Wisconsin, Madison.

Muhs, D. R., T. A. Ager, E. A. Bettis, III, J. McGeehin, J. M. Been, J. E. Begét, M. J. Pavich, T. W. Stafford, and D. Stevens. 2003. Stratigraphy and Palaeoclimatic Significance of Late Quaternary Loess–Palaeosol Sequences of the Last Interglacial–Glacial Cycle in Central Alaska. *Quaternary Science Reviews* 22 (18-19):1947-1986.

Muhs, D. R., and E. A. Bettis, III. 2000. Geochemical Variations in Peoria Loess of Western Iowa Indicate Paleowinds of Midcontinental North America During Last Glaciation. *Quaternary Research* 53 (1):49-61.

Nadelhoffer, K. J., and B. Fry. 1988. Controls on Natural Nitrogen-15 and Carbon-13 Abundances in Forest Soil Organic Matter. *Soil Science Society of America Journal* 52 (6):1633-1640.

Nelson, D. M., and F. S. Hu. 2008. Patterns and Drivers of Holocene Vegetational Change near the Prairie-Forest Ecotone in Minnesota: Revisiting Mcandrews' Transect. *New Phytologist* 179 (2):449-459.

Nelson, D. M., F. S. Hu, E. C. Grimm, B. B. Curry, and J. E. Slate. 2006. The Influence of Aridity and Fire on Holocene Prairie Communities in the Eastern Prairie Peninsula. *Ecology* 87 (10):2523-2536.

Nelson, D. M., F. S. Hu, J. Tian, I. Stefanova, and T. A. Brown. 2004. Response of C3 and C4 Plants to Middle-Holocene Climatic Variation near the Prairie-Forest Ecotone of Minnesota. *Proceedings of the National Academy of Sciences of the United States of America* 101 (2):562-567.

Odom, I. E. 1975. Feldspar-Grain Size Relations in Cambrian Arenites, Upper Mississippi Valley. *Journal of Sedimentary Research* 45 (3):636-650.

Ostrom, M. E. 1970. Lithologic Cycles in Lower Paleozoic Rocks of Western Wisconsin. Information Circular No. 11. Wisconsin Geological and Natural History Survey: Madison, WI. 131.

Overpeck, J. T., R. S. Webb, and T. Webb, III. 1992. Mapping Eastern North American Vegetation Change of the Past 18 Ka: No-Analogs and the Future. *Geology* 20 (12):1071-1074.

Péwé, T. L. 1966. Paleoclimatic Significance of Fossil Ice Wedges. *Biuletyn Peryglacjalny* 15:65-73.

———. 1984. Present and Past Permafrost in the Temperate United States. *Me 'langes offerts a' Andre' Journaux*: 255-66.

——— ed. 1983. *The Periglacial Environment in North America During Wisconsin Time*.

Price, L. W. 1972. *The Periglacial Environment, Permafrost, and Man*. Washington, DC: Association of American Geographers.

Putman, B. R., I. J. Jansen, and L. R. Follmer. 1988. Loessial Soils: Their Relationship to Width of the Source Valley in Illinois. *Soil Science* 146 (4):241-247.

Pye, K. 1984. Loess. *Progress in Physical Geography* 8 (2):176-217.

Rawling, J. E., III, P. R. Hanson, A. R. Young, and J. W. Attig. 2008. Late Pleistocene Dune Construction in the Central Sand Plain of Wisconsin, USA. *Geomorphology* 100 (3-4):494-505.

Reheis, M. C. 1990. Influence of Climate and Eolian Dust on the Major-Element Chemistry and Clay Mineralogy of Soils in the Northern Bighorn Basin, USA. *CATENA* 17 (3):219-248.

Reimer, P. J., M. G. L. Baillie, E. Bard, A. Bayliss, J. W. Beck, P. G. Blackwell, C. B. Ramsey, C. E. Buck, G. S. Burr, R. L. Edwards, M. Friedrich, P. M. Grootes, T. P. Guilderson, I. Hajdas, T. J. Heaton, A. G. Hogg, K. Hughen, K. F. Kaiser, B. Kromer, F. G. McCormac, S. W. Manning, R. W. Reimer, D. A. Richards, J. Southon, S. Talamo, C. S. M. Turney, J. van der Plicht, and C. E. Weyhenmeyer. 2009. Intcal09 and Marine09 Radiocarbon Age Calibration Curves, 0-50,000 Years Cal Bp. *Radiocarbon* 51 (4):1111-1150.

Reynolds, R., J. Belnap, M. Reheis, P. Lamothe, and F. Luiszer. 2001. Aeolian Dust in Colorado Plateau Soils: Nutrient Inputs and Recent Change in Source. *Proceedings of the National Academy of Sciences* 98 (13):7123-7127.

Reynolds, R., J. Neff, M. Reheis, and P. Lamothe. 2006. Atmospheric Dust in Modern Soil on Aeolian Sandstone, Colorado Plateau (USA): Variation with Landscape Position and Contribution to Potential Plant Nutrients. *Geoderma* 130 (1–2):108-123.

Riise, G., P. Van Hees, U. Lundström, and L. Tau Strand. 2000. Mobility of Different Size Fractions of Organic Carbon, Al, Fe, Mn and Si in Podzols. *Geoderma* 94 (2-4):237-247.

Ritter, D. F., R. C. Kochel, and J. R. Miller. 2011. *Process Geomorphology*. 5th ed: Waveland Press, INC.

Rosenbloom, N. A., J. W. Harden, J. C. Neff, and D. S. Schimel. 2006. Geomorphic Control of Landscape Carbon Accumulation. *Journal of Geophysical Research* 111 (G1):G01004.

Ross, D. S., G. Matschonat, and U. Skyllberg. 2008. Cation Exchange in Forest Soils: The Need for a New Perspective. *European Journal of Soil Science* 59 (6):1141-1159.

Ruegg, G. H. J., M. E. Brookfield, and T. S. Ahlbrandt. 1983. Periglacial Eolian Evenly Laminated Sandy Deposits in the Late Pleistocene of NW Europe, a Facies Unrecorded in Modern Sedimentological Handbooks. In *Developments in Sedimentology*, 455-482: Elsevier.

Ruhe, R. V. 1954. Relations of the Properties of Wisconsin Loess to Topography in Western Iowa. *American Journal of Science* 252 (11):663-672.

———. 1983. Depositional Environment of Late Wisconsin Loess in the Midcontinental United States. In *Late-Quaternary Environments of the United States*, ed. H. E. Wright, Jr., 130–137. Minneapolis, MN: University of MN press.

Ruhe, R. V., and C. G. Olson. 1979. Estimate of Clay-Mineral Content - Additions of Proportions of Soil Clay to Constant Standard. *Clays and Clay Minerals* 27 (5):322-326.

———. 1980. Clay-Mineral Indicators of Glacial and Non-Glacial Sources of Wisconsinan Loesses in Southern Indiana, USA. *Geoderma* 24 (4):283-297.

Schaetzl, R. J. 1992. Texture, Mineralogy, and Lamellae Development in Sandy Soils in Michigan. *Soil Science Society of America Journal* 56 (5):1538-1545.

———. 2012. Comment On: Mississippi Valley Regional Source of Loess on the Southern Green Bay Lobe Land Surface, Wisconsin (Quat. Res. 75 (3), 574–583, 2011). *Quaternary Research* 78:149-151.

Schaetzl, R. J., and S. Anderson. 2005. *Soils: Genesis and Geomorphology*. New York: Cambridge University Press.

Schaetzl, R. J., and J. W. Attig. 2013. The Loess Cover of Northeastern Wisconsin. *Quaternary Research* 79 (2):199-214.

Schaetzl, R. J., and W. L. Loope. 2008. Evidence for an Eolian Origin for the Silt-Enriched Soil Mantles on the Glaciated Uplands of Eastern Upper Michigan, USA. *Geomorphology* 100 (3-4):285-295.

Schaetzl, R. J., and M. D. Luehmann. 2013. Coarse-Textured Basal Zones in Thin Loess Deposits: Products of Sediment Mixing and/or Paleoenvironmental Change? *Geoderma* 192 (0):277-285.

Scheel, T., C. Dörfler, and K. Kalbitz. 2007. Precipitation of Dissolved Organic Matter by Aluminum Stabilizes Carbon in Acidic Forest Soils. *Soil Science Society of America Journal* 71 (1):64-74.

Schoeneberger, P. J., D. A. Wysocki, E. C. Benham, and W. D. Broderson. 2002. Field Book for Describing and Sampling Soils, Version 2.0. *Natural Resources Conservation Service, National Soil Survey Center, Lincoln, NE*.

Schuur, E., and P. Matson. 2001. Net Primary Productivity and Nutrient Cycling across a Mesic to Wet Precipitation Gradient in Hawaiian Montane Forest. *Oecologia* 128 (3):431-442.

Schwan, J. 1988. The Structure and Genesis of Weichselian to Early Hologene Aeolian Sand Sheets in Western Europe. *Sedimentary Geology* 55 (3–4):197-232.

———. 1991. Palaeowetness Indicators in a Weichselian Late Glacial to Holocene Aeolian Succession in the Southwestern Netherlands. *Z. Geomorph. NF*:155-169.

Schwendenmann, L., and E. Veldkamp. 2005. The Role of Dissolved Organic Carbon, Dissolved Organic Nitrogen, and Dissolved Inorganic Nitrogen in a Tropical Wet Forest Ecosystem. *Ecosystems* 8 (4):339-351.

Scull, P., J. Franklin, O. A. Chadwick, and D. McArthur. 2003. Predictive Soil Mapping: A Review. *Progress in Physical Geography* 27 (2):171-197.

Semmel, A., and B. Terhorst. 2010. The Concept of the Pleistocene Periglacial Cover Beds in Central Europe: A Review. *Quaternary International* 222 (1–2):120-128.

Shearer, G., D. H. Kohl, and S.-H. Chien. 1978. The Nitrogen-15 Abundance in a Wide Variety of Soils1. *Soil Science Society of America Journal* 42 (6):899-902.

Smalley, I. J. 1966. The Properties of Glacial Loess and the Formation of Loess Deposits. *Journal of Sedimentary Research* 36 (3):669-676.

———. 1975. *Loess: Lithology and Genesis*: Dowden Hutchinson and Ross.

Smith, G. D. 1942. *Illinois Loess: Variations in Its Properties and Distribution, a Pedologic Interpretation*: University of Illinois, Agricultural Experiment Station.

Snowden, J. O., and R. R. Priddy. 1968. *Geology of Mississippi Loess*. Mississippi Geological Survey Bulletin. 111. 13–203.

Sollins, P., C. Swanston, M. Kleber, T. Filley, M. Kramer, S. Crow, B. A. Caldwell, K. Lajtha, and R. Bowden. 2006. Organic C and N Stabilization in a Forest Soil: Evidence from Sequential Density Fractionation. *Soil Biology and Biochemistry* 38 (11):3313-3324.

Sommer, M., D. Halm, C. Geisinger, I. Andruschkewitsch, M. Zarei, and K. Stahr. 2001. Lateral Podzolization in a Sandstone Catchment. *Geoderma* 103 (3-4):231-247.

Sommer, M., D. Halm, U. Weller, M. Zarei, and K. Stahr. 2000. Lateral Podzolization in a Granite Landscape. *Soil Science Society of America Journal* 64 (4):1434-1442.

Sommer, M., and E. Schlichting. 1997. Archetypes of Catenas in Respect to Matter - a Concept for Structuring and Grouping Catenas. *Geoderma* 76 (1-2):1-33.

Stablein, N. K., and E. C. Dapples. 1977. Feldspars of the Tunnel City Group (Cambrian), Western Wisconsin. *Journal of Sedimentary Research* 47 (4):1512-1538.

Stanley, K. E. 2008a. The Characterization and and Paleoenvironmental Significance of the North Central Wisconsin Loess Sheet. MS Thesis, Geography, Michigan State University, East Lansing.

———. 2008b. Unpublished Data. East Lansing, MI: Michigan State Univeristy

Stanley, K. E., and R. J. Schaetzl. 2011. Characteristics and Paleoenvironmental Significance of a Thin, Dual-Sourced Loess Sheet, North-Central Wisconsin. *Aeolian Research* 2 (4):241-251.

Stiles, C. A., and K. A. Stensvold. 2008. Loess Contribution to Soils Forming on Dolostone in the Driftless Area of Wisconsin. *Soil Science Society of America Journal* 72 (3):650-659.

Stone, E. L., W. G. Harris, R. B. Brown, and R. J. Kuehl. 1993. Carbon Storage in Florida Spodosols. *Soil Science Society of America Journal* 57 (1):179-182.

Sweeney, M. R., D. R. Gaylord, and A. J. Busacca. 2007. Evolution of Eureka Flat: A Dust-Producing Engine of the Palouse Loess, USA. *Quaternary International* 162–163 (0):76-96.

Trumbore, S. 2000. Age of Soil Organic Matter and Soil Respiration: Radiocarbon Constraints on Belowground C Dynamics. *Ecological Applications* 10 (2):399-411.

Trumbore, S. E., and C. I. Czimczik. 2008. An Uncertain Future for Soil Carbon. *Science* 321 (5895):1455-1456.

Tsoar, H., and K. Pye. 1987. Dust Transport and the Question of Desert Loess Formation. *Sedimentology* 34 (1):139-153.

Umbanhowar, C. E., Jr. 2004. Interaction of Fire, Climate and Vegetation Change at a Large Landscape Scale in the Big Woods of Minnesota, USA. *The Holocene* 14 (5):661-676.

Umbanhowar, C. E., Jr. , P. Camill, C. E. Geiss, and R. Teed. 2006. Asymmetric Vegetation Responses to Mid-Holocene Aridity at the Prairie-Forest Ecotone in South-Central Minnesota. *Quaternary Research* 66 (1):53-66.

Volkoff, B., and C. C. Cerri. 1987. Carbon Isotopic Fractionation in Subtropical Brazilian Grassland Soils. Comparison with Tropical Forest Soils. *Plant and Soil* 102 (1):27-31.

Wada, E., R. Imaizumi, and Y. Takai. 1984. Natural Abundance of $^{15}N$ in Soil Organic Matter with Special Reference to Paddy Soils in Japan: Biogeochemical Implications on the Nitrogen Cycle. *Geochem. J* 18:109–123.

Waroszewski, J., K. Kalinski, M. Malkiewicz, R. Mazurek, G. Kozlowski, and C. Kabala. 2013. Pleistocene–Holocene Cover-Beds on Granite Regolith as Parent Material for Podzols — an Example from the Sudeten Mountains. *CATENA* 104 (0):161-173.

Waroszewski, J., M. Malkiewicz, R. Mazurek, B. Labaz, P. Jezierski, and C. Kabala. 2015. Lithological Discontinuities in Podzols Developed from Sandstone Cover Beds in the Stolowe Mountains (Poland). *CATENA* 126 (0):11-19.

Webb, T., III, E. J. Cushing, and H. E. Wright Jr. 1983. Holocene Changes in the Vegetation of the Midwest. In *Late-Quaternary Environments of the United States*, ed. H. E. Wright, Jr., 142-165.

Webb, T., III, B. Shuman, and J. W. Williams. 2004. Climatically Forced Vegetation Dynamics in Eastern North America During the Late Quaternary Period. *The Quaternary Period in the United States*:459–478.

Weisenborn, B. N., and R. J. Schaetzl. 2005. Range of Fragipan Expression in Some Michigan Soils: I. Morphological, Micromorphological, and Pedogenic Characterization. *Soil Science Society of America Journal* 69 (1):168-177.

West, L. T., E. M. Rutledge, and D. M. Barber. 1980. Sources and Properties of Loess Deposits on Crowley's Ridge in Arkansas. *Soil Science Society of America Journal* 44 (2):353-358.

Williams, J. W., B. Shuman, P. J. Bartlein, N. S. Diffenbaugh, and T. Webb. 2010. Rapid, Time-Transgressive, and Variable Responses to Early Holocene Midcontinental Drying in North America. *Geology* 38 (2):135-138.

Williams, J. W., B. N. Shuman, and T. Webb, III. 2001. Dissimilarity Analyses of Late-Quaternary Vegetation and Climate in Eastern North America. *Ecology* 82 (12):3346-3362.

Williams, J. W., B. N. Shuman, T. Webb, III, P. J. Bartlein, and P. L. Leduc. 2004. Late-Quaternary Vegetation Dynamics in North America: Scaling from Taxa to Biomes. *Ecological Monographs* 74 (2):309-334.

Willman, H. B., and J. C. Frye. 1970. Pleistocene Stratigraphy of Illinois. Bulletin 94. Illinois State Geological Survey Bulletin: Urbana, IL.

Wright, H. E., I. Stefanova, J. Tian, T. A. Brown, and F. S. Hu. 2004. A Chronological Framework for the Holocene Vegetational History of Central Minnesota: The Steel Lake Pollen Record. *Quaternary Science Reviews* 23 (5-6):611-626.

Yoo, K., R. Amundson, A. M. Heimsath, and W. E. Dietrich. 2006. Spatial Patterns of Soil Organic Carbon on Hillslopes: Integrating Geomorphic Processes and the Biological C Cycle. *Geoderma* 130 (1-2):47-65.

*Appendix 1: Laser particle size data for profile samples in central Jackson County, Wisconsin.*

| Sample | Depth (cm) | Median µm | Mean µm | Mean Φ | SD Φ | Sort | Sk Φ | Sk | Tx | Clay | Silt | Sand | 2 -30 | 30-63 µm | VFS | FS | MS | CS | VCS |
|---|---|---|---|---|---|---|---|---|---|---|---|---|---|---|---|---|---|---|---|
| R12 A | 0-5 | 59.2 | 116.0 | 4.3 | 2.4 | VPS | 0.2 | CSk | FSL | 4.0 | 46.6 | 49.4 | 36.1 | 10.5 | 8.4 | 20.9 | 18.6 | 1.5 | 0.0 |
| R12 Bw1 | 5-37 | 121.2 | 133.4 | 3.9 | 2.4 | VPS | 0.5 | SCSk | FSL | 4.4 | 36.7 | 58.9 | 29.3 | 7.4 | 9.8 | 29.6 | 19.2 | 0.3 | 0.0 |
| R12 Bw2 | 37-59 | 180.0 | 176.2 | 3.3 | 2.1 | VPS | 0.6 | SCSk | LS | 2.8 | 21.4 | 75.8 | 17.1 | 4.3 | 9.7 | 35.3 | 28.6 | 2.2 | 0.0 |
| R12 Bt1 | 59-76 | 172.8 | 172.7 | 3.6 | 2.4 | VPS | 0.6 | SCSk | FSL | 4.1 | 26.5 | 69.4 | 21.5 | 5.0 | 7.7 | 30.9 | 27.9 | 2.9 | 0.0 |
| R12 Bt2 | 76-80 | 206.8 | 200.5 | 3.4 | 2.5 | VPS | 0.7 | SCSk | SL | 4.3 | 24.4 | 71.3 | 20.4 | 4.0 | 4.2 | 27.3 | 34.2 | 5.6 | 0.0 |
| R12 2E/Bt (E) | 80-84 | 349.9 | 363.7 | 1.5 | 0.6 | MWS | 0.1 | Sym | S | 0.4 | 3.6 | 96.1 | 2.8 | 0.7 | 0.0 | 16.6 | 62.2 | 17.2 | 0.0 |
| R12 2E&Bt (Bt) | 87-89 | 312.9 | 257.3 | 2.9 | 2.3 | VPS | 0.8 | SCSk | LS | 3.5 | 17.0 | 79.5 | 14.8 | 2.2 | 0.0 | 10.6 | 61.2 | 7.7 | 0.0 |
| R12 2E/Bt (E) | 90-93 | 303.1 | 323.1 | 1.7 | 0.6 | MWS | 0.0 | Sym | S | 0.1 | 1.1 | 98.8 | 1.1 | 0.0 | 0.9 | 31.3 | 53.7 | 12.8 | 0.0 |
| R12 2E&Bt (Bt) | 95-98 | 337.0 | 345.8 | 1.7 | 1.7 | PS | 0.5 | SCSk | LS | 5.8 | 7.6 | 86.6 | 7.2 | 0.5 | 0.2 | 16.6 | 49.4 | 20.4 | 0.0 |
| R12 2E/Bt (E) | 109-114 | 321.4 | 343.1 | 1.7 | 0.8 | MS | 0.1 | CSk | S | 0.4 | 2.8 | 96.8 | 2.5 | 0.3 | 2.7 | 26.5 | 48.9 | 18.8 | 0.0 |
| R12 2E&Bt (Bt) | 122-127 | 391.0 | 400.3 | 1.4 | 1.4 | PS | 0.4 | SCSk | S | 3.4 | 4.8 | 91.7 | 4.8 | 0.0 | 0.0 | 6.3 | 61.0 | 24.4 | 0.0 |
| R12 2E/Bt (E) | 140-145 | 314.1 | 332.8 | 1.7 | 0.6 | MWS | 0.0 | Sym | S | 0.0 | 1.1 | 98.9 | 1.1 | 0.0 | 0.7 | 28.8 | 55.4 | 14.0 | 0.0 |
| R12 2E&Bt (Bt) | 166-170 | 256.4 | 268.3 | 2.0 | 0.6 | MWS | 0.1 | Sym | S | 1.2 | 2.1 | 96.6 | 2.1 | 0.0 | 1.9 | 42.2 | 49.1 | 3.3 | 0.0 |
| R12 2E&Bt (E) | 170-180 | 266.5 | 285.8 | 1.9 | 0.7 | MWS | 0.0 | Sym | S | 0.0 | 0.5 | 99.5 | 0.5 | 0.0 | 4.9 | 39.5 | 46.7 | 8.4 | 0.0 |
| W40 AE | 1-6 | 212.9 | 218.6 | 3.2 | 2.3 | VPS | 0.6 | SCSk | LS | 2.0 | 25.5 | 72.4 | 21.9 | 3.6 | 5.2 | 24.9 | 32.3 | 10.0 | 0.0 |
| W40 Bs | 6-12 | 184.2 | 184.2 | 3.4 | 2.3 | VPS | 0.6 | SCSk | LS | 2.7 | 23.7 | 73.6 | 21.3 | 2.5 | 8.3 | 31.4 | 29.6 | 4.3 | 0.0 |
| W40 Bw1 | 12-30 | 196.8 | 199.8 | 3.2 | 2.2 | VPS | 0.6 | SCSk | LS | 2.7 | 19.9 | 77.4 | 17.9 | 2.1 | 8.6 | 31.6 | 30.0 | 7.1 | 0.2 |
| W40 Bw2 | 30-45 | 218.6 | 218.6 | 2.9 | 2.1 | VPS | 0.6 | SCSk | LS | 2.3 | 16.4 | 81.3 | 14.7 | 1.6 | 7.4 | 31.4 | 33.7 | 8.8 | 0.0 |
| W40 Bw2 | 45-59 | 212.7 | 231.8 | 2.4 | 1.6 | PS | 0.4 | SCSk | LS | 1.8 | 12.5 | 85.7 | 11.4 | 1.1 | 10.0 | 35.2 | 32.5 | 7.9 | 0.0 |
| W40 2Bw3 | 59-80 | 210.1 | 231.8 | 2.3 | 1.4 | PS | 0.3 | SCSk | S | 1.4 | 9.4 | 89.2 | 7.9 | 1.5 | 12.4 | 37.5 | 32.4 | 6.9 | 0.0 |
| W40 2Bt | 80-84 | 182.9 | 183.1 | 3.4 | 2.3 | VPS | 0.6 | SCSk | FSL | 4.0 | 22.5 | 73.5 | 19.1 | 3.3 | 8.6 | 31.4 | 29.4 | 4.0 | 0.0 |
| W40 3E&Bt (E) | 90-103 | 194.9 | 220.0 | 2.4 | 1.3 | PS | 0.3 | CSk | S | 1.0 | 8.3 | 90.7 | 7.8 | 0.5 | 16.0 | 39.7 | 29.0 | 6.0 | 0.1 |
| W40 3E&Bt (Bt) | 94-96 | 290.1 | 286.5 | 2.5 | 2.1 | VPS | 0.6 | SCSk | LS | 2.4 | 17.1 | 80.5 | 12.7 | 4.3 | 4.1 | 19.0 | 37.9 | 19.3 | 0.2 |
| W40 3E&Bt (Bt) | 107-108 | 226.3 | 241.0 | 2.5 | 1.8 | PS | 0.5 | SCSk | LS | 2.8 | 13.5 | 83.8 | 10.6 | 2.9 | 8.3 | 30.9 | 33.5 | 11.1 | 0.0 |

| Sample | Depth (cm) | Median µm | Mean µm | Mean Φ | SD Φ | Sort | Sk Φ | Sk | Tx | Clay | Silt | Sand | 2 -30 | 30-63 µm | VFS | FS | MS | CS | VCS |
|---|---|---|---|---|---|---|---|---|---|---|---|---|---|---|---|---|---|---|---|
| W41 A | 3-13 | 160.7 | 197.6 | 3.6 | 2.7 | VPS | 0.5 | SCSk | SL | 3.6 | 37.0 | 59.4 | 32.7 | 4.3 | 4.4 | 19.4 | 24.4 | 10.2 | 1.0 |
| W41 EBg | 13-17 | 205.8 | 208.2 | 3.2 | 2.2 | VPS | 0.6 | SCSk | LS | 2.3 | 21.0 | 76.7 | 18.9 | 2.0 | 6.7 | 30.5 | 30.7 | 8.0 | 0.8 |
| W41 Bhg | 17-26 | 218.9 | 220.3 | 2.8 | 1.9 | PS | 0.5 | SCSk | LS | 1.3 | 18.5 | 80.1 | 14.3 | 4.3 | 6.6 | 31.1 | 33.6 | 8.8 | 0.1 |
| W41 Bhs | 26-42 | 252.9 | 275.2 | 2.0 | 1.3 | PS | 0.3 | SCSk | S | 0.8 | 9.4 | 89.9 | 7.6 | 1.8 | 6.0 | 33.1 | 39.3 | 11.1 | 0.3 |
| W41 Bg | 42-51 | 285.1 | 314.6 | 1.8 | 0.8 | MS | 0.1 | Sym | S | 0.1 | 3.4 | 96.5 | 3.1 | 0.3 | 5.4 | 32.3 | 42.7 | 15.4 | 0.7 |
| W41 Bhg' | 51-70 | 214.4 | 244.8 | 2.2 | 1.1 | PS | 0.2 | CSk | S | 0.4 | 5.4 | 94.2 | 4.7 | 0.7 | 14.2 | 39.4 | 31.3 | 8.7 | 0.6 |
| W41 2Cg | 70+ | 266.8 | 284.6 | 1.9 | 0.8 | MS | 0.1 | CSk | S | 0.0 | 1.0 | 99.0 | 0.7 | 0.3 | 9.0 | 35.4 | 45.2 | 9.5 | 0.0 |
| W42 A | 5-16 | 216.8 | 223.2 | 3.3 | 2.5 | VPS | 0.6 | SCSk | SL | 2.8 | 30.8 | 66.4 | 27.3 | 3.5 | 2.3 | 20.4 | 32.4 | 11.3 | 0.1 |
| W42 E | 16-27 | 282.2 | 269.2 | 2.7 | 2.1 | VPS | 0.6 | SCSk | LS | 1.9 | 16.7 | 81.4 | 14.7 | 2.1 | 1.6 | 22.6 | 41.4 | 15.8 | 0.1 |
| W42 Bhs | 27-31 | 248.1 | 239.3 | 3.2 | 2.5 | VPS | 0.7 | SCSk | SL | 3.7 | 25.8 | 70.5 | 22.6 | 3.2 | 1.2 | 19.7 | 37.6 | 12.0 | 0.0 |
| W42 Bs | 31-35 | 261.7 | 256.4 | 3.0 | 2.5 | VPS | 0.6 | SCSk | SL | 3.4 | 24.1 | 72.5 | 20.8 | 3.3 | 1.3 | 18.9 | 36.8 | 15.3 | 0.1 |
| W42 Bw1 | 35-47 | 252.5 | 245.5 | 3.0 | 2.4 | VPS | 0.6 | SCSk | LS | 3.1 | 22.3 | 74.7 | 19.0 | 3.3 | 1.9 | 22.2 | 37.4 | 12.8 | 0.4 |
| W42 Bw2 | 47-63 | 256.6 | 252.9 | 2.6 | 2.0 | PS | 0.6 | SCSk | LS | 2.1 | 14.9 | 83.0 | 12.8 | 2.1 | 3.9 | 27.6 | 38.7 | 12.8 | 0.0 |
| W42 BC | 63-81 | 247.5 | 267.0 | 2.1 | 1.1 | PS | 0.3 | CSk | S | 0.6 | 5.3 | 94.1 | 4.6 | 0.6 | 8.7 | 36.1 | 40.7 | 8.6 | 0.0 |
| W42 Cg | 81+ | 219.7 | 239.0 | 2.2 | 0.7 | MS | 0.0 | Sym | S | 0.0 | 1.2 | 98.8 | 1.0 | 0.2 | 11.2 | 47.9 | 34.5 | 4.6 | 0.8 |
| L43 E | 4-8 | 38.8 | 115.1 | 4.6 | 2.6 | VPS | 0.0 | Sym | SiL | 4.8 | 50.6 | 44.6 | 40.9 | 9.7 | 5.7 | 17.0 | 18.3 | 3.5 | 0.1 |
| L43 Bt1 | 8-19 | 39.7 | 109.2 | 4.6 | 2.6 | VPS | 0.1 | Sym | FSL | 5.9 | 49.0 | 45.1 | 39.7 | 9.4 | 6.5 | 18.6 | 18.1 | 1.9 | 0.0 |
| L43 Bt2 | 19-30 | 56.2 | 121.7 | 4.4 | 2.6 | VPS | 0.2 | CSk | FSL | 5.3 | 45.6 | 49.0 | 36.2 | 9.4 | 6.3 | 19.8 | 20.4 | 2.6 | 0.0 |
| L43 Bw | 30-42 | 53.7 | 120.1 | 4.4 | 2.6 | VPS | 0.2 | CSk | FSL | 5.3 | 46.1 | 48.5 | 36.1 | 10.0 | 6.4 | 19.5 | 20.0 | 2.6 | 0.0 |
| L43 Ex | 42-54 | 59.8 | 116.7 | 4.4 | 2.5 | VPS | 0.2 | CSk | FSL | 5.6 | 44.8 | 49.6 | 35.5 | 9.3 | 7.1 | 21.7 | 19.4 | 1.4 | 0.0 |
| L43 Btx | 54-69 | 109.3 | 149.5 | 4.0 | 2.7 | VPS | 0.5 | SCSk | FSL | 5.7 | 40.7 | 53.5 | 33.6 | 7.1 | 5.4 | 20.8 | 23.4 | 4.0 | 0.0 |
| L43 2C | 69+ | 247.6 | 258.7 | 2.2 | 1.4 | PS | 0.4 | SCSk | S | 1.2 | 12.9 | 85.8 | 9.2 | 3.8 | 5.4 | 31.0 | 39.8 | 9.6 | 0.0 |

| Sample | Depth (cm) | Median µm | Mean µm | Mean Φ | SD Φ | Sort | Sk Φ | Sk | Tx | Clay | Silt | Sand | 2 -30 | 30-63 µm | VFS | FS | MS | CS | VCS |
|---|---|---|---|---|---|---|---|---|---|---|---|---|---|---|---|---|---|---|---|
| L44 A | 11-14 | 22.6 | 73.4 | 5.0 | 2.3 | VPS | -0.2 | FSk | SiL | 4.0 | 70.1 | 25.8 | 55.7 | 14.4 | 4.4 | 10.4 | 10.2 | 0.8 | 0.0 |
| L44 E | 14-18 | 21.5 | 83.8 | 5.1 | 2.5 | VPS | -0.2 | FSk | SiL | 5.9 | 62.5 | 31.6 | 52.0 | 10.6 | 5.7 | 12.2 | 12.0 | 1.7 | 0.0 |
| L44 EB | 18-25 | 22.4 | 82.1 | 5.1 | 2.5 | VPS | -0.1 | FSk | SiL | 5.6 | 62.7 | 31.7 | 51.6 | 11.2 | 5.7 | 12.9 | 11.8 | 1.2 | 0.0 |
| L44 Bt | 25-38 | 23.0 | 83.2 | 5.1 | 2.5 | VPS | -0.1 | FSk | SiL | 5.6 | 64.8 | 29.6 | 51.6 | 13.2 | 4.9 | 11.3 | 12.0 | 1.4 | 0.0 |
| L44 Bt | 38-52 | 21.3 | 78.7 | 5.2 | 2.6 | VPS | -0.1 | FSk | SiL | 7.1 | 61.5 | 31.5 | 51.0 | 10.5 | 5.2 | 14.8 | 11.1 | 0.4 | 0.0 |
| L44 Ex | 52-57 | 26.0 | 96.3 | 5.0 | 2.7 | VPS | -0.1 | Sym | SiL | 6.9 | 56.3 | 36.8 | 46.1 | 10.2 | 5.4 | 14.5 | 14.8 | 2.0 | 0.0 |
| L44 Btx1 | 57-70 | 22.5 | 96.6 | 5.1 | 2.7 | VPS | -0.1 | FSk | SiL | 7.7 | 57.2 | 35.2 | 48.3 | 8.9 | 4.4 | 13.5 | 15.1 | 2.3 | 0.0 |
| L44 Btx1 | 70-89 | 25.5 | 103.5 | 5.0 | 2.7 | VPS | -0.1 | Sym | SiL | 7.2 | 55.2 | 37.7 | 46.0 | 9.2 | 4.1 | 14.2 | 17.3 | 2.1 | 0.0 |
| L44 2Btx2 | 89-109 | 177.5 | 180.4 | 3.4 | 2.3 | VPS | 0.6 | SCSk | SL | 3.4 | 30.1 | 66.5 | 23.0 | 7.1 | 5.6 | 27.7 | 29.4 | 3.8 | 0.0 |
| L44 2C | 109+ | 296.2 | 314.0 | 1.8 | 0.7 | MS | 0.1 | CSk | S | 0.4 | 4.6 | 95.0 | 3.4 | 1.1 | 1.4 | 30.0 | 51.5 | 12.2 | 0.0 |
| L48 E | 6-14 | 63.8 | 147.8 | 4.1 | 2.6 | VPS | 0.1 | CSk | FSL | 4.0 | 45.8 | 50.2 | 34.1 | 11.7 | 12.5 | 12.4 | 16.5 | 8.6 | 0.3 |
| L48 Bw | 14-34 | 44.5 | 109.5 | 4.8 | 2.8 | VPS | 0.2 | CSk | L | 8.2 | 47.3 | 44.6 | 36.7 | 10.6 | 13.1 | 13.0 | 15.0 | 3.4 | 0.0 |
| L48 2Ex | 34-51 | 35.2 | 92.0 | 5.0 | 2.7 | VPS | 0.1 | Sym | SiL | 7.8 | 51.5 | 40.7 | 39.6 | 11.9 | 12.4 | 13.4 | 11.0 | 3.9 | 0.1 |
| L48 2Btx1 | 51-70 | 31.7 | 98.9 | 5.0 | 2.8 | VPS | 0.0 | Sym | SiL | 8.6 | 51.8 | 39.6 | 40.4 | 11.3 | 10.4 | 12.3 | 13.7 | 3.2 | 0.0 |
| L48 2Btx2 | 70-83 | 47.4 | 116.8 | 4.6 | 2.7 | VPS | 0.1 | CSk | FSL | 6.9 | 47.4 | 45.7 | 35.6 | 11.7 | 10.5 | 14.7 | 15.9 | 4.5 | 0.1 |
| L48 3BC | 83-114 | 248.9 | 292.3 | 3.0 | 2.7 | VPS | 0.5 | SCSk | SL | 4.0 | 25.7 | 70.4 | 18.9 | 6.8 | 6.8 | 13.7 | 26.3 | 19.4 | 4.2 |
| L48 4C | 114-125 | 309.7 | 300.8 | 2.3 | 1.9 | PS | 0.6 | SCSk | LS | 1.8 | 15.2 | 83.0 | 10.7 | 4.4 | 4.9 | 16.8 | 41.3 | 20.0 | 0.0 |
| L48 5Ab | 125-131 | 12.6 | 17.4 | 6.5 | 1.9 | PS | 0.1 | CSk | Si | 11.2 | 81.8 | 7.0 | 67.2 | 14.6 | 2.8 | 1.1 | 1.8 | 1.3 | 0.0 |
| L48 5Eb | 131-142 | 11.1 | 15.9 | 6.7 | 2.1 | VPS | 0.0 | Sym | SiL | 12.0 | 79.6 | 8.5 | 69.2 | 10.4 | 1.8 | 3.4 | 3.1 | 0.1 | 0.0 |
| L48 5Bsb | 142-153 | 22.1 | 100.5 | 5.5 | 3.3 | VPS | 0.1 | Sym | L | 18.0 | 45.5 | 36.5 | 36.9 | 8.6 | 5.6 | 12.3 | 15.4 | 3.1 | 0.0 |
| L48 6Cr | 153+ | 164.6 | 179.8 | 3.5 | 2.4 | VPS | 0.6 | SCSk | SL | 4.0 | 33.0 | 63.0 | 26.0 | 7.0 | 5.9 | 24.2 | 27.3 | 5.6 | 0.0 |
| L48 6Cr | 195-200 | 193.1 | 197.9 | 3.1 | 2.2 | VPS | 0.6 | SCSk | LS | 2.9 | 21.6 | 75.4 | 16.4 | 5.2 | 9.3 | 29.1 | 30.8 | 6.2 | 0.0 |

SD=Standard deviation; Sort=Sorting; Sk=Skew; Tx=Texture class; VFS=63-125 µm; FS=125-250 µm; MS=250-500 µm; CS=500-1000 µm; VCS= 1000-2000 µm.
Skewness: FSk= fine skewed; Sym=nearly symmetrical; SCSk= slightly coarse skewed; CSk= coarse skewed.
Texture: Si=silt; SiL= silty loam; L= loam; SL= sandy loam; LS= loamy sand; S= sand

## *Appendix 2: Profile descriptions*

| Site | Horizon | Depth (cm) | Moist color (Munsell) | Structure | | | Cons. (m) | Tx | Boundary | | Coarse Frag % | | Comments |
|---|---|---|---|---|---|---|---|---|---|---|---|---|---|
| | | | | Gr | Sz | Sh | | | D | T | Gr | Co | |
| W40 | Oi | 0-1 | | | | | | | c | s | 0 | 0 | Less than 1cm Oe below |
| | AE | 1-6 | 10YR 2/2 | w | med + c | gr | vf - L | LS | a | w | 0 | 0 | 50/50 clean sand grains; parting to loose; many fine to med roots |
| | Bs | 6-12 | 7.5YR 3/4 | m | med-f | sbk | fr | S | a | w | 0 | 0 | Common med roots |
| | Bw1 | 12-30 | 10YR 4/4 | w | f | sbk-sg | fr | LFS | c | s | 0 | 0 | Moderately-few med. roots |
| | Bw2 | 30-59 | 10YR 5/4 | w | med-f | sbk-sg | fr-L | LFS | c | s | 2 | 0 | No gravels at the top of the horizon, increasing towards base; m-few med roots |
| | 2Bw3 | 59-80 | 10YR 6/4 | w | c | sbk-M | fr | LS | c | w | 10 | 15 | Moderately-few med. roots; thin (2-5mm) lamellae (7.5YR 4/4, strong med. sbk firm) between flaggy gravels; gravels are randomly oriented around 2 large flaggy cobbles, which are sub-horizontal (do not appear imbricated), but are oriented parallel to the slope; lamellae appear to be bioturbated and/or disrupted by mass-wasting; redox concentrations present |
| | 2Bt | 80-84 | 7.5YR4/4 | s | med | sbk | firm | SL | c | w | 10 | 15 | |
| | 3E&Bt | 84-135+ | 10YR 7/4 | | | M | fr | LS | - | - | 2 | 0 | Moderately-few med. roots; 40% of horizon is 10YR 6/6 strong, med, sbk, firm lamellae; Fe concentrations 7.5YR 5/8 are common, fine, irregular, and distinct |

| Site | Horizon | Depth (cm) | Moist color (Munsell) | Structure | | | Cons. (m) | Tx | Boundary | | Coarse Frag % | | Comments |
|---|---|---|---|---|---|---|---|---|---|---|---|---|---|
| | | | | Gr | Sz | Sh | | | D | T | Gr | Co | |
| W41 | Oi | 1-3 | | | | | | | | | 0 | 0 | A lot of hemic material too |
| | A | 3-13 | 10YR 2/1 | w | f | gr | vf | S | c | w | 0 | 0 | Common uncoated sand grains |
| | EBg | 13-17 | 7.5YR 4/1 | w | f | sbk to M | fr | S | gual | w | | | |
| | Bhg | 17-26 | 7.5YR 3/1 | w | f & med | sbk | fr | S | c | w | 0 | 0 | Many uncoated sand grains |
| | Bhsm | 26-42 | 2.5YR 2.5/1 | w | lg | sbk to M | firm | S | c | w | 0 | 0 | |
| | Bg | 42-51 | 7.5YR 3.5/2 | w | lg | sbk to M | fr | S | gual | w | 0 | 0 | Some 7.5YR 6/2 and streaks of 7.5YR 3/1 throughout |
| | Bhg' | 51-70 | 7.5YR 3/3 and 5YR 2.5/1 | w | lg | sbk | fr - firm | S | c | w | 2 | 0 | Where the color is darker, the structure is m-strong sbk; glauconite lenses at the base of the horizon |
| | 2Cg | 70+ | 10YR 6/2 | | | M | fr | S | - | - | 2 | 0 | Tends to become more consolidated with depth; sandstone fragments increase; Water table @ 79 cm, smells like sulfur, and seems to stain the bedrock residuum |

| Site | Horizon | Depth (cm) | Moist color (Munsell) | Structure | | | Cons. (m) | Tx | Boundary | | Coarse Frag % | | Comments |
|---|---|---|---|---|---|---|---|---|---|---|---|---|---|
| | | | | Gr | Sz | Sh | | | D | T | Gr | Co | |
| W42 | Oe | 0-5 | | | | | | | | | 0 | 0 | <1cm of Oi at the surface; moss common |
| | A | 5-16 | 10YR 2/1 | m | f - med | gr | fr to L | S | c | w | 0 | 0 | Bioturbated; many fine, med, and coarse roots |
| | E | 16-27 | 10YR 4/3 with patches of 3/1 | w | med | sbk | fr to L | S | c | w | 0 | 0 | Bioturbated lower boundary; face 10YR 6/2; tends to get darker towards surface |
| | Bhs | 27-31 | 7.5YR 3/3 | s | med | sbk | fr to L | LS | c | w | 0 | 0 | Bioturbated with overlying E horizon |
| | Bs | 31-35 | 5YR 4/6 | w | f to med | sbk | vfr to L | S | c | w | 0 | 0 | Fine, med, and coarse roots common; ants presently feeding on dead roots |
| | Bw1 | 35-47 | 7.5YR 4/6 | w | med | sbk | vfr to L | S | gual | s | 2 | 0 | Fine roots common, med and coarse roots are m. Few; few mottles along root traces |
| | Bw2 | 47-63 | 10YR 5/4 | w | med | sbk | fr | S | gual | w | 2 | 5 | Mottles: 2.5YR 4/8 along root traces (prominent, few-common); gravels and cobbles are concentrated at the top of the horizon and are subhorizontal, but do not appear imbricated; fine roots common, few med. Roots |
| | BC | 63-81 | 10YR 6/4 | w | med | sbk-abk | fr | S | gual | w | 0 | 0 | Mottles: 5YR 6/8 prominent, common, along root traces |
| | Cg | 81+ | 2.5 8/1 (gley) | | | M | fr | S | gual | w | 0 | 0 | Gley matrix, few prominent Fe concentrations 10YR 6/8 around root traces |

| Site | Horizon | Depth | Moist color | Structure | | | Cons. | Tx | Boundary | | Coarse Frag % | | Comments |
|---|---|---|---|---|---|---|---|---|---|---|---|---|---|
| | | (cm) | (Munsell) | Gr | Sz | Sh | (m) | | D | T | Gr | Co | |
| L43 | Oi | 0-2 | | | | | | | c | s | | | |
| | Oe | 2-4 | | | | | | | c | w | | | |
| | E | 4-8 | 10YR 5/2-4/1 | w | med | gr | vfr-L | LS | c | w | | | |
| | Bt1 | 8-19 | 10YR 4/4 | s | med-f | sbk | fr | FSL | c | s | | | |
| | Bt2 | 19-30 | 10YR 4/4 | s | med | sbk | fr | FSL | gual | s | | | |
| | Bw | 30-42 | 10YR 6/4 | m-w | med | sbk | fr | FSL | c | w | | | Weak diffuse Fe concentratons |
| | Ex | 42-54 | 10YR 6/3 (ped face) 10YR 4/4 (inside ped) | s | med-lg | sbk-M | firm | FSL | c | i | | | Inside of peds appear to be Bt material; bioturbation evident |
| | Btx | 54-69 | 10YR 5/6 | s | lg | sbk | firm | SL | c | i | | | Clay films (7.5YR 3/3); appears bioturbated; differences in colors are distinct |
| | C | 69+ | 10YR 7/3 | | | M | L-sg | FS | | | | | Dark colored laminae |

| Site | Horizon | Depth (cm) | Moist color (Munsell) | Structure | | | Cons. (m) | Tx | Boundary | | Coarse Frag % | | Comments |
|---|---|---|---|---|---|---|---|---|---|---|---|---|---|
| | | | | Gr | Sz | Sh | | | D | T | Gr | Co | |
| L44 | Oi | 0-8 | | | | | | | | | | | Fluffy; mostly leaves from this year and last |
| | Oe | 8-11 | | | | | | | c | w | | | |
| | A | 11-14 | 10YR 3/1 | m-s | f & med | gr | fr | L | c | w | | | Clean sand grains |
| | E | 14-18 | 10YR 5/2 | m-s | vf-f | gr | vfr | VFSL | c | w | | | |
| | EB | 18-25 | 10YR 4/4 | w | f-vf | sbk | vfr | L | | | | | |
| | Bt | 25-52 | 10YR 4/4 | w-m | f-med | sbk | fr | L | gual | w | | | Fine and very fine roots common, decreasing with depth |
| | Ex | 52-57 | 10YR 5/4 | m | med | sbk | firm | VFSL | c | w | | | Parting to platy; inside of peds seem like they have clay inside (10YR4/4); fine and medium roots, few. |
| | Btx1 | 57-89 | 7.5YR 4/6 | s | med | sbk | f | FSL | c | w | | | Parts to platy structure; few fine and medium roots towards the top of the horizon; prominent clay films (7.5YR 3/3 with flecks of 7.5YR 2/1) |
| | 2Btx2 | 89-109 | 10YR 5/6 | w | med | sbk-p | firm | SL | a | s | | | Lamellae between 1 and 4 cm thick (7.5 YR 3/4); very few fine roots; seems bioturbated |
| | 2C | 109+ | 2.5YR 8/2 | | | sg | L | S | - | - | | | Fe concentrations (7.5YR 6/8); Lamellae (7.5YR 3/4) |

| Site | Horizon | Depth (cm) | Moist color (Munsell) | Structure Gr | Sz | Sh | Cons. (m) | Tx | Boundary D | T | Coarse Frag % Gr | Co | Comments |
|---|---|---|---|---|---|---|---|---|---|---|---|---|---|
| L48 | Oi | 0-3 | | | | | | | | | | | Mostly oak leaves, some maple leaves |
| | Oa | 3-6 | | | | | | | | | | | Many fine roots |
| | E | 6-14 | 10YR 5/2 | m | med | p | fr | SL | c | w | 20 | 5 | Cobble size are channers |
| | Bw | 14-34 | 10YR 5/6 | w | f | sbk | fr-vfr | SL | c | w | 10 | 40 | Gravels: coarse to very coarse; channery cobbles; no sense of imbrication - randomly oriented and unsorted |
| | 2EX | 34-51 | 10YR 6/4 (inside peds: 10YR 5/6) | m | med | sbk | fr-f | VFSL | g | w | 0 | 0 | 2% fine roots |
| | 2Btx1 | 51-70 | 10YR 5/6 | m | f | sbk-M | f | VFSL | g | w | 0 | 0 | 10% med and coarse roots |
| | 2Btx2 | 70-83 | 10YR 5/4 (cutans: 7.5YR 3/4) | s | med-c | sbk-abk | f | VFSL | c | w | 0 | 0 | |
| | 3BC | 83-112 | 10YR 5/4 | w | m | sbk | fr | v. grav S | a | w | 60-70 | 15 | stratified, very gravelly |
| | 4C | 112-125 | 10YR 6/4 | w | med | sbk-M | fr | S | a | w | 0 | 0 | sand appears to be horizontally stratified; 1cm thick clay lamella (10YR 4/2) that coats gravels at base of 3BC horizon, which is difficult to dig through |
| | 5Ab | 125-131 | 10YR 4/3 | w | f | gr-M | vf | SiL | c | s | 0 | 0 | Some 10YR 4/2 flecks; mottles: 10YR 7/2; contains OM in charcoal form that look like coniferous (spruce?) needles. |
| | 5Eb | 131-142 | 10YR 6/2 | s | m | abk | f | SiL | c | w | 0 | 0 | Fe concentrations: 5YR 5/8, strong and prominent ; one med. root noted. |
| | 5BsB | 142-153 | 5YR 4/6 | m | m | p-M | f | VFSL | c | s | | | Mottles: 5YR 3/3 and some 5YR 5/8; Fe-Mn concretions: 5YR 2.5/1 |
| | 6Cr | 153+ | 10YR 6/4 | | | M | f-fr | S | - | - | 0 | 0 | weakly consolidated |

Structure: Gr=grade (w=weak, m=medium, s=strong) ; Sz=size (vf=very fine, f=fine, m=medium, lg=large); Sh=shape (gr=granular, p=platy, sbk=subangular blocky, abk=angular blocky, M=massive, sg= single grain)
Consistence (moist): fr=friable, vfr=very friable, f=firm, vf=very firm
Texture: Si=silt; SiL= silty loam; L= loam; FSL= fine sandy loam; VFSL= very fine sandy loam; SL= sandy loam; LS= loamy sand; S= sand
Boundary: D=distinctness (a=abrupt, c=clear, g=gradual); T=topography (s=smooth, w=wavy, ir=irregular).

***Appendix 3: Silt (2-63 µm) XRD data.***

| Profile | Horizon | Depth (cm) | % Quartz | % K-spar | % Plag | K/Q | P/Q |
|---|---|---|---|---|---|---|---|
| ***Windward profiles*** | | | | | | | |
| W40 | AE | 0 | 79.3 | 8.4 | 12.3 | 2.7 | 4.4 |
| | Bs | 6 | 66.7 | 23.4 | 9.9 | 8.8 | 4.2 |
| | Bw1 | 12 | 73.5 | 14.7 | 11.8 | 5.0 | 4.6 |
| | Bw2 | 30 | 77.1 | 13.0 | 9.9 | 4.2 | 3.7 |
| | Bw2 | 45 | 75.4 | 12.8 | 11.8 | 4.3 | 4.5 |
| | 2Bw3 | 59 | 66.6 | 19.8 | 13.6 | 7.4 | 5.8 |
| | 2Bt | 80 | 70.1 | 15.1 | 14.9 | 5.4 | 6.1 |
| | 3E&Bt | 94 | 62.6 | 22.1 | 15.3 | 8.8 | 7.0 |
| | 3E&Bt | 97 | 60.8 | 29.6 | 9.7 | 12.2 | 4.5 |
| | 3E&Bt | 107 | 75.3 | 12.0 | 12.7 | 4.0 | 4.8 |
| W41 | A | 3 | 86.0 | 6.1 | 7.9 | 1.8 | 2.6 |
| | Ebg | 13 | 86.5 | 6.9 | 6.6 | 2.0 | 2.2 |
| | Bhg | 17 | 83.7 | 9.5 | 6.8 | 2.8 | 2.3 |
| | Bhsm | 26 | 75.0 | 10.6 | 14.3 | 3.5 | 5.4 |
| | Bg | 42 | 68.2 | 17.4 | 14.4 | 6.4 | 6.0 |
| | Bhg' | 51 | 75.7 | 11.4 | 12.8 | 3.8 | 4.8 |
| | 2Cg | 70 | 70.5 | 19.4 | 10.0 | 6.9 | 4.1 |
| W42 | A | 5 | 73.5 | 7.3 | 19.2 | 2.5 | 7.4 |
| | E | 16 | 77.3 | 10.4 | 12.4 | 3.4 | 4.6 |
| | Bhs | 27 | 77.1 | 9.4 | 13.5 | 3.0 | 5.0 |
| | Bs | 31 | 79.3 | 8.5 | 12.3 | 2.7 | 4.4 |
| | Bw1 | 35 | 75.4 | 12.1 | 12.6 | 4.0 | 4.8 |
| | Bw2 | 47 | 76.9 | 10.9 | 12.2 | 3.6 | 4.5 |
| | BC | 63 | 72.9 | 13.3 | 13.8 | 4.6 | 5.4 |
| | 2Cg | 100 | 70.8 | 12.0 | 17.2 | 4.2 | 7.0 |
| *Mean* | | | *74.2* | *13.4* | *12.3* | *4.7* | *4.8* |
| *Median* | | | *75.3* | *12.0* | *12.4* | *4.0* | *4.6* |
| *High* | | | *86.5* | *29.6* | *19.2* | *12.2* | *7.4* |
| *Low* | | | *60.8* | *6.1* | *6.6* | *1.8* | *2.2* |
| ***Ridge complex profile*** | | | | | | | |
| R12 | Bw1 | 5 | 75.8 | 11.5 | 12.7 | 3.8 | 4.8 |
| | Bw2 | 37 | 64.4 | 18.4 | 17.2 | 7.1 | 7.6 |
| | Bt1 | 59 | 66.2 | 15.5 | 18.2 | 5.9 | 7.9 |
| | Bt2 | 80 | 69.7 | 14.6 | 15.7 | 5.2 | 6.4 |
| | 2E&Bt | 87 | 62.9 | 13.8 | 23.3 | 5.5 | 10.6 |
| | 2E&Bt | 95 | 57.6 | 15.9 | 26.5 | 6.9 | 13.1 |
| *Mean* | | | *66.1* | *15.0* | *18.9* | *5.7* | *8.4* |
| *Median* | | | *65.3* | *15.1* | *17.7* | *5.7* | *7.7* |
| *High* | | | *75.8* | *18.4* | *26.5* | *7.1* | *13.1* |
| *Low* | | | *57.6* | *11.5* | *12.7* | *3.8* | *4.8* |

| Profile | Horizon | Depth (cm) | % Quartz | % K-spar | % Plag | K/Q | P/Q |
|---|---|---|---|---|---|---|---|
| ***Lee profiles*** | | | | | | | |
| L43 | E | 4 | 71.7 | 17.1 | 11.3 | 5.9 | 4.5 |
| | Bt1 | 8 | 69.8 | 18.2 | 12.0 | 6.5 | 4.9 |
| | Bt2 | 19 | 71.0 | 16.2 | 12.8 | 5.7 | 5.1 |
| | Bw | 30 | 70.7 | 16.2 | 13.1 | 5.7 | 5.3 |
| | Ex | 42 | 68.9 | 15.2 | 15.9 | 5.5 | 6.6 |
| | Btx | 54 | 71.4 | 16.3 | 12.4 | 5.7 | 5.0 |
| | C | 69 | 70.2 | 15.6 | 14.3 | 5.5 | 5.8 |
| L44 | E | 14 | 71.5 | 13.0 | 15.5 | 4.6 | 6.2 |
| | EB | 18 | 75.3 | 13.8 | 11.0 | 4.6 | 4.2 |
| | Bt | 25 | 70.8 | 14.8 | 14.4 | 5.2 | 5.8 |
| | Bt | 38 | 71.5 | 15.3 | 13.2 | 5.3 | 5.3 |
| | Ex | 52 | 75.0 | 12.4 | 12.6 | 4.1 | 4.8 |
| | Btx | 57 | 71.1 | 15.2 | 13.7 | 5.4 | 5.5 |
| | Btx | 70 | 71.4 | 16.4 | 12.2 | 5.7 | 4.9 |
| | 2Btx2 | 89 | 73.7 | 10.7 | 15.6 | 3.6 | 6.0 |
| | 2C | 109 | 63.3 | 19.8 | 16.8 | 7.8 | 7.6 |
| L48 | E | 6 | 71.6 | 21.9 | 6.5 | 7.7 | 2.6 |
| | Bw | 14 | 64.6 | 28.8 | 6.5 | 11.1 | 2.9 |
| | 2Ex | 34 | 64.5 | 26.6 | 8.9 | 10.3 | 3.9 |
| | 2Btx1 | 51 | 62.0 | 27.2 | 10.8 | 11.0 | 5.0 |
| | 2Btx2 | 70 | 63.8 | 24.9 | 11.3 | 9.8 | 5.0 |
| | 3BC | 83 | 63.6 | 26.7 | 9.7 | 10.5 | 4.3 |
| | 4C | 112 | 62.5 | 27.4 | 10.1 | 11.0 | 4.6 |
| | 5Ab | 125 | 64.7 | 24.9 | 10.4 | 9.6 | 4.6 |
| | 5Eb | 131 | 72.6 | 14.8 | 12.7 | 5.1 | 5.0 |
| | 5Bsb | 142 | 72.1 | 11.4 | 16.5 | 3.9 | 6.5 |
| | 6Cr | 153 | 68.4 | 17.1 | 14.4 | 6.3 | 6.0 |
| *Mean* | | | *69.2* | *18.4* | *12.4* | *6.8* | *5.1* |
| *Median* | | | *70.8* | *16.3* | *12.6* | *5.7* | *5.0* |
| *High* | | | *75.3* | *28.8* | *16.8* | *11.1* | *7.6* |
| *Low* | | | *62.0* | *10.7* | *6.5* | *3.6* | *2.6* |
| ***Mean (all)*** | | | ***71.0*** | ***15.9*** | ***13.0*** | ***5.8*** | ***5.3*** |
| ***Median*** | | | ***71.2*** | ***15.1*** | ***12.7*** | ***5.4*** | ***5.0*** |
| ***High*** | | | ***86.5*** | ***29.6*** | ***26.5*** | ***12.2*** | ***13.1*** |
| ***Low*** | | | ***57.6*** | ***6.1*** | ***6.5*** | ***1.8*** | ***2.2*** |

K/Q= peak height ratio of K-feldspar to quartz; P/Q = peak height ratio of plagioclase to quartz.

***Appendix 4: Clay mineralogy XRD and pH data for profiles in central Jackson County, WI.***

| Horizon | Depth (cm) | % EXP | % V | % I | % K+C | $H_2O$ pH | CaCl pH | Clay % |
|---|---|---|---|---|---|---|---|---|
| W40 AE | 0 | 3.4 | 39.0 | 14.4 | 43.3 | 3.45 | 3.37 | 2.05 |
| W40 Bs 9cm | 6 | 3.0 | 47.0 | 13.0 | 37.0 | 4.03 | 4.14 | 2.68 |
| W40 Bw 21cm | 12 | 0.7 | 49.1 | 8.6 | 41.6 | 4.51 | 4.59 | 2.66 |
| W40 Bw2 30 | 30 | 2.2 | 49.1 | 6.7 | 42.0 | 4.72 | 4.8 | 2.31 |
| W40 Bw2 45 | 45 | 2.5 | 49.5 | 10.3 | 37.7 | 4.64 | 4.62 | 1.84 |
| W40 2Bw3 | 59 | 0.9 | 38.8 | 17.2 | 43.1 | 4.81 | 4.77 | 1.36 |
| W40 2Bt | 80 | 2.1 | 29.7 | 24.6 | 43.6 | 5.31 | 4.76 | 4.03 |
| W40 3EnBt 90 | 90 | 1.1 | 10.9 | 29.3 | 58.6 | 4.83 | 4.79 | 0.98 |
| W40 3EnBt 94 | 94.0 | 4.3 | 37.1 | 13.0 | 45.7 | 4.87 | 4.82 | 2.43 |
| W40 3EnBt 107 | 107.0 | 5.5 | 40.1 | 13.7 | 40.6 | 5.17 | 4.58 | 2.77 |
| W41 A | 3 | 27.7 | 12.6 | 18.0 | 41.7 | 3.38 | 4.32 | 3.55 |
| W41 EBg | 13 | 38.2 | 17.8 | 5.4 | 38.6 | 3.45 | 3.46 | 2.34 |
| W41 Bhg | 17 | 46.2 | 16.4 | 7.7 | 29.6 | 3.37 | 3.43 | 1.34 |
| W41 Bhs | 26 | 37.2 | 4.4 | 28.0 | 30.4 | 3.48 | 3.65 | 0.77 |
| W41 Bg | 42 | 19.4 | 3.0 | 27.3 | 50.3 | 3.47 | 3.81 | 0.13 |
| W41 Bhg’ | 51 | 25.4 | 8.1 | 24.4 | 42.2 | 3.64 | 3.87 | 0.43 |
| W41 2Cg | 70.0 | 2.3 | 10.1 | 29.3 | 58.4 | 3.95 | 4.34 | 0.00 |
| W42 A | 5 | 2.0 | 20.4 | 43.3 | 34.3 | 3.41 | 3.17 | 2.79 |
| W42 E | 16 | 7.9 | 16.6 | 40.3 | 35.2 | 3.83 | 3.68 | 1.90 |
| W42 Bhs | 27 | 3.7 | 42.6 | 17.3 | 36.4 | 3.79 | 3.75 | 3.70 |
| W42 Bs | 31 | 5.6 | 26.5 | 30.3 | 37.6 | 4.08 | 3.95 | 3.43 |
| W42 Bw1 | 35 | 9.0 | 39.2 | 14.9 | 36.9 | 4.21 | 4.34 | 3.07 |
| W42 Bw2 | 47.0 | 5.4 | 47.5 | 10.9 | 36.2 | 4.23 | 4.44 | 2.11 |
| W42 BC | 63 | 0.8 | 43.7 | 8.5 | 47.0 | 4.22 | 4.45 | 0.59 |
| W42 Cg | 100 | 8.6 | 19.3 | 19.8 | 52.3 | 4.41 | 4.86 | 0.00 |
| | ***Max*** | ***9.0*** | ***49.5*** | ***43.3*** | ***58.6*** | ***5.3*** | ***4.9*** | ***4.03*** |
| | ***Min*** | ***0.7*** | ***10.1*** | ***6.7*** | ***34.3*** | ***3.4*** | ***3.2*** | ***0.00*** |
| | ***Ave*** | ***3.7*** | ***34.5*** | ***19.2*** | ***42.5*** | ***4.1*** | ***4.2*** | ***1.97*** |
| | ***Median*** | ***3.0*** | ***39.0*** | ***14.9*** | ***41.6*** | ***4.1*** | ***4.3*** | ***2.11*** |

| Horizon | Depth (cm) | % EXP | % V | % I | % K+C | $H_2O$ pH | CaCl pH | Clay % |
|---|---|---|---|---|---|---|---|---|
| R12 Bw1 | 5 | 0.9 | 41.1 | 12.8 | 45.3 | 4.63 | 4.14 | 4.39 |
| R12 Bw2 | 37 | 3.9 | 18.5 | 32.8 | 44.9 | 4.57 | 4.06 | 2.84 |
| R12 Bt1 | 59 | 14.3 | 24.0 | 25.1 | 36.5 | 4.65 | 3.97 | 4.14 |
| R12 Bt2 | 76 | 20.8 | 25.1 | 21.3 | 32.8 | 4.68 | 3.94 | 4.33 |
| R12 2E_Bt 87-89 | 87 | 18.0 | 24.4 | 20.0 | 37.7 | 4.6 | 4 | 3.52 |
| R12 2E_Bt 95-98 | 95 | 11.5 | 20.9 | 19.6 | 48.0 | 4.66 | 4.07 | 5.81 |

| Horizon | Depth (cm) | % EXP | % V | % I | % K+C | $H_2O$ pH | CaCl pH | Clay % |
|---|---|---|---|---|---|---|---|---|
| L43 E | 4 | 5.3 | 22.9 | 29.0 | 42.8 | 3.79 | 3.55 | 4.78 |
| L43 Bt1 | 8 | 7.7 | 44.7 | 8.4 | 39.2 | 4.17 | 4.22 | 5.86 |
| L43 Bt2 | 19 | 5.2 | 44.0 | 8.2 | 42.6 | 4.3 | 4.28 | 5.31 |
| L43 Bw | 30 | 6.6 | 29.5 | 16.3 | 47.5 | 4.47 | 4.38 | 5.35 |
| L43 Ex | 42 | 5.1 | 33.0 | 13.9 | 48.1 | 4.56 | 4.38 | 5.61 |
| L43 Btx | 54 | 2.3 | 23.7 | 27.5 | 46.4 | 4.28 | 4.25 | 5.75 |
| L43 C | 69.0 | 4.8 | 19.3 | 28.1 | 47.7 | 4.25 | 4.12 | 1.25 |
| L44 A | 11.0 | 1.8 | 24.9 | 23.4 | 49.9 | 4 | 3.7 | 4.05 |
| L44 E | 14 | 17.1 | 37.1 | 9.2 | 36.6 | 3.76 | 3.55 | 5.89 |
| L44 EB | 18 | 0.7 | 53.1 | 9.9 | 36.3 | 3.91 | 3.94 | 5.61 |
| L44 Bt 25 | 25 | 9.1 | 41.2 | 17.7 | 32.0 | 4.11 | 4.03 | 5.62 |
| L44 Bt 38 | 38 | 10.9 | 35.0 | 14.7 | 39.4 | 4.01 | 3.94 | 7.07 |
| L44 Ex 2 | 52 | 2.3 | 31.1 | 22.9 | 43.7 | 3.98 | 3.89 | 6.87 |
| L44 Btx 57 | 57 | 2.0 | 31.7 | 20.0 | 46.3 | 3.95 | 3.79 | 7.66 |
| L44 Btx 70 | 70 | 10.1 | 33.0 | 19.9 | 37.0 | 3.94 | 3.73 | 7.18 |
| L44 2Btx2 | 89 | 9.9 | 28.2 | 27.8 | 34.1 | 3.96 | 3.87 | 3.36 |
| L44 2C | 109 | 11.0 | 15.8 | 35.2 | 38.1 | 4.05 | 4.17 | 0.43 |
| L48 E | 6 | 3.3 | 4.4 | 59.4 | 32.9 | 3.64 | 3.55 | 3.98 |
| L48 Bw | 14 | 6.8 | 39.2 | 13.2 | 40.8 | 4.15 | 4.18 | 8.17 |
| L48 2Ex | 34 | 9.9 | 29.8 | 19.4 | 40.9 | 4.32 | 4.31 | 7.77 |
| L48 2Btx1 | 51 | 6.4 | 20.9 | 29.4 | 43.3 | 4.06 | 4.01 | 8.63 |
| L48 2Btx2 | 70 | 8.2 | 24.7 | 19.7 | 47.5 | 4.14 | 4.02 | 6.93 |
| L48 3BC | 83 | 8.0 | 13.0 | 42.3 | 36.8 | 4.12 | 4.04 | 3.97 |
| L48 4C | 112 | 6.7 | 10.9 | 56.2 | 26.1 | 4.22 | 4.21 | 1.81 |
| L48 5Ab | 125 | 18.5 | 17.3 | 35.5 | 28.7 | 4.09 | 3.89 | 11.25 |
| L48 5Eb | 131 | 16.6 | 20.5 | 29.6 | 33.3 | 4.03 | 3.87 | 11.98 |
| L48 5Bsb | 142 | 12.3 | 29.0 | 29.7 | 29.0 | 4.07 | 4.22 | 18.00 |
| L48 6Cr | 153 | 8.7 | 15.0 | 34.4 | 41.9 | 4.1 | 4.03 | 4.00 |
| L48 Cr 160-165 | 160 | 11.1 | 18.6 | 34.3 | 36.0 | | | |
| L48 Cr 195-200 | 195 | 16.6 | 19.6 | 26.9 | 36.9 | | | 2.94 |
| | ***Max*** | ***20.8*** | ***53.1*** | ***59.4*** | ***49.9*** | ***4.7*** | ***4.4*** | ***18.00*** |
| | ***Min*** | ***0.7*** | ***4.4*** | ***8.2*** | ***26.1*** | ***3.6*** | ***3.6*** | ***0.43*** |
| | ***Ave*** | ***8.7*** | ***26.8*** | ***24.8*** | ***39.6*** | ***4.2*** | ***4.0*** | ***5.77*** |
| | ***Median*** | ***8.1*** | ***24.8*** | ***23.1*** | ***39.3*** | ***4.1*** | ***4.0*** | ***5.61*** |
| ***(All samples)*** | ***Max*** | ***46.2*** | ***53.1*** | ***59.4*** | ***58.6*** | ***5.3*** | ***4.9*** | ***18.00*** |
| | ***Min*** | ***0.7*** | ***3.0*** | ***5.4*** | ***26.1*** | ***3.4*** | ***3.2*** | ***0.00*** |
| | ***Ave*** | ***9.5*** | ***27.6*** | ***22.5*** | ***40.4*** | ***4.2*** | ***4.1*** | ***4.19*** |
| | ***Median*** | ***6.7*** | ***25.1*** | ***20.0*** | ***40.6*** | ***4.1*** | ***4.0*** | ***3.63*** |

Exp. = expandable clays (14.5-18 Å); V = vermiculite or HI (~14 Å); K = kaolinite, C=chlorite (~7 Å); clay percent (<2 µm).

***Appendix 5: Photograph of profile L48 with horizons drawn in. Photo by K Gruley 2012***

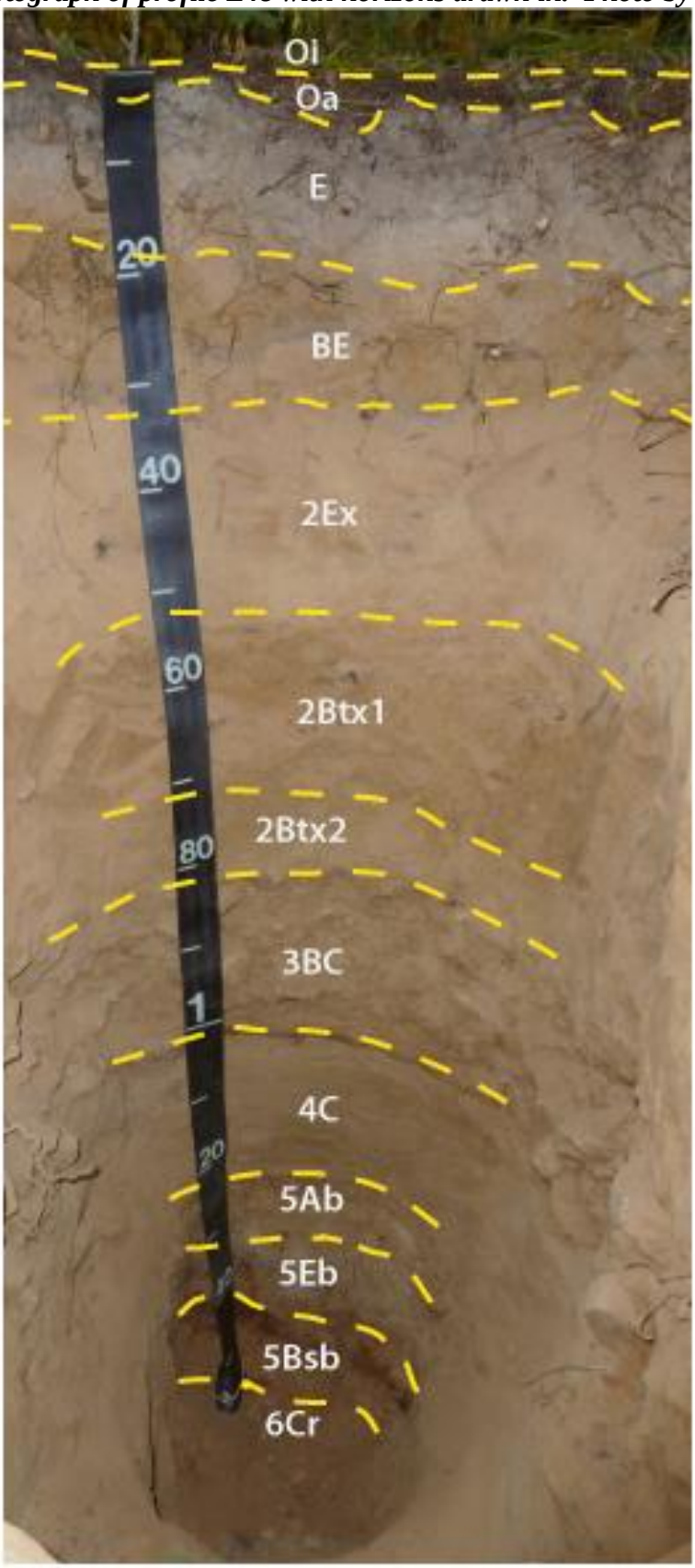

***Appendix 6: SOM data from mineral soil samples for profiles in central Jackson County.***

| Sample ID | Depth (cm) | $\delta^{13}C$ | OC (µg) | $\delta^{15}N$ | Total N (µg) | Sample (mg) | CN | C% | N% |
|---|---|---|---|---|---|---|---|---|---|
| W40 Oi | 0 | -28.34 | 1364.88 | -5.02 | 57.41 | 3.1 | 23.78 | 44.03 | 1.85 |
| W40 AE | 1 | -27.08 | 967.29 | 1.85 | 51.16 | 37.7 | 18.91 | 2.57 | 0.14 |
| W40 Bs 6 | 6 | -26.57 | 376.47 | 3.94 | 26.24 | 51.9 | 14.35 | 0.73 | 0.05 |
| W40 Bw1 | 12 | -25.88 | 224.54 | 5.03 | 20.05 | 73.7 | 11.20 | 0.30 | 0.03 |
| W40 Bw2 | 30 | -25.56 | 126.54 | 4.59 | 9.64 | 74.8 | 13.13 | 0.17 | 0.01 |
| W40 Bw2 | 45 | -25.43 | 86.99 | 4.63 | 6.69 | 75.1 | 13.00 | 0.12 | 0.01 |
| W41 Oi | 1 | -28.75 | 808.84 | -4.75 | 25.51 | 2 | 31.70 | 40.44 | 1.28 |
| W41 A 3 | 3 | -26.37 | 2535.10 | 1.79 | 123.12 | 36.1 | 20.59 | 7.02 | 0.34 |
| W41 EBg | 13 | -26.80 | 429.49 | 4.55 | 25.76 | 72.9 | 16.67 | 0.59 | 0.04 |
| W41 Bhg | 17 | -27.50 | 517.88 | 5.08 | 27.78 | 60.5 | 18.64 | 0.86 | 0.05 |
| W41 Bhsm | 26 | -26.86 | 708.88 | 2.59 | 22.47 | 63.8 | 31.55 | 1.11 | 0.04 |
| W41 Bg | 42 | -27.26 | 96.88 | -0.96 | 3.69 | 64 | 26.26 | 0.15 | 0.01 |
| W41 Bhg’ | 51 | -27.08 | 289.90 | 1.64 | 9.54 | 65.2 | 30.39 | 0.44 | 0.01 |
| W42 Oe | 1 | -27.04 | 1163.46 | -0.54 | 47.86 | 3.4 | 24.31 | 34.22 | 1.41 |
| W42 A | 5 | -26.27 | 1316.34 | 3.60 | 58.88 | 43.7 | 22.36 | 3.01 | 0.13 |
| W42 E | 16 | -25.64 | 133.60 | 4.28 | 8.95 | 52.9 | 14.93 | 0.25 | 0.02 |
| W42 Bhs | 27 | -25.80 | 434.79 | 5.69 | 27.88 | 55.6 | 15.60 | 0.78 | 0.05 |
| W42 Bs | 31 | -25.58 | 475.45 | 5.48 | 31.82 | 69.9 | 14.94 | 0.68 | 0.05 |
| W42 Bw1 | 35 | -25.26 | 390.61 | 5.70 | 24.41 | 75.2 | 16.01 | 0.52 | 0.03 |

| Sample ID | Depth (cm) | $\delta^{13}C$ | OC (µg) | $\delta^{15}N$ | Total N (µg) | Sample (mg) | CN | C% | N% |
|---|---|---|---|---|---|---|---|---|---|
| L43 Oi | 0 | -29.85 | 943.03 | -5.66 | 29.86 | 2.8 | 31.58 | 33.68 | 1.07 |
| L43 Oe | 2 | -28.38 | 1160.87 | -3.32 | 57.87 | 3.9 | 20.06 | 29.77 | 1.48 |
| L43 E | 4 | -27.02 | 954.90 | 1.69 | 55.78 | 46.4 | 17.12 | 2.06 | 0.12 |
| L43 Bt1 | 8 | -24.95 | 351.74 | 6.53 | 28.84 | 73.1 | 12.20 | 0.48 | 0.04 |
| L43 Bt2 | 19 | -24.90 | 205.12 | 8.01 | 16.17 | 71.7 | 12.69 | 0.29 | 0.02 |
| L43 Ex | 42 | -23.85 | 80.99 | 6.07 | 9.44 | 73.8 | 8.58 | 0.11 | 0.01 |
| L43 Btx | 54 | -23.90 | 79.58 | 5.69 | 11.98 | 74.5 | 6.64 | 0.11 | 0.02 |
| L44 Oi | 0 | -29.11 | 1354.81 | -2.84 | 53.99 | 3.2 | 25.09 | 42.34 | 1.69 |
| L44 Oe | 8 | -28.21 | 1369.67 | -2.43 | 87.36 | 6.30 | 15.68 | 21.74 | 1.39 |
| L44 A | 11 | -26.60 | 3426.65 | 0.45 | 221.65 | 43.7 | 15.46 | 7.84 | 0.51 |
| L44 E | 14 | -25.78 | 1422.73 | 3.82 | 98.01 | 55.2 | 14.52 | 2.58 | 0.18 |
| L44 EB | 18 | -25.38 | 807.97 | 5.78 | 63.38 | 67.1 | 12.75 | 1.20 | 0.09 |
| L44 Bt | 25 | -24.98 | 323.47 | 7.19 | 33.26 | 69.9 | 9.73 | 0.46 | 0.05 |
| L44 Ex | 52 | -24.28 | 243.97 | 7.25 | 24.70 | 73.8 | 9.88 | 0.33 | 0.03 |
| L44 Btx | 57 | -24.17 | 170.33 | 7.06 | 22.38 | 74.6 | 7.61 | 0.23 | 0.03 |
| L48 Oi | 0 | -29.68 | 1465.61 | -5.17 | 66.55 | 3.1 | 22.02 | 47.28 | 2.15 |
| L48 Oa | 3 | -29.24 | 1819.98 | -4.31 | 91.63 | 4.404 | 19.86 | 41.33 | 2.08 |
| L48 E | 6 | -27.27 | 383.54 | 5.04 | 25.76 | 50.2 | 14.89 | 0.76 | 0.05 |
| L48 Bw | 14 | -26.64 | 562.08 | 6.68 | 38.05 | 69.8 | 14.77 | 0.81 | 0.05 |
| L48 2Ex | 34 | -25.34 | 167.33 | 7.19 | 17.33 | 70.1 | 9.65 | 0.24 | 0.02 |
| L48 2Btx1 | 51 | -25.05 | 133.43 | 6.43 | 14.03 | 73.6 | 9.51 | 0.18 | 0.02 |
| L48 2Btx2 | 70 | -24.66 | 61.40 | 5.27 | 7.87 | 75 | 7.81 | 0.08 | 0.01 |
| L48 5Ab | 125 | -24.94 | 176.69 | 5.63 | 21.70 | 60.5 | 8.14 | 0.29 | 0.04 |
| L48 5Eb | 131 | -24.37 | 168.39 | 5.72 | 27.78 | 70.5 | 6.06 | 0.24 | 0.04 |
| L48 5Bsb | 142 | -23.47 | 149.67 | 6.72 | 17.92 | 74.7 | 8.35 | 0.20 | 0.02 |

OC = organic carbon; N = total nitrogen; C:N = carbon-to-nitrogen ratio; $\delta^{13}C$ = relative deviation of $^{13}C$ from standard; $\delta^{15}N$ = relative deviation of $^{15}N$ from standard.